EXPERIMENTAL STUDIES ON THE STABILITY AND TRANSITION OF THREE-DIMENSIONAL BOUNDARY LAYERS

P. Nitschke-Kowsky

IN-34

82598

114 P.

NATIONAL AERONAUTICS AND SPACE ADMINISTRATION
WASHINGTON, DC   20546   JUNE 1987

1. Report No. NASA TM-88539	2. Government Accession No.	3. Recipient's Catalog No.
4. Title and Subtitle EXPERIMENTAL STUDIES ON THE STABILITY AND TRANSITION OF THREE-DIMENSIONAL BOUNDARY LAYERS		5. Report Date June 1987
		6. Performing Organization Code
7. Author(s) P. Nitschke-Kowsky		8. Performing Organization Report No.
		10. Work Unit No.
9. Performing Organization Name and Address The Corporate Word, inc. 3 Gateway Ctr., 18 S. Pittsburgh, PA 15222		11. Contract or Grant No. NASW-4006
		13. Type of Report and Period Covered Translation
12. Sponsoring Agency Name and Address National Aeronautics and Space Administration Washington, DC 20546		14. Sponsoring Agency Code

15. Supplementary Notes   Translation of "Experimentelle Untersuchungen zu Stabilitaet und Umschlag dreidimensionaler Grenzschichten," Deutsch Forschungs- und Versuchsanstalt fuer Luft- und Raumfahrt, DFVLR-FB 86-24, June 19, 1986.

16. Abstract

By means of various experimental methods, three-dimensional unstable boundary layers are examined concerning their characteristic instabilities which lead to turbulence. Using a swept cylinder, it was possible, using the hydrogen bubble method, to make standing cross flow instabilities and travelling waves visible in the boundary layer above the wall. Other experiments were conducted using the sublimation method and hot film technique on a model consisting of a swept flat plate with a pressure-inducing displacement body in the 1-meter wind tunnel. These experiments also produced both standing cross flow instabilities ($\lambda \approx 4.\delta_{99.9\%}$) and travelling waves in a broad frequency band. The instabilities observed in the model are a close approximation of the theoretical predictions.

17. Key Words (Selected by Author(s))		18. Distribution Statement Unlimited	
19. Security Classif. (of this report) Unclassified	20. Security Classif. (of this page) Unclassified	21. No. of Pages 114	22. Price

NASA-HQ

TABLE OF CONTENTS

LIST OF SYMBOLS

c	0.50 m, plate depth
$c_p = \dfrac{p - p_\infty}{\rho/2 \cdot U_\infty^2}$	correction value for pressure, relative to the velocity component perpendicular to leading edge
d	0.20 m, cylinder diameter
$E(t)$	hot wire or hot film signal at output end of anemometer
$E_s(t)$	hot wire or hot film signal after taking off
$E_\zeta(t)$	a constant voltage and amplification
f	frequency of travelling wave
$F_\delta = 2\pi f \cdot \delta / Q_e$	normed frequencies
$F = 2\pi f \cdot \sqrt{\nu x / U_e} / Q_e$	normed frequencies
H_{12}	shape parameter of the velocity profile projected onto the (x_t, z) plane
K	constant discretionary voltage
$k = (\alpha, \beta)$	wave vector
$k_i = (\alpha_i, \beta_i)$	excitation vector
L	standardization length
P	pressure
p	nonstationary pressure variations
Q	velocity vector
Q_0	standardization velocity
q	disturbance velocity vector
Re	Reynolds number, obtained with c or d
$R = V_e \cdot \eta / \nu$	characteristic Reynolds number for the flow in stagnation area where
	$\eta = \sqrt{\dfrac{\nu}{dU_e/dx\big|_{x=0}}}$
t	time

Tu		amount of turbulence
U,V,W		velocity components of the main flow in the body coordinate system
U_t,V_t,W		velocity components of the main flow in the streamline coordinate system
u,v,w		nonstationary velocity components
x,y,z		body coordinate system
	x:	wall coordinate perpendicular to leading edge
	y:	wall coordinate parallel to leading edge
	z:	perpendicular to wall
x_t,y_t,z		streamline coordinate system
	x_t:	wall coordinate tangential to local streamline at edge of boundary layer
	y_t:	wall coordinate normal to local streamline at edge of boundary layer
$\alpha = \alpha_r + \alpha_i$		complex non-dimensional wave number in direction x
$\beta = \beta_r + \beta_i$		complex non-dimensional wave number in direction y
γ		angle at circumference between stagnation line and bubble wire on the cylinder
δ		99.9% boundary layer thickness
δ^*		non-dimensional 99.9% boundary layer thickness
λ		wavelength measured perpendicular to propagation direction of wave
λ''		wavelength measured parallel to leading edge
v		kinematic viscosity
p		density
ϕ_0		sweep angle, i.e. angle between the vector of undisturbed forward flow Q_∞ and x, the perpendicular to the leading edge
$\phi(x)$		local sweep angle of the streamline at the boundary layer edge, i.e. angle between x and x_t
$\phi_{QI}(x)$		local sweep angle of the stationary waves to the x axis

$\chi = V_{t max} \cdot \Delta / \nu$ cross flow Reynolds number where
$$\Delta = \int V_t / V_{t max} dy$$

angle between x_t and the propagation direction of a wave

ψ angle between x_t and the propagation direction of a wave

ψ' angle between x and the propagation direction of a wave

$\omega = \omega_r + \omega_i$ complex non-dimensional frequency

EXPERIMENTAL STUDIES ON THE STABILITY AND TRANSITION
OF THREE-DIMENSIONAL BOUNDARY LAYERS

P. Nitschke-Kowsky
DFVLR Institute for Experimental Flow Mechanics, Göttingen

1. INTRODUCTION   /11*

The occurrence of instability in a laminar boundary layer and the accompanying turbulent transition are highly significant for many technical applications. For example, the transition causes the resistance of a laminar wing to change considerably. If it is possible to keep the boundary layer on this airfoil laminar by influencing its physical properties, an aircraft's fuel consumption can be decreased as a result of diminished friction.

However, sufficient understanding of the physics of the instability which occurs is required. The present work is intended to provide new depth to this understanding.

Reynolds was the first to develop the notion that a laminar flow will become unstable when very small initial disturbances grow under certain conditions until they finally cause transition. This idea led to the mathematical concept of introducing small disturbance factors into the Navier-Stokes equation and calculating the excitation or attenuation of these disturbances.

For two-dimensional boundary layers, the Orr-Sommerfeld equation can be applied with a few simplifications. This equation was solved for the Blasius boundary layer by Tollmien in 1929 (see Schlichting [38]. He created a stability diagram which was confirmed experimentally by Schubauer and Skranstad [40]. In spite of some simplification, the theory was able to correctly describe the boundary layer's reaction to induced disturbances. The theory also provides useful criteria for the behavior of flat boundary layers with pressure gradients and for boundary layers on slightly curved surfaces as far as stability is concerned. After surpassing a certain excitation of disturbance waves all the way up to turbulence, the other processes can no longer be described by the linear theory of stability. For practical applications, various empirical criteria or, when the results of the theory /12 of stability were used, semi-empirical theories were developed, such as the so-called e^n method. These methods predicted the site of transition in two-dimensional boundary layers with satisfactory accuracy.

However, these criteria, which were found for flat boundary layers, are not valid for three-dimensional boundary layer profiles as they occur in the case of swept wings. The theoretical treatment of the three-dimensional boundary layer with

---

*Numbers in the margins indicate pagination of the foreign text.

regard to stability is much more complicated. Since velocity profiles are warped, one can no longer assume a preferred direction of the propagation of disturbing waves, as one could at the two-dimensional level.

Experimentally Gray [12] and Owen and Randall [25] observed the characteristic peculiarities of transition of three-dimensional boundary layers on arrowhead wings.

- As the angle of sweep increases, the site of transition is transferred to smaller Reynolds numbers and transition takes place, especially in the area of decreasing pressure, which is very stable in a two-dimensional model.

- In all experiments, before actual transition took place, regular stationary striations were observed in the area of decreased pressure using the sublimation method.

- As a third conspicuous phenomenon, Owen and Randall discovered that under certain experimental conditions the boundary layer even became turbulent in the region of the leading edge.

In spite of these crucial observations, there is a lack of systematic experimental studies in which the theory can be examined or which point the way to potential simplifications of the theory.

It is the goal of the present work to experimentally examine three-dimensional boundary layers in the areas of decreasing pressure. First, in Section 2, a brief summary of the experimental and theoretical results of other authors will be /13 presented. Section 3 deals with an experiment based on a suggestion by Hirschel and Dallmann [17]. They seized upon an idea of van den Berg and Elsenaar [4], who had built a model out of a swept plate with impressed pressure gradient in order to study turbulent, three-dimensional boundary layers. They suggested the construction of a similar model to study laminar turbulent transition. This model meets the requirements of the theory quite well, thereby enabling direct comparison of results. Such a model was constructed for the DFVLR 1-meter wind tunnel in Göttingen. The resulting boundary layer was examined by making the flow visible on the surface of the plate (sublimation and painting method) and using hot film measurements for stationary and travelling waves. The results were compared with computations done by Bieler [5] at the institute for theoretical flow mechanics of the DFVLR Göttingen. The actual site of the transition was compared with the prediction using a criterion developed by Coustols (1983) for the transition of three-dimensional boundary layers.

It was the aim of another experiment using an adjusted circular cylinder with a semispherical head in a model water tunnel to make the flow in the boundary layer visible. Until that time, the standing cross flow instabilities on swept wings were observed only directly on the wall in sublimation and petroleum

painting pictures. Making things visible in the boundary layer can yield other insights about the physical processes involved. The model water tunnel is particularly well-suited to stability experiments due to the low level of instability in the inflow. With the hydrogen bubble technique, a good method of making things visible is available. The design and results of this experiment are described in Section 4. Finally, Section 5 presents a summary of the results and prospects for further studies.

2. STABILITY AND TRANSITION OF THREE-DIMENSIONAL BOUNDARY LAYERS - KNOWLEDGE TO DATE /14

2.1 THEORETICAL BASIS

In three-dimensional boundary layers, the direction of velocity parallel to the wall changes with the distance from the wall. Such boundary layer profiles always develop where flow lines are bent in levels parallel to the wall and thus centrifugal force has an effect, for example, on rotating bodies, or on the flow around three-dimensional bodies. Normally, the boundary layer profile is dismantled by projecting it on one level tangential to the local streamline on the edge of the boundary layer and by projecting it on one level in a normal relationship to the former into the so-called main flow and cross flow profile (see Fig. 2.1).

Stuart (Gregory, Stuart, Walker, [14]) derived the linearized disturbance differential equations for such twisted velocity profiles with temporally excited disturbances as early as 1955. In the process, he took the curvature of surface and streamline parameters into account. The equations are quite general and they contain some of the previously derived special cases, such as the Orr-Sommerfeld equation for a flat boundary layer. With such generality, the equations could not be solved. Not until very recently did Malik and Poll's [23] results appear.

Attempts were made, however, to arrive at an equation similar to the Orr-Sommerfeld equation through simplification. Many authors (such as Reshotko [33], Mack [22], and Habiballah [15]) have already dealt with the theory and its results at length. For that reason, just a brief overview will be presented in the next section. Its thrust will center around a discussion of the simplifications, and it determines the goals of the present experiments.

In the present work, only the simplest instance of a three-dimensional boundary layer is dealt with: an incompressible flow around an infinitely long, swept, two-dimensional model. The magnitude of the flow and all the basic magnitudes of the /15 boundary layer do not depend on the coordinates parallel to the leading edge (y); a so-called quasi-two-dimensional boundary layer is the result.

Fig. 2.2 introduces two more suitable systems of coordinates: a system which is physically constant (x, y, z) with the velocity

components of the main flow (U, V, W), and (x_t, y_t, z) which is oriented toward the line of flow, together with (U_t, V_t, W_t), whose x_t axis runs tangentially to the local flow line of the external flow. ϕ_0 is the model's angle of sweep. x and x_t include the streamlines local sweep angle $\phi(x)$.

As is customary in the stability theory, disturbances q and p, which are supposed to be very small, are superimposed upon the main flow Q and P. The total resulting from main flow and disturbance flow is:

$$Q_g = Q + q$$

$$P_g = P + p \ .$$

(1)

Inserting this statement into the Navier-Stokes equation yields:

$$\frac{DQ_g}{Dt} = \frac{\partial Q_g}{\partial t} + (Q_g, \nabla) \, Q_g =$$

$$= \nabla P_g + \frac{1}{Re} \, (\nabla, \nabla) \, Q_g \ .$$

(2a)

and the continuity equation

$$\nabla \cdot Q_g = 0 \ .$$

(2b)

In equations 2a and 2b, non-dimensional coordinates have already been introduced. Finally, the following simplifications are undertaken.

LINEARIZATION

First the equations are linearized by ignoring all products of the variable quantities q and p, together with their derivations, since, according to the prediction, these are supposed to be small.

ASSUMING PARALLEL FLOW

In addition, the velocity component perpendicular to the wall of the main flow is assumed to be zero.

$$W = 0.$$

The requirements for a completely formed boundary layer flow in a flat tunnel are met exactly; for other types of boundary layers, the requirement is not met entirely. This is so because the boundary layer grows with the length of the run.

LOCAL ANALYSIS

Due to the requirements of a quasi-two-dimensional flow, not all main flow quantities depend upon coordinate y:

$$\partial/\partial y = 0 .$$

Furthermore, the changes of velocity components U and V in direction x as opposed to the changes perpendicular to wall z are disregarded

$$\partial U/\partial x \quad << \quad \partial U/\partial z$$
$$\partial V/\partial x \quad << \quad \partial V/\partial z .$$

In disregarding these things, one is limited to local analysis, since all information on the influence of the growth of the boundary layer is lost.

In addition, curvature of the surface and of the streamline is disregarded. This gives:

$$\frac{\partial u}{\partial t} + U \frac{\partial u}{\partial x} + V \frac{\partial u}{\partial y} + w \frac{\partial U}{\partial z} = - \frac{\partial p}{\partial x} + \frac{1}{Re} \left(\frac{\partial^2 u}{\partial x^2} + \frac{\partial^2 u}{\partial y^2} + \frac{\partial^2 u}{\partial z^2} \right)$$

$$\frac{\partial v}{\partial t} + U \frac{\partial v}{\partial x} + V \frac{\partial v}{\partial y} + w \frac{\partial V}{\partial z} = - \frac{\partial p}{\partial y} + \frac{1}{Re} \left(\frac{\partial^2 v}{\partial x^2} + \frac{\partial^2 v}{\partial y^2} + \frac{\partial^2 v}{\partial z^2} \right) \tag{3}$$

$$\frac{\partial w}{\partial t} + U \frac{\partial w}{\partial x} + V \frac{\partial w}{\partial y} \qquad = - \frac{\partial p}{\partial z} + \frac{1}{Re} \left(\frac{\partial^2 w}{\partial x^2} + \frac{\partial^2 w}{\partial y^2} + \frac{\partial^2 w}{\partial z^2} \right)$$

THE DISTURBANCE STATEMENT

A small disturbance q, p of the boundary layer flow can be broken down with the aid of a Fourier analysis into a sum of harmonic waves. Thus, for the disturbance statement, a harmonic wave can be chosen and real disturbances simulated by superimposing partial vibrations.

By assuming parallel flows, it can be supposed that the coefficient of the system of equations depends only upon z. This makes it possible to split the disturbance statement into an amplitude which depends solely on z and a harmonic wave dependent on x and y.

$$\begin{pmatrix} p \\ u \\ v \\ w \end{pmatrix} = \begin{pmatrix} \hat{p} \\ \hat{u} \\ \hat{v} \\ \hat{w} \end{pmatrix} (z) \cdot e^{i(\alpha x + \beta y - \omega t)} \tag{4}$$

$\hat{u}(z)$, $\hat{v}(z)$, $\hat{w}(z)$, $\hat{p}(z)$ are those amplitudes which have complex values; α, β, and ω are complex in general. Usually, however, the

12

computations are limited to either a temporal or spatial excitation of the disturbances.

In the case of temporal disturbances

$$\alpha = (2\pi/\lambda_x)L, \quad \beta = (2\pi/\lambda_y)L$$

are the non-dimensional components of the wave vector

$$\underline{k} = (\alpha,\beta),$$

which, together with the x axis, includes the angle

$$\psi' = \arctan \beta/\alpha.$$

is complex

$$\omega = \omega_r + \omega_i$$

with

$$\omega_r = 2\pi f \; L/Q_0$$

as a non-dimensional frequency of the wave. ω_i is an excitation or squelching factor:

$$\begin{pmatrix}u\\v\\w\end{pmatrix} = \begin{pmatrix}\hat{u}\\\hat{v}\\\hat{w}\end{pmatrix} e^{\omega_i t} \cdot e^{i(\alpha x + \beta y - \omega_r t)}.$$

Placing statement (4) in (3) and eliminating $\hat{u}$, $\hat{v}$, $\hat{p}$ gives:

$$1/iRe \; (\hat{w}'''' -2(\alpha^2+\beta^2)\hat{w}''+(\alpha^2+\beta^2)^2 \; \hat{w}) =$$

$$(5)$$

$$= (\alpha U+\beta V-\omega)[\hat{w}''-(\alpha^2+\beta^2)\hat{w}]-(\alpha U''+\beta V'')\hat{w} \; .$$

This equation is a generalization of the Orr-Sommerfeld equation for three-dimensional velocity profiles and any possible direction of propagation of the wave. In the case of V ≡ 0 and β ≡ 0, it is transformed to the latter.

By means of a simple transformation, Squire (1933) was able to prove for level boundary layer profiles (V ≡ 0) in cases of temporally excited disturbances that every wave travelling at a slant corresponds to a wave in the streamline direction (β ≡ 0) with a smaller Reynolds number. Thus, if the critical Reynolds number for a flat speed profile is to be calculated, it suffices to solve the Orr-Sommerfeld equation for β ≡ 0.

A similar transformation can be introduced for temporally excited waves ($\alpha_i = \beta_i = 0$, $\omega_i \neq 0$) in three-dimensional speed

profiles ($V \neq 0$) (Stuart [14], Mack [22]). The wave vector $\underline{k}$ is expressed by the amount and angle against the x axis.

$$\underline{k} = |k| (\cos \psi', \sin \psi').$$

It follows that

$\alpha = |k| \cos \psi', \quad \beta = |k| \sin \psi'$

$\alpha^2 + \beta^2 = |k|^2 .$

Substituting the values into (5) gives:

$$1/iRe(\hat{w}'''' - 2k^2\hat{w}'' + k^4\hat{w}) = [|k| (U \cos \psi' + V \sin \psi') - \omega] \cdot$$

$$\cdot [\hat{w}'' - |k|^2\hat{w}] - |k| (U \cos \psi' + V \sin \psi')'' \hat{w} . \tag{6}$$

Now this equation corresponds exactly to the Orr-Sommerfeld equation for a velocity profile $U(z)$

$$U(z) = (U \cos \psi' + V \sin \psi')$$

which results from the projection of the three-dimensional profile $Q(z) = (U(z), V(z), 0)$ onto the propagation direction of the wave.

Thus the mathematical stability problem of a three-dimensional boundary layer has been traced back to the solution of the Orr-Sommerfeld equation for projection profiles. However, /20 solutions to this equation must be found for all projection angles, and only the total of the resulting calculated flat waves for different directions allows a determination of the three-dimensional profile's stability.

Not until theoretical and experimental results have been compared can it be determined whether using equation (6) to consider projection profiles does in fact accurately describe the physical processes and whether the simplifications are therefore justified. Various authors have already discussed the effect of linearization, assumption of parallel flow, and local analysis in the course of dealing with the plane problem.

Small disturbances can be correctly calculated by linearization. Larger disturbances such as those occurring before the transition or their non-linear interaction cannot be accounted for.

By assuming parallel flow, not only is the velocity component perpendicular to the wall neglected, but the prerequisite for a simplified approach to disturbance is created. Gaster [11] and Saric and Nayfeh [35] discussed this problem and showed that the impact of this simplification is not very great as long as the disturbances are followed only over a few wavelengths. In particular, its impact is smaller for an accelerated flow, since the boundary layer does not grow as much there.

Neglecting the curve of the surface and streamlines is quite a bit more problematic, because they can play a large role in cases of practical interest, especially when cross flow instabilities are induced. Calculations for the swept cylinder by Poll and Malik [23] show that significantly different excitation results are obtained when the curve effects for several disturbance modes are considered. It is therefore extremely important, when comparing calculations which are based on the generalized Orr-Sommerfeld equation (6) and on an experiment, to approximate the condition of negligible surface and streamline curvature.

The transformation which changes equation (5) into the standard Orr-Sommerfeld equation (6), thereby allowing the observation of projection profiles, is only possible for temporally excited waves. However, in a stationary boundary layer flow, temporal origin is not realistic. The disturbances are actually spatially caused, making the components of the wave vector α and β complex while the frequency is real. For the wave, we find

$$\begin{pmatrix} u \\ v \\ w \end{pmatrix} = \begin{pmatrix} \hat{u} \\ \hat{v} \\ \hat{w} \end{pmatrix} e^{\alpha_i x + \beta_i y} \, e^{i(\alpha_r x + \beta_r y - \omega t)} \; .$$

In this equation, the frequency is expressed by

$$\omega = 2\pi f \, L/Q_0 \; .$$

The real parts of α and β correspond to the wave vector

$$\underline{k} = (\alpha_r , \beta_r)$$

and the excitation vector

$$\underline{k}_i = (\alpha_i , \beta_i)$$

can also be introduced, which need not have the same direction as k. The direction represents an additional free parameter.

However, Mack [23] was able to show that the transformation of temporally excited solutions to spatially excited ones introduced by Gaster for two-dimensional boundary layers is also valid for three-dimensional boundary layers with low excitation rates. Therefore, temporally excited solutions also can correctly describe the stability characteristics.

2.2 THEORETICAL AND EXPERIMENTAL FINDINGS TO DATE

Although equation (6) contains several simplifications, it has been possible, with the idea of considering the stability of projection profiles based on it, to explain several phenomena of transition in three-dimensional boundary layers. (Stuart [14])

- As already mentioned in the introduction, the transition for swept airfoils already occurs at much smaller Reynolds

numbers and can even begin even at the area of the pressure
drop. Fig. 2.3 shows projection profiles of a typical
three-dimensional boundary layer in accelerated flow
dependent on the angle ψ from the tangent to the outer
streamline. It is important that profiles with turning-points
occur in a certain range of angles. It is known of such
profiles that they become unstable even at very small critical
Reynolds numbers. In addition, the excitation of
instabilities is significantly more powerful there. This
offers an explanation for the early transition of swept
airfoils.

—　In all transition experiments in three-dimensional boundary
layers, the occurrence of stationary disturbances has been
observed in the pressure drop area. They were found to be
band structures with a direction corresponding roughly to the
local frictionless streamline. In the family of profiles in
Fig. 2.3 there exist profiles with a change of sign and a
turning-point after a certain angle. Outstanding among these
profiles is one with projection angle ψ_J, where the turning-
point coincides with the zero point (often called the J-
profile in the literature). It is possible, for velocity
profiles in this angle range around ψ_J, to calculate excited
disturbances with decreasing phase velocity

$$\omega_r = 0 .$$

These disturbances have the form

$$\begin{pmatrix} u \\ v \\ w \end{pmatrix} = \mathrm{Re} \left\{ \begin{pmatrix} \hat{u} \\ \hat{v} \\ \hat{w} \end{pmatrix} e^{i\omega_i t} e^{ik_\psi x_\psi} \right\} .$$

They cause stationary vortices spinning in a contrary　　　/23
direction, whose axes lie perpendicular to the projection
plane of the velocity profile and are therefore approximately
in the direction of the main flow, cf. Fig. 2.4 (cf. Arnal
[2]). If this disturbance flow is overlaid on the main flow,
the result for the stationary observer is a streamline
configuration with half the number of vortices spinning in the
same direction. The observed striated structures can be
explained by these stationary vortex patterns.

More exact measurements in the unstable area of a quasi-two-
dimensional boundary layer, which make possible a quantitative
comparison of theory and experiment, were obtained by Poll [28]
and [30], Arnal et al. [3], and Saric [37].

Poll conducted extensive studies of disturbances in the
stagnation area and of the stability of the three-dimensional
boundary layer using a swept circular cylinder whose trailing edge
was constructed with a wedge attached tangentially to the
cylinder. This flow is characterized by strong wall and
streamline curvature and by great acceleration, see Fig. 2.5.

Poll used the petroleum painting method to determine the first
appearance of cross flow instability and to measure its wavelength λ
and its direction relative to the x axis. In addition, he found
strongly negative excited travelling waves of about 1,000 Hz.
With Malik, he later carried out stability calculations (Malik and
Poll [23]) which took curvature terms into consideration. The
findings showed a satisfactory match between wavelength and
direction of the stationary modes. However, the truly significant
aspect of their calculations is that not stationary but travelling
waves undergo the strongest integral continuous excitation. In
particular, a wave of approximately 1,000 Hz was also found for
the above mentioned case. It is astounding that the stationary
waves nonetheless show up so clearly in petroleum painting   /24
images. The role of stationary waves in the area of turbulence
remains unclear.

     In addition to transition measurements, Arnal et al. conducted
investigations in the boundary layer on the pressure surface of a
swept (ϕ_o = 40°), set ($\propto$ = -6°) ONERA-D wing. Fig. 2.6 shows the
velocity progression on the edge of the boundary layer. All
measurements were made for $y/c \geq 0.2$, i.e. in a range where the
profile is only slightly curved, no great acceleration exists,
and, therefore, no great streamline curvature is present.

     Arnal et al. utilized the sublimation method to determine the
transition and to make the traces of the cross flow vortex visible
on the wall. Measurements with a hot wire at a constant distance
from the wall showed that the average spanwise velocity is greatly
modulated (up to 15% of the external velocity) by the cross flow
vortices. The measured wavelength corresponds to that measured in
sublimation images; it increases with growing distance x/c from
the leading edge. A widening or disappearance of single "bands"
in the sublimation image corresponds to the increase of the
wavelength.

     In detailed measurements with reduced velocity of flow from
initial direction, Arnal shows the modulation of the average
velocity in an entire field with a height of δ and a width of a
wavelength λ (field (δ,λ)) perpendicular to the local streamline.
Arnal compares the measurements to solutions of the Orr-Sommerfeld
equation (6) for the local velocity profile assuming temporally
negatively excited, stationary disturbances. In fact, he finds
that modes of the measured wavelength are the most strongly
negatively excited for all STATIONARY disturbances. Also the form
of the calculated velocity modulation for this disturbance is
quite a good representation of those measured.

     However, he himself critically notes that the disturbances are
already so great that the linear stability theory is no longer
valid and that the choice of the locally most negatively excited
wave is somewhat arbitrary, since it is possible that other
disturbances with that travelling length could have undergone a
stronger integral continuous excitation. It is therefore   /25
planned and necessary to calculate the integral continuous
excitation of the stationary modes.

Measurements of the nonstationary velocity in field (δ, λ) show that frequencies below 200 Hz are continuously excited. Stability measurements show that, in addition to the stationary waves, travelling waves with frequencies of this order are continuously excited as well.

The continuous disturbances show very great amplitudes. They can effectively surpass a level of 15% of the external velocity. Yet the effective levels in field (δ, λ) are also modulated by double the wavelength of the stationary modes. Thus there is a strong interaction between both disturbances. The travelling disturbances, whose amplitude approximates the amplitude of the stationary ones, are superimposed on the stationary mode, while the travelling wave's amplitude is closely dependent on that of the stationary one.

Saric studies a three-dimensional boundary layer on a swept plate in a closed tunnel. A pressure gradient roughly corresponding to that of an airfoil is imposed by a camber of the tunnel wall lying opposite the plate (Fig. 2.7).

In the first part of the plate, great acceleration exists, and a strong cross flow accompanied by cross flow instabilities are anticipated. With increasing run length, the acceleration decreases and Tollmien-Schlichting waves of the main flow profile may be continuously excited. Also using the sublimation method, however, Saric observed stationary disturbances whose wavelength was independent of the run length and velocity (10 and 14 m/s). Hot wire measurements at various positions x/c and at varying distances from the wall showed a span velocity modulation of half the wavelength. Reed [32] interpreted this discrepancy as follows. First, in accordance with the linear theory, stationary modes of the observed wavelength are continuously excited, which then enter into interaction with likewise stationary modes of half the wavelength, with the latter undergoing strong continuous excitation.

In summary, it can be stated that within certain bounds, it is possible to correctly calculate the stationary modes observed in the experiments and their wavelength by using the linear stability theory. The theory says, however, that stationary waves do not always undergo the greatest local or integral continuous excitation, but that travelling waves are also continuously excited. The latter are also observed in the experiments, but the observed and the calculated frequencies still have not been systematically compared. In particular, the question arises of whether the stationary modes play a more important role in the experiment than the travelling ones. It also has not been experimentally tested whether and how the two disturbance modes interact.

2.3 KNOWLEDGE OF LAMINAR-TURBULENT TRANSITION

The linear theory of stability cannot describe the transition to turbulence, due to its requirements. From numerous experiments (Klebanoff et al. [19]; Kachanov et al. [18]; Saric et al. [34]; Nishioka [24]; Kovasznay et al. [20]), however, the processes at work in a flat boundary layer up to transition are better understood. Herbert [16] was able to interpret these processes as an instability in the disturbed main flow against three-dimensional disturbances (secondary instability) through the use of linear disturbance differential equations. This theory can describe a few other phases of increasing instability in the case of two-dimensional boundary layers for experiments under strictly controlled conditions.

For determining the site of transition in wind tunnel experiments, the e^n method was developed. It relies on the results of the linear theory of stability on the one hand, yet on the other, while disregarding the complicated processes in the transition area, includes the surpassing of a critical threshold of excitation as an experimental criterion for transition.

There are still no more precise studies dealing with the processes which take place in three-dimensional boundary layers from becoming unstable to transition. In the first instance, one can associate the observations with three different phenomena:

A DISTURBANCES IN THE STAGNATION AREA

It is possible that disturbances along the leading edge spread and lead to turbulence in the stagnation area (Poll [28]). If relaminarization does not occur in the area immediately behind the stagnation line, an area of strong acceleration, this causes turbulence in the entire boundary layer.

A characteristic Reynolds number for this flow is

$$Re = V_e\, \eta/\nu$$

V_e : velocity parallel to the leading edge, at the edge of the boundary layer

η = the measure of length $\eta = \sqrt{\dfrac{\nu}{dU_e/dx\,|_{x=0}}}$

with the velocity gradient dU_e/dx perpendicular to the leading edge given $x = 0$.

This number was indicated by Pfenninger [27], Cumpsty and Head [10], and Poll [28].

For $R \leq 250$

the boundary layer remains laminar, even with the introduction of artificial disturbances (such as the boundary layer of a lateral wall or something similar) (Poll [28]).

B TOLLMIEN-SCHLICHTING WAVES

In the case of delayed flow, the main flow profile can become unstable against Tollmien-Schlichting waves before another projection profile has reached its critical Reynolds number (Bieler [5]). In this case, according to Arnal, the flow can be viewed as two-dimensional. A wonderful method of separating this instability from the cross flow instability is provided by Coustols [9]; see also Arnal et al. [2].

C CHARACTERISTIC INSTABILITY OF THE THREE-DIMENSIONAL BOUNDARY LAYER

The characteristic instability of the three-dimensional boundary layer appears not when the main flow profile, but rather projection profiles in other directions   first become unstable. As was already mentioned, both standing cross flow vortices as well as continuous waves can be excited. Exactly which physical mechanisms lead to transition in these cases is still unknown to a large extent.

It is conceivable that the stationary cross flow vortices play a decisive role. Studies of transition on concave walls have shown that, between the Taylor-Görtler vortices, unstable velocity profiles occur which lead to a secondary instability (Bippes [6]). Similarly, the cross flow vortices could deform the velocity profile and thus lead to turbulence. On the other hand, one knows from calculations of stability that, together with stationary waves, travelling waves are excited as well. In point of fact, it is not the standing ones that exhibit the lowest critical Reynolds number. Computations by Malik and Poll [23] show that, for the infinitely long swept cylinder, travelling waves experience the greatest total excitation if one integrates over the run length. It is thus possible that travelling waves play the decisive role.

Just as was the case with a flat flow, attempts have been made to calculate the site of transition using an e^n method. However, such calculations are markedly more difficult than in the case of two-dimensional ones, because in addition to frequency and wavelength of the disturbance, one also has the direction of propagation as a free parameter. In addition, it is not certain whether the generalized Orr-Sommerfeld equation provides the proper excitations. Calculations by Reed [32] show that the excitation of travelling waves in the presence of cross flow vortices can increase greatly. The effects of curvature, as calculations by Poll and Malik showed, can also have a great effect on excitation.

Coustols [9] developed an empirical criterion to determine transition. He summarized a few of the more recent transition experiments (among them, Poll [28], Boltz, Kenyon & Allen [7], and

the DERAT's experiments) and he correlated the cross flow Reynolds number χ at the site of transition with the shape factor H_{12} of the main flow profile at the same site:

$$\chi = 300/\pi \; arctan \; [0.106/(H_{12}-2.3)^{2.052}] \; .$$

Since only four different experiments were available to him, further data on the examination of the suggested criterion for transition are needed.

2.4 GOAL OF THE PRESENT WORK

It is the goal of the present work to conduct experimental studies in three-dimensional boundary layers which will contribute to a better understanding of the instatilities and the subsequent laminar-turbulent transition. In addition to the stationary cross flow instabilities observed in prior experiments, investigations are to be carried out to determine whether travelling waves are excited and how both of these disturbances interact with one another.

Another goal is to examine the theoretical results of the generalized Orr-Sommerfeld equation given the experimental findings. In order to make a direct comparison of theory and experiment possible, it is necessary to come as close as possible to meeting the requirements set forth in Section 2.1. The curvature of the wall in particular can have a decisive /30 influence. For this reason a model consisting of a swept plate with an impressed pressure gradient was chosen, just as Hirschel and Dallman suggested in 1974 for stability studies. The pressure gradient is applied by means of a pressure-inducing displacement body.

Further advantages of this model are:

—   The lack of an express stagnation area so that no disturbances coming from that area influence the boundary layer,

—   Mechanical simplifications,

—   The possibility of variation of pressure by means of changing the displacement body or its position with regard to the position of the plate.

Saric used a similar configuration for his studies. Whereas he selected his pressure progression in such a way that at first cross flow instabilities and then Tollmien-Schlichting waves of the main flow profile are caused in order to study their interchangeability, in this instance a negative pressure gradient was to be produced across the whole plate just to preserve cross flow instabilities.

The first partial assignment of this work is the development of such a model for the 1-meter wind tunnel of the DFVLR in

21

Göttingen. It is shown in Section 3.2. The dependence of the site of transition upon the Reynolds number as well as the change in the wavelength of stationary modes and the frequency of travelling waves is studied in the described model. After a description of the construction, methods of measurement, and preliminary tests, the results are described in Section 3.6.

In experiments to date on swept airfoils, only the traces of the stationary disturbances were made visible on the surface of the model (sublimation method, petroleum painting method). A second aspect of this work involves studying the origin of disturbances by rendering flows visible in the boundary layer. In this way it is possible to observe stationary and travelling waves and to gain some insight into their interaction. A circular /31 cylinder with a semispherical head was available for use as a model. The hydrogen bubble method in the model water tunnel served to make the phenomena visible. The first visible appearance of disturbances and the transition to turbulence in dependence from the Reynolds number and sweep angle were investigated. The experimental design and methods of measurement are described in Sections 4.1 and 4.2; Section 4.3 presents the results.

3. EXPERIMENTS ON THE SWEPT PLATE

3.1 EXPERIMENTAL FACILITIES

3.1.1 THE 1-METER WIND TUNNEL

A 1-meter wind tunnel with a 1.3 m long open working section and a closed gust return (Fig. 3.1) was used for experiments on the basic model. While measuring, a 1.0-m x 0.7-m rectangular nozzle with a contraction ration of 1:3.5 was used. The velocity can be regulated continuously from 0.7 to 45 m/s. Approximately 5 m before the end of the nozzle in the calming section there is a honeycomb and 3 screens with a 4.6 to 5 mm and 2.4- to 2.8-mm mesh of 1- and 0.5-mm thick wire. For all attained velocities, the amount of turbulence in the open working section is less than 0.1%. The development of a model consisting of a plate and a pressure-imposing displacement body is described in Section 3.2.

3.1.2 THE CIRCULATING WATER TUNNEL

In order to construct a suitable displacement body, it was necessary to make the flow around the model visible. These experiments were conducted in the small circulating water tunnel, for which the hydrogen bubble technique (cf. Section 4) provided a good visualization method. Fig. 3.2 shows a sketch of the /32 tunnel. The measuring section, which was passed through horizontally, has a cross-section measuring 0.25 m x 0.33 m and a length of 1.25 m, and it is open at the top. The mechanical return is trained toward a round diffusor. At a contraction ratio of 1:3.4, the jet creates the transition from the round mechanical

return to the rectangular cross-section in the measuring section.
This velocity can be controlled without any steps to a maximum of
5 m/s.

3.2 CONSTRUCTION OF THE MODEL

The goal is to create a three-dimensional boundary layer which
becomes unstable and finally turbulent on a flat swept plate by
imposing a pressure gradient. This boundary layer comes very
close to the requirements of theory, as mentioned above in Section
2.4. The development of such a model encompasses two tasks:

-   Choice of a "suitable" pressure gradient,

-   Development of a displacement body which creates the desired
    pressure progression.

The intention is to create a pressure progression resembling
that on a swept airfoil. The area of great acceleration on the
profile is of particular importance here. That is where the
boundary layer is very stable in two-dimensional cases, whereas
with swept airfoils, turbulence can occur even there.

Several preliminary tests conducted in the 1-meter wind tunnel
on a NACA-0010 airfoil provide an impressive example of this. A
15° angle of incidence $\propto$ was chosen to obtain a long stretched-out
area with a negative pressure gradient. The transition line was
made visible by the sublimation method. Fig. 3.3 shows such a
sublimation image for a 48° sweep angle ϕ_0 and a Reynolds number
of Re = 1.5 $\cdot$ 10^6 with the associated pressure progression.
Transition, visible at the separation of the white area from the
dark, occurs already at x/c = 0.28. In the laminar area in front
of the transition a marked striated structure formation is   /33
noticeable. In this area, the projection profile in the direction
of the main flow is still stable. The striated structure
formation can be explained by a continuously excited, stationary
instability of a projection profile in a direction close to the
normal one of the streamline at the edge of the boundary layer.
It can therefore be supposed that the transition is influenced by
cross flow instability. Since the main subject of this paper is
the clarification of this question, a displacement body must be
designed which imposes a pressure progression on the plate like it
does on a 15° NACA-0010 set airfoil.

Since no inverse methods of calculation were available which
could be used to figure a displacement body from a pressure
progression, this body was developed and optimized experimentally.
A 1:3 scaled-down first model was built for the small circulating
water tunnel. In this tunnel, it is very easy to make the flow
around the model visible by using the hydrogen bubble technique
(cf. Section 4.2). By means of pulsed current on the bubble wire,
so-called time lines are obtained at regular time intervals.
Their spatial distances provide a measure of the velocity
distribution in the direction of flow. The acceleration and the
pressure gradient can be derived from them. The displacement body

was varied until it created the desired velocity progression on the plate. At the same time, while the model was being developed, care was taken that no nonstationary separation areas were created. As the observation of flow has shown, they can react on the flow and thereby on the boundary layer. Fig. 3.4 shows a cross-section of the final model. The slat prevents the formation of a large separation area close to the nose of the displacement body. The side of the displacement body facing the plate is very curved at first with a gradual transition to a flat plane. This form sesults in a weaker pressure gradient than the NACA-0010 wing has. A greater drop in pressure requires a considerably greater curvature of the displacement body, because the pressure gradient affecting the displacement body normally decreases toward its surface, i.e. toward the plate as well. However, the flow no longer follows such a curve; a separation bubble forms on the /34 side of the displacement body facing the plate, which should be avoided for the above named reasons. As will be shown later, however, the pressure gradient is sufficient to bring the boundary layer on the plate to transition. The final design (Fig. 3.4) was built for the 1-meter wind tunnel in a 3:1 enlargement.

Another important task was the simulation of a quasi-two-dimensional flow, i.e. a flow which is independent of the span coordinate y. Initial experiments with the plate and displacement body showed that deflectors are necessary for reaching this goal. For an exact directing of the flow by the walls, they would have to be formed under quasi-two-dimensional conditions following the three-dimensional warped plane of flow between the plate and displacement body. This plane of flow is only obtainable from a calculation of the entire velocity field. It is a simpler solution to form the lateral plates with only two dimensions following the streamline at the edge of the plate boundary layer. This streamline can be easily calculated from the measured pressure progression under the assumption that
$V = V_\infty$ = const (condition for an infinitely long swept wing):

$$y = x_0 + V_e/U_\infty \cdot \int (\sqrt{1-cp(x)})^{-1} \, dx \ .$$

With built-on lateral plates, the pressure progression demonstrated a slight change from the measurement without deflectors. The streamlines calculated for both pressure distributions, however, differ only very little (Fig. 3.5); their differences are, in particular, only near the leading edge of the plate. But that is precisely where the three-dimensional warp of the flow plane is especially great, since the streamline near the plate is greatly distorted by the strong pressure gradient in the stagnation zone, whereas just a little above the plate the effect of the stagnation area diminishes. Therefore, it is not a good idea to simulate the strong curvature of the streamline near the plate by means of the deflectors. As will be shown below in Section 3.5.4, measurements of velocity at the edge of the boundary layer showed that these deflectors provide a good simulation of a quasi-two-dimensional flow, and this justifies the simplified form.

3.3.1 GENERAL DESIGN

Fig. 3.6 shows the final design of the experiment in the 1-meter wind tunnel. The leading edge of the plate is at a 45° sweep angle to the displacement body fastened above it. The windward sides are attached outside the free jet, whereas the downwind sides end at the collecting cone due to the short length of the speed course. The two deflectors S are formed below the zero friction streamline at the edge of the plate boundary layer. The plate is outfitted with a series of pressure piercings P and a sweep mechanism V. The individual parts of the model are described in more detail below.

3.3.2 THE PLATE

The plate, made of double-glued plywood, is 2.30 m long, 0.5 m deep, and 30 mm thick. The surface was carefully primed, sprayed black, and wet sanded to produce a very smooth surface. The leading edge of the plate has the nose profile of a Clark-y airfoil. This profile was chosen to keep the suction point small and to insure that the stagnation line lies on the side of the plate being tested.

The plate has 22 pressure piercings placed on a cut at a 40° angle to the leading edge. A small steel pipe with an internal diameter of 0.7 mm and an external diameter of 1 mm is inserted into the plate for each pressure piercing before the final finishing of the surface. Any roughness brought about in the process is also primed and sanded.

A sweep mechanism is built into the plate (Fig. 3.7) for measurements using hot wire and hot film. It consists of two eccentric disks that can turn against each other, supported in bearings, in an outer ring that is tightly fastened to the plate. The inner disk can take up two different cylinders, which are in turn supported by bearings allowing them to turn. The cylinders serve as a mounting for a hot wire or hot film. By turning the disks, any point within two concentric circles whose radius ranges from 30 mm to 66 mm (smallest possible and greatest possible distance from anemometer and center of the larger disk) can be reached. An additional disk with a sweep mechanism can be attached inside the plate. It moves the anemometer mounting on a straight line, whose angle to the leading edge can be set in 5° steps by the swing angle of the disk. This makes it possible to move the anemometer along parallel paths to the leading edge at distances of 27 cm and 33 cm, and to move it on paths perpendicularly or at various angles to the leading edge. A sweep mechanism such as this was chosen in order to be able to measure the stationary disturbances with a hot film. Only very small variation of the average wall shearing stress is to be expected, and since it is very difficult to calibrate hot films, measuring the stationary cross flow instabilities with several fixed hot films would not be possible.

In constructing and installing the sweep mechanism, extreme care was taken to avoid surface flaws. The outer fixed ring was placed in the plywood plate and finished so well with a fine filler that no measurable flaws were caused. The surface flaws between the rotating disks supported by bearings were smaller than 0.02 mm for all positions. Subsequent tests making the flow visible showed that these flaws had no influence on the site of transition.

3.3.3 THE DISPLACEMENT BODY

The development of the displacement body was described in Section 3.1 and a cross-section was shown by means of the model (Fig. 3.3). Precise data concerning the profile are presented in the appendix. During the experiments, the boundary layer was rendered turbulent by the attachment of artificial roughness to the side of the displacement body turned toward the plate in order to avoid separation at the curvature.

3.3.4 THE LATERAL PLATES

The lateral plates were shaped following the calculated streamline at the edge of the plate boundary layer. They are made of 2-mm sheet aluminum, attached to streamline-shaped struts and fixed between the displacement body and the plate. The deflector, which is situated windward, was extended in front of the model, since it was necessary to guide the flow in front of the model as well. Both lateral plates, the extended windward one, as well as the one downwind, were struck tangentially by the flow.

3.4 METHODS OF MEASUREMENT

3.4.1 MEASUREMENTS OF PRESSURE

The static pressures were measured by a pressure pickup whose initial signal was averaged using a digital voltmeter for over 20 s. The data were stored on punch cards and evaluated on the IBM computer. The pre-chamber pressure of the 1-meter wind tunnel was measured using a Betz manometer to a tolerance of 0.5%.

3.4.2 MEASURING VELOCITY WITH A FIVE-HOLE ANEMOMETER

In order to measure the amount and direction of velocity, a five-hole anemometer with a very small head (1.5 mm in diameter) was used. Pressures were measured by means of pressure pickups, and they were fed into a data acquisition subsystem (see Fig. 3.8). The anemometer and the acquisition system were described in Landhäußer [21]. The inaccuracy of the velocity measurements is 5% at most; that in determination of the angle, 1.2°.

SUBLIMATION METHOD

By means of the sublimation method, various shearing stresses
of the walls can be made visible on the surface of the model with
the aid of sublimating crystals. In the present experiments,
naphthalene was dissolved in acetone and sprayed in thin layers on
the plate. The acetone evaporates very quickly and leaves behind
a thin layer of crystals. Between sprayings, thicker crystals are
carefully removed with a soft brush. After repeating this process
three times, a dense white layer of crystals covers the white
lacquered model. If one exposes this plate to the flow, the
naphthalene sublimates completely on those places first in which a
higher shearing stress of the wall, and thus, a higher temperature
prevails: near the leading edge, where, as a result of the thin
boundary layer, high shearing stresses occur and in that area in
which the shearing stress increases as a result of the turbulence.
Depending upon the surrounding temperature, after 10-30 minutes of
wind a picture emerges with a line of demarcation between the
naphthalene which was left behind in the laminar area and the
sublimated naphthalene in the area of turbulence. Thus, a simple
method exists for determining the course of the transition line.
The cross flow instabilities also show up in the sublimation
picture.

PETROLEUM PAINTING

To make the wall streamlines and the traces of the stationary
cross flow vortices visible, the petroleum painting method was
used. A suspension of petroleum and very fine colored pigments is
sprayed on the plate, which is then exposed to the flow. After
the petroleum has evaporated, the wall streamlines can be
discerned in the residue of colored pigments.

3.4.4 HOT WIRE AND HOT FILM MEASUREMENTS

Three anemometers were used for hot wire and hot film
measurements, see Fig. 3.9. With a surface hot film anemometer
(3), changes in the wall shearing stress were measured. The
anemometer consists of a small cylindrical quartz body, on the /39
face of which the hot film, a 0.2 mm wide and 0.75 mm long nickel
layer, is steamed on. The film is covered by a 0.5 micron thick
protective layer made of quartz.

The hot wire angle anemometer (1) is used to measure the
nonstationary velocity in the boundary layer. The hot wire, with
a diameter of 5 microns, is 1 mm long.

Both anemometers were swept parallel to the leading edge with
the help of the sweep mechanism (Fig. 3.7). For each of the
anemometers, a mounting cylinder was built and installed in the
smaller disk of the sweep mechanism, ending flush with it.

An additional hot wire anemometer (2) was also used for measurement in the boundary layer. The hot wire was 1 mm long and 5 microns in diameter. The anemometer mounting can be attached to the plate at any desired point. The anemometer wire is 0.25 mm from the surface. To allow measuring standing waves with this hot wire anemometer, the mounting of the hot wire was fastened to the large disk of the sweep mechanism and directed along the local streamline. By turning the disk, the hot wire moves in an arc with a radius of r = 156 mm. Measurements were made up to angles of ± 7.5° so that the arc only deviates from a straight line perpendicular to the local streamline by ± 0.7 mm (Fig. 3.10). The movement of the hot wire can thus be described in the streamline oriented coordinate system as movement along the y_t axis with constant x_t. In the body system, x changes by ± 2 cm. Due to the rotation of the hot wire and the variable distance from the leading edge, errors in the measurement of the average velocity occur. However, since only the wavelength was determined, these deviations are insignificant.

All three anemometers were run by a Disa constant temperature bridge. The superheating relationships were 1.7 for hot film and hot wire (2), and 1.5 for hot wire (1). Since the variation of the averaged output signals is very small when there is sweeping along the y coordinate, amplification is necessary. To accomplish this, the output signal of the bridge E and a fixed discretionary voltage K were put on a differential amplifier and amplified 20 times. The amplified signal E_s was directly obsevable on the oscillograph. With an integrating digital voltmeter, the mean values were registered (averaging interval 20 s). A quantitative analysis of the variations in velocity is possible using an FFT-analyzer, which carries out a frequency analysis of the time signal. Temporal disturbances containing large numbers of low frequencies were observed. For this reason, at no point while making or using measurements was a high-pass filtering undertaken, which could have distorted the signal. Fig. 3.11 shows a block diagram of the entire apparatus.

3.5 PRELIMINARY MEASUREMENTS AND CALCULATIONS

3.5.1 METHODS OF CALCULATION

Along with the experiments, boundary layer and stability investigations were conducted at Bieler's theoretical institute. The velocity at the edge of the boundary layer was calculated from the measured pressure progression. Under the assumption of an infinitely long swept model, it holds that:

$$V_e = V_\infty = Q_\infty \sin \phi_0$$

$$U_e = \sqrt{1-c_p} \cdot U_\infty =$$

$$= \sqrt{1-c_p} \cdot Q \cos\phi_0.$$

As will be shown in Section 3.5.4, these calculated velocities describe the experiment within defined boundaries quite well. To

which are marked in the photo. Next to these there are areas in which the flow remains laminar for a longer time.

To render this qualitative overview complete, the velocity vector on the edge of the boundary layer was measured using a five-hole anemometer to determine the quantitative deviations of the assumed quasi-two-dimensional flow. The measurements were carried out at a velocity of Q_∞ = 25 m/s. A sketch of the experimental design is presented in Fig. 3.17. The anemometer was set against the leading edge at a 45° angle so that the angle of flow lies within the anemometer's calibration range. For anemometer head distances from the leading edge less than x = 35 cm, the anemometer was extended by means of a tubular mount. Fig. 3.18 shows the measurements of the velocity along parallels to the leading edge at the following distances:

    x = 20 cm
    x = 28 cm
    x = 40 cm .

The coordinate origins of the three parallels are swept <u>/43</u> against one another in the direction of the wing span in such a way that the points of crossing of a flow line with the parallels in the picture lie across each other in a perpendicular arrangement. At x = 20 cm and x = 28 cm, the velocity components show a slight change with the direction of wingspan. If the margins of the field of flow, in which deviations of 4% occur, are removed, the deviations for the area (y = 10-40 cm and at x = 20 cm) are under 2% and thus within the anemometer's tolerance limits. For x = 40 cm, particularly in the right portion of the surveyed area, greater deviations occur (maximally 4% for y = -12 cm).

The results can be compared with computations obtained from the measured distribution of pressure and the sweep angle ϕ_0 assuming an infinitely swept wing (V = const). For V_e/Q_∞ and U_e/Q_∞, it holds that:

$$V_e/Q_\infty \equiv V_\infty/Q_\infty = \sin \phi_0$$

$$U_e/Q_\infty \equiv \sqrt{1-cp} \cdot \cos \phi_0 .$$

It became apparent that the results of the measurements agreed with those of the calculation to a great degree if one takes as sweep angle not the geometrical 45° sweep angle, but rather an effective sweep angle of ϕ_0 = 46.6°, an angle which might arise from the great displacement of the free jet in the wind tunnel because of the model. Thus, for the velocities, the results are:

$V_{\infty}/Q_{\infty} = 0.727$

$U_e /Q_{\infty}(x/c = 0.40) = 0.541$

$U_e /Q_{\infty}(x/c = 0.56) = 0.617$

$U_e /Q_{\infty}(x/c = 0.80) = 0.712$.

These values are drawn in as straight lines in Fig. 3.18. Fig. 3.19 shows the velocity U_{te} and the angle of the velocity vector Q_e to the axis of the tunnel in comparison with the quantities computed from the pressure progression. Except for areas of the near trailing edge, deviations are under 2%. The angle of flow at x < 40 cm deviates from the calculated flow by less than 1°.

To summarize, it may be concluded:

Making the flow visible and quantitative measurements show that the flow in a "central area" agrees in velocity at 2% and in the direction of the streamlines from the pressure progression at 1%. The flow can best be described assuming an effective sweep angle of 46.6°. In this way it is shown that the calculated values of the main flow can be related as reference quantities in comparison with the theory within the range of deviations from Figs. 3.18 and 3.19.

3.5.5 STABILITY AGAINST DISTURBANCES IN THE STAGNATION AREA

In studying transition due to cross flow instability, it is important that disturbances do not occur in the area of the stagnation line and become excited ("leading edge contamination").

Poll's results show that for a Reynolds number R in the stagnation line boundary layer of

$R \leq 250$

strong disturbances are baffled and thus cannot lead to turbulence (see Section 2.3). For a maximal flow velocity of $Q_{\infty} = 45$ m/s and with

$$\frac{\partial U_e/U_{\infty}}{\partial x/c} \cdot \frac{U_{\infty}}{c} \approx 30 \cdot \frac{U_{\infty}}{c}$$

from the measured pressure progression, a maximum Reynolds number of the contact line of

$R = 192$

results for the present experiment so that in the vicinity of the leading edge no disturbances are excited. Hot film measurements at a distance of 5 cm from the leading edge confirm that Poll's results can be used in this case as well.

3.6 RESULTS AND DISCUSSION

3.6.1 TRANSITION

In defining a transition site in a three-dimensional boundary layer, two problems must be considered. For one thing, just as with two-dimensional boundary layers, the transition comprises a certain length of run length x. For another, the transition line, which is shown in sublimation images, is sharply zig-zagged (Fig. 3.16). In this case, the transition line was indicated as a middle line between those zig-zags.

For comparison, for a few of the experiments, Preston tube measurements were also carried out along the depth of the plate. The Preston tube also addresses the changes in wall shearing stress. Fig. 3.20 shows the progression of the Preston pressure across the depth of the plate. With the aid of this curve it is possible to measure the beginning and end of transition. The comparison with the sublimation pictures shows that the latter indicate a central site x between the beginning and end of transition. This site x is defined as the transition site in the following.

Between the laminar and turbulent area of the petroleum painting there are likewise characteristic differences, and these can be used in the determination of transition.

- In similar fashion to the sublimation picture, the rate of evaporation depends upon the wall shearing stress. As the image develops, a clear demarcation line is recognazable between the area which is still wet (small wall shearing stress, laminar) and the area which is already dry (great wall shearing stress, turbulent).

- In the turbulent area the drawing of the picture is   /46 markedly finer.

- Small disturbances can produce turbulent wedges in a laminar surrounding; in a turbulent area they leave only narrow bands behind them (Fig. 3.21). However, disturbances can sometimes cause mere "bands" in a laminar, very stable flow. Therefore the conclusion that the surroundings are laminar should be drawn only from turbulent wedges and not the other way around from missing wedges to turbulent bands.

- In the transition area, the wall shearing stress increases markedly, and accordingly, few particles of pigment remain there. In the dried petroleum painting picture this transition area is recognizable as a narrow dark band (see Fig. 3.22).

When they are looked at carefully, the pictures obtained from the petroleum painting process provide the same site of transition as the sublimation images. Since the petroleum painting method is

32

easier to manage and poses less of a health hazard, it was used in addition to the naphthalene method.

The results of the measurements for various Reynolds numbers are summarized in Fig. 3.23.

Hot film measurements with anemometer 2 provide additional information about the condition of the boundary layer. The anemometer was attached at the following distances from the leading edge:

    x/c = 0.36
    x/c = 0.52
    x/c = 0.62
    x/c = 0.75
    x/c = 0.85.

At increasing velocity, observations were made when spots occur or when the initial signal is completely turbulent. The occurence of the first spots is labeled S in the picture; a completely turbulent signal is labeled T.

In addition to the experimentally determined line of transition, the site of transition was determined according to the Coustols criterion (see Section 2.3) /47

$$x = f(H_{12})$$

and entered into the picture. The criterion's prediction and the experiment are in very close agreement. Thus it is proven that the criterion, which was developed for various experiments on airfoils, can predict the site of transition on the plate very well.

3.6.2 STANDING WAVES

In petroleum painting pictures and naphthalene pictures, the traces of stationary disturbances become visible. The cross flow instability produces a variation of the average velocity in amount and direction as wide as the wingspan, and thus a variation of the wall shearing stress. In petroleum painting pictures, the modulation of amount and direction of wall shearing stress works itself out. In the laminar area before transition, a strong formation of band structures is evident, as was shown in Fig. 3.15. Following the flow downwind from the leading edge, undisturbed laminar flow is observed at first. In a few places, individual "bands" occur that change to uniform striated structures after some distance and disappear again in the turbulent area. The striated structures run more or less in the same direction as the streamline at the edge of the boundary layer. If isolated "bands" are observed very far forward in the area of pronounced curvature of the streamline, they are also greatly curved. This method of rendering the flow visible amounts to a simple and rapid aid to studying cross flow instability. Wavelength and direction of the striated structures can be

measured in the picture. The site at which isolated bands could be seen was identified as site x_i/c, the site of the first excitation.

The flow on the plate was made visible at various Reynolds numbers. To determine the wavelength, averages were taken at several places on the plate across a few bands in each case. The wavelengths determined in this way do not depend upon their   /48 distance from the leading edge as far as the accuracy of their measurement is concerned. A unification of individual "bands" or the disappearance of "bands," and thus a variation of wavelength, as Arnal [3] describes it, was not observed.

The results of the wavelength measurements are compiled in Fig. 3.24. For various experiments with one Reynolds number and also within one picture, wavelength changes of up to 17% were shown. The error lines shown in the illustration cover the range of these changes.

In naphthalene pictures, a striated formation in the laminar area was shown before transition too. Just as in the case of making transition visible, the wingspan-wide change of the wall shearing stress becomes clear in the sublimation picture due to varying degrees of sublimation of the crystals. The wavelengths measured in these pictures are also registered in Fig. 3.24. They agree with the results from the petroleum painting pictures.

Measurements by Saric have shown that it is possible for other wavelengths to occur in the boundary layer besides those observed on the wall. In addition, no experiments are known which directly measure the variations of wall shearing stress. For this reason, the wavelength measurements in the sublimation and painting pictures were supplemented by measurements of the wall shearing stress using a mobile surface hot film at $x/c = 0.66$ and by measurement in the boundary layer at $x/c = 0.40$ and $x/c = 0.66$ with two mobile hot wire anemometers.

The sweep mechanism for the hot film and for both hot wire anemometers was described in Sections 3.3.2 and 3.4.4.

The variation of the average velocity is shown in Fig. 3.26 a-h.

Table 3.1 summarizes the results.

Measurement Number	Anemometer	Re 10^{-5}	x/c	y/δ	χ''	λ
a	2	6.67	0.40	0.11	–	–
b	2	8.08	0.40	0.12	–	8.0
c	2	9.69	0.40	0.13	–	6.3
d	2	10.10	0.40	0.13	–	6.8
e	3	5.65	0.66	–	18.7	12.8
f	3	6.61	0.66	–	16	10.7
g	1	6.61	0.66	0.36	16	10.7
h	1	7.44	0.66	0.39	16	10.7

TABLE 3.1

Measurements a-d were carried out in the streamline oriented coordinate system. The measurements are corrected for temperature, for the alteration of the average velocity due to the hot wire rotation, and for the change in distance x from the leading edge. The wavelengths from measurements b to d are entered in Fig. 3.24 as circles.

The measurements of wavelength (λ'') in the series of measurements e-h were carried out in a body coordinate system. Measurements were not carried out perpendicular to the stationary waves. With the local sweep angle of the striated structures, known through the painted pictures, it is possible to convert to. The values are characterized by the squares in Fig. 3.24. The wavelengths measured by means of the anemometers are in agreement with those determined in the process of making the flow visible; contrary to Saric [37], no wavelengths in the ratio 1:2 are found in the boundary layer or on the surface of the model.

In Fig. 3.25, the measured wavelengths with the calculated boundary layer thickness δ at x = x_i are normed. The site x_i, that is the smallest distance from the leading edge at which band formation could be observed, was determined from the petroleum painting pictures. Within the context of accuracy of measurement, the ratio is constant:

λ/δ_i = 4.1 .

The angle $\phi_{QI}(x)$ of the cross flow instability to the <u>/50</u> x axis was measured with an accuracy of ± 1° for three different Reynolds numbers. The results are presented in Tab. 3.2. For all measured Reynolds numbers and distances of x, $\phi_{QI}(x)$ is about 4° less than the local sweep angle of the streamline.

Re 10^{-5}	x/c	$\phi_{QI}(x)$	$\phi(x)$	$\Delta\phi$
6.6	0.36	50°	54.5°	4.5°
7.8	0.55	47°	49.8°	2.8°
9.62	0.47	47.5°	51.5°	4°
9.62	0.32	51°	55.6°	4.6°

TABLE 3.2

COMPARISON WITH THEORY

Calculations of the boundary layers' stability were carried out by Bieler [5] at the theoretical institute. He computed the Orr-Sommerfeld equation using different Reynolds numbers and different sites x/c in the flow field for several projection profiles in turn. Stationary disturbances with $\omega_r = 0$ are possible for several projection directions ψ lying close together from 85° to 87°. The wavelengths of these modes vary with the projection angle. Their excitation differs only very little from a wavelength band having a width of about 10% of the average, most excited wave. Thus, stationary modes whose wavelengths differ from each other by about 10% undergo practically the same excitation. This corresponds to the experimental observations.

For further comparison with the experiment, the wavelengths of the stationary modes for the combinations of Reynolds numbers and site x_i of the first observation were considered. In Fig. 3.24 the wavelengths of the disturbance with the greatest excitation are paired with the experimental values. The theory is very well able to give the course of change in wavelengths with the Reynolds number; however, the calculated wavelength lies below the experimental values by about 1 mm for all Reynolds numbers. This comes as no surprise inasmuch as the experimentally observed disturbances underwent the strongest integral excitation and /51 not the strongest local excitation. For a more accurate comparison, the local excitation of the stationary disturbances would have to be integrated over the run length x.

For all Reynolds numbers, the stationary disturbance with the greatest excitation occurs at a projection angle ψ of 85° to 87°. The wave fronts (band structures) have an angle of (90° − ψ), that is, 2° to 4° from the local streamline. Within the interpretation accuracy of a painting image, this amounts to experimental angle measurements of 4° on the average.

In summary:
The theory is able to explain why the wavelengths of the standing disturbances in the experiment vary by about 17%. The course of the wavelength with the Reynolds number is also described quite well. However, predictions of the wavelengths are a little too small. The directions of the excited standing waves are well described within the limits of the accuracy of measurement.

3.6.3 TRAVELLING WAVES

In addition to the standing waves, travelling waves were also found in the boundary layer. To investigate these waves, the hot wire anemometer (2) was fixed at six different positions x/c in the flow field: x/c = 0.1; 0.36; 0.52; 0.62; 0.75; and 0.85. The signal was observed on the oscillograph for increasing incoming

flow velocity. With the exception of x/c = 0.1, strong periodic variations in velocity were found at all positions, even in the areas in which the stationary waves were observed. Fig. 3.27 shows some examples. For systematic study, spectra of the variations of velocity were calculated using an FFT-analyzer and shown on a screen.

Hot wire signals and spectra change with the velocity in the same characteristic way at all sites x/c. Fig. 3.28 shows a typical series of velocity signals and their spectra for x/c = 0.52. First the flow is undisturbed; the spectrum has only <u>/52</u> low RMS-values for frequencies below 50 Hz and has a "round shape," i.e. a slow drop in amplitude with growing frequency (Shape A in Fig. 3.28a). With increasing Reynolds number, growing amplitudes of the nearly periodic velocity variations are observed. In the respective spectrum, the effective value of the variations increases. It is striking that the spectrum has a very broad peak and not only the frequency at the peak but all lower frequencies as well are greatly excited. In contrast to the spectrum of shape A, this spectrum has a steep flank for excited disturbances, i.e. the amplitudes drop off sharply with increasing frequency (Shape B in Fig. 3.28 b-d). With further increasing Reynolds number, the amplitudes of the disturbances become greater and their frequencies shift to larger values. From a certain velocity on, the first spots appear, like the ones also observed in the transition in two-dimensional boundary layes. They contain large amounts of high frequencies. With further increases in velocity, the spots become more numerous until finally a fully turbulent flow exists, whose spectrum has the typical shallow drop (Shape T in Fig. 3.28e). A similar evolution with rising velocity has been observed at all sites x/c of the unstable area.

With increasing distance from the leading edge, a change occurs in the Reynolds number Re starting at which the strong disturbances (spectrum shape B) were observed. In Fig. 3.29, the measured spectra labeled according to their shape are entered in an x/c-Re-diagram, which also shows the experimental transition curve and the first continuous excitation of stationary waves according to the petroleum painting images. The boundary between the spectrum shapes A and B corresponds to the first occurrence of travelling waves. It can be represented very well by a curve with a constant cross flow Reynolds number

χ = 115 .

The frequencies of the peak in the spectrum are determined <u>/53</u> for different Reynolds numbers and at different sites. Since the peaks are very broad, these values are only accurate to about 10%. The peak shifts for increasing Reynolds numbers at a fixed site x/c to higher frequency (see Fig. 3.30). For growing distance at a constant Reynolds number, the frequency of the peak decreases very slightly in the example shown, as well as for other Reynolds numbers. Fig. 3.31 summarizes the results. Norming the

frequencies for x/c = 0.36, 0.52, and 0.62 with δ/Q_e, a constant value results within the limits of measurement accuracy (see Fig. 3.32).

$$F = 2 \pi (f \, \delta/Q_e) = 10.6 \cdot 10^{-2} \quad .$$

Thus, the frequencies of the most excited travelling waves are dependent only on the local velocity at the boundary layer's edge and on the thickness of the boundary layer.

COMPARISON WITH THEORY

Calculations by Bieler [5] show that the projection profile in the direction of the main flow ($\psi = 0$) and neighboring profiles ($\psi < 35°$) are stable for small disturbances. In a range of angles $90° < \psi < 35°$, on the other hand, one finds excited travelling waves in an entire frequency band. The continuous excitation of the travelling waves for different projection directions ψ was calculated for a velocity profile at x/c = 0.52 and a Reynolds number Re = $8 \cdot 10^5$. In Fig. 3.33, this non-dimensional continuous excitation is shown superimposed in double logarithms upon the frequency. In the experiment, a mixture of travelling waves whose directions can not be differentiated by the hot wire are observed. It is therefore a good idea to consider the envelope of the curves in Fig. 3.33 when comparing theory and experiment. It has, like the measured spectra, a broad peak underneath which excited waves also appear at all frequencies. The shape of the calculated spectrum along with the location of the peak closely resembles the measured spectrum from Fig. 3.28c, which was recorded at the site x/c = 0.52 with the somewhat larger Reynolds number Re = $8.5 \cdot 10^5$.

For further comparison between theory and experiment, the excited frequencies were computed for several sites x/c and different Reynolds numbers. In all these calculations, the most strongly excited non-dimensional frequency occurs at:

$$F = 2\pi \, f \cdot \sqrt{vx/U_e} \cdot Q_e \simeq 2.2 \cdot 10^{-2} \quad .$$

The experimentally determined frequency F can be transformed using the non-dimensional boundary layer thickness

$$\delta^* = \delta \cdot \sqrt{U_e/vx} \quad .$$

For x/c = 0.36, 0.52, and 0.62, δ^* is nearly constant because of the accelerated flow:

x/c	δ^*
0.36	4.68
0.52	4.60
0.62	4.57 .

With an averaged $\delta^* = 4.62$ one obtains

With an averaged $\delta^* = 4.62$ one obtains

$$F = (F/\delta^*) = 2.29 \cdot 10^{-2} \quad .$$

The calculated value of $F = 2.2 \cdot 10^{-2}$ comes very close to this value.

With an averaged $\delta^* = 0.45$ and an F_{δ} between 0.85 and 0.95 (see Fig. 3.32), a non-dimensional frequency F

$$F = 1.88 \text{ to } 2.11 \cdot 10^{-2}$$

is obtained for the sites $x/c = 0.75$ and $x/c = 0.85$. This F is not as much in line with the theory. This discrepancy can be attributed to the deviation from a quasi-two-dimensional flow in the measuring area.

Thus, the observed travelling waves can be understood in /55 their entirety, using the Orr-Sommerfeld equation, as instabilities of the different projection profiles. The frequency of the most strongly excited wave is also correctly predicted by the theory.

3.6.4 INTERACTION BETWEEN STANDING AND TRAVELLING WAVES

In the present experiment, standing and travelling waves were observed. The first excitation of travelling waves can be represented by the curve $\chi = 115$, as was mentioned. In Fig. 3.29, in addition to this curve, the first stimulation of stationary vortices as they were observed in petroleum painting pictures was entered. As described previously, the registered sites x_i/c are those where the formation of bands could be observed in isolated instances. Regular band structures could be found somewhat later. Therefore, for the present experiment, it can be concluded that stationary and travelling waves are excited by approximately the same cross flow Reynolds number. More precise statements can only be made as a result of further experiments, since both the determination of x_i/c and the determination of the boundary curve for travelling waves are still fraught with uncertainty.

With measurements of stationary waves at $x/c = 0.66$, the effective value of travelling waves in a Reynolds number range of $Re = 6.65 \cdot 10^5$ to $Re = 7.45 \cdot 10^5$ were measured simultaneously when both disturbances were excited. The variations of wall shearing stress resulting from both disturbances are of the same magnitude. That means that the difference of the averaged signals in time between the wave peaks and valleys on a stationary wave is of the same magnitude as the difference between the maximum and minimum of the time signal of a travelling wave at the same site. The same is also true of the hot wire signals from the boundary layers. In this area, both disturbances are of equal significance.

At the same time, an alternation is also evident between both disturbances. The effective value of velocity variations changes with the site y within the stationary wave. In longitudinal /56 zones of low velocity it is up to 10% greater than at sites of great velocity and great wall shearing stress. This is in keeping with the notion that in the "wave valley" of a stationary wave, due to the lower velocity and velocity gradients at the wall, a velocity profile which is on the average more unstable develops, a profile in which travelling waves are excited to a greater degree. More precise statements concerning the question whether that is a significant instability mechanism in this three-dimensional boundary layer cannot be made until more measurements are taken.

4. EXPERIMENTS IN THE MODEL WATER TUNNEL

4.1 DESIGN OF THE EXPERIMENT

4.1.1 THE MODEL WATER TUNNEL

The model water tunnel was available for experiments involving the semispherical cylinder. Such a tunnel is particularly well-suited to stability experiments since a flow which is quite free of disturbances can be achieved. The hydrogen bubble technique offers a further advantage in that a tried-and-true method of rendering things visible is made available.

The model water tunnel is presented in Fig. 4.1. Basically, it consists of a basin which is 18 m long, whose side walls and floor are made of glass for the most part. The tunnel is attached to the floor in such a way as to be insulated against vibration. The tracks upon which the car is led are set up apart from the tunnel so that the vibrations which occur thus are not transferred to the flowing medium. The tow wagon is driven by a rope tow powered by a D.C. shunt motor. As a result of the motor's revolutions, which can be regulated without intermediate steps, any speed at all between 0 and 5 m/s can be selected. The acceleration can be regulated to such a degree that after 1 m of warm-up, the desired final velocity is reached. The wagon is /57 stopped at the end of the tunnel by two pneumatic shock absorbers at a path length of 1.0 m. Thus, 16.0 meters are available for stationary towing velocity.

4.1.2 THE SEMISPHERICAL CYLINDER

An engaged (swept) circular cylinder with a semispherical head having a diameter of 0.2 m was selected as a model. It was constructed of plexiglass. The length of the model, including the semispherical head, is 900 mm. The cylinder is held at the downstream end by a short rod which as attached to a brace (Fig. 4.2). By moving the mounting on the semicircular brace the angle of incidence α can be set from +30° to -35°. This corresponds to sweep angles of 55° to 90°. The brace is held in a steel framework which is fastened to the towing wagon (Fig. 4.3) in such a way as to be insulated from vibrations. The insulation is set up so that a transfer of vibrations to the model

above 30 Hz is avoided to a great extent. In order to make the flow visible, a 375 mm long and 25-30 microns thick wire is attached to the model. Since the wire acts as a cathode, hydrogen bubbles form on it. The wire runs parallel to the cylinder's axis, and it can be soldered to two pins at various distances from the surface of the cylinder (from 0.2 to 1.0 mm). The pins jut out from the model's surface. The total angle between the wire and the stagnation line can be varied by rotating the cylinder around its axis. Thus, in the experiment, the two flow parameters, namely sweep angle ϕ_0 and inflow or towing velocity Q_∞ and the parameters of making the flow visible, namely angle of roll γ and distance of the bubble wire from surface z, can be varied.

4.2 THE HYDROGEN BUBBLE METHOD

4.2.1 PRODUCING HYDROGEN BUBBLES

As mentioned, the hydrogen bubble method was utilized to make the flow visible. An electrical current was laid between a wire anemometer as cathode and a long copper track on the bottom of the basin of the model water tunnel as anode. This current actuates electrolysis. Along the wire anemometer, hydrogen bubbles are formed, which are carried along by the flow and – within certain limits – follow the paths of the particles. If the bubbles are illuminated from appropriate angles, they can easily be observed and photographed.

In the experiment, the bubbles were produced by two means. To make a "skimming area" visible, a constant voltage was set up. Then a continuous layer of bubbles lifts off, composed of skimming lines, i.e. a combination of all particles which emanate from a site. In a stationary flow, this area is identical to a flow area. In nonstationary flows, skimming lines or areas can be interpreted only with difficulty.

To create so-called time lines, a pulsating voltage was laid on the wire. Making things visible in this way is especially appropriate when changes in the flow field of the velocity component perpendicular to the wire occur with the coordinate along the wire, for these changes show up clearly as distortion of the time line.

When considering and interpreting the snapshots of skimming areas and time lines it is important to realize that this method of making things visible is integrative. Once structures have formed, they move downstream and can therefore be observed in areas where they no longer exist.

4.2.2 ELECTRICAL POWER SUPPLY

A mains-connected unit was available to produce hydrogen bubbles. It supplies direct-current voltage which can be set between 0 V and 1,000 V with a maximum amperage of 5 A. With this

apparatus, it is possible to obtain sufficient hydrogen bubbles to provide visibility of the flow for any velocity.

To produce time lines, the current coming from the mains-connected unit is interrupted at regular time intervals. The duration of pulse and pauses can be chosen independently of each other as multiples of the period duration of a given basic frequency. This basic frequency, in turn, can be set between 10 Hz and 10^5 Hz.

A detailed description of the switching is found in Bippes [6].

4.2.3 ILLUMINATION

Photoflash lamps manufactured by the Heimann Company (DGQ 8760ZWl) were used for lighting. The flash duration is approximately 0.02 ms. The white light produced by the flash was filtered to prevent an unclear image due to color dispersion at the refraction of the water-glass-air surfaces. The filter used let through wavelengths above 510 nm, and the photographic layer, depending on the film, is only sensitive up to 600 or 670 nm, so that only light in a frequency band from 510 nm to a maximum of 670 nm contributes to blackening the film.

Further, it is important to carefully set an angle of 115° between the optical axis and the entering cone of light in order to achieve an optimal contrast and maximal blackening of the film.

4.2.4 PHOTOGRAPHY

During the experiments, both simple and stereo photographs were taken in order to be able to observe a possible three-dimensional distortion of the bubble layer in the boundary layer.

For the stereo pictures, a stereo camera made at the institute with two lenses corrected for closeness (1:8, 75 mm) was available. The distance between both the optical axes can be set between 100 and 128 mm. During the experiments, the distance was adjusted so that the stereo pictures, while providing a maximal impression of depth, were still able to be put together to a three-dimensional picture.

For the mono pictures, a Linhof camera with lenses which were likewise corrected for closeness (1:9, 150 mm) was used.

All pictures were made by using the flash with an open shutter in a darkened room. Thus, the length of exposure is determined by the flash duration of 0.02 ms so that even at the greatest velocity, the movement blur stays very small. The moment of shooting the picture is determined by the towing wagon setting off a movable flash contact. The films used were Agfa Ortho and Agfa Pan roll film or flat film with 25 or 100 ASA.

4.2.5 ACCURACY OF THE METHOD

In this experiment, the photos of the visualized flow are analyzed qualitatively for the most part. No conclusions as to the local distribution of velocity are drawn from the bubble movement. Thus, it remains to be decided only whether the bubbles follow the streamlines with sufficient accuracy and whether the influence of the bubble wire on the flow can be disregarded.

In the report by Schraub et al. [39], the error potential of the hydrogen bubble method is discussed in detail. The /61 authors arrive at the conclusion that the lifting power of the hydrogen bubbles against the velocity along the streamline can be disregarded at velocities above 0.02 m/s. Schraub et al. also investigated the influence of the bubble wire itself up to Reynolds number of Re = 15 (derived from the diameter of the wire) and came to the conclusion that up to 75 diameter, a velocity deficit is measurable behind the wire. However, this is significant only for quantitative measurements.

In this experiment, the wire has a diameter of 25 microns. With a towing speed of 2.5 m/s, this leads to a Reynolds number of approximately 50 derived from the diameter of the wire and the velocity component perpendicular to the wire. The velocity component perpendicular to the wire was created under consideration of the angle of incidence, the super velocity at the location of the wire, and the height of the wire in the boundary layer. At such small Reynolds numbers, according to Schlichting [38], it can be assumed that no vortex street forms in the wire's wake. In isolated experiments under extreme conditions (e.g. α = 35°, γ = 90°, height in the boundary layer at U/U_e = 0.7), Reynolds numbers up to 70 can occur, at which shedding of vortices is possible. However, it has not yet been determined whether shedding of vortices occurs for gassing wire anemometers with this Reynolds number. However, the possibility must be reckoned with in these experiments.

If the Reynolds number surpasses about 15 to 20, narrow strips, in which no bubbles separate, can arise at regular intervals (5-10 mm). This might be caused by a characteristic vibration of the wire. Böttcher [8] studied this phenomenon more closely. As far as possible, an attempt was made to keep the velocity component perpendicular to the wire and thereby the wire Reynolds number small by choosing small angles of roll γ and small distances from the wall in these experiments. In experiments in which the wire Reynolds number becomes greater than 20, two questions must be settled.

Does the wire influence the formation of disturbances?

If this is not the case, how can the structures caused by regular interruptions of the separation of bubbles and those caused by the flow be kept apart?

These two questions are discussed in the appendix under consideration of the experimental results.

4.3   RESULTS AND DISCUSSION

In making the flow visible, different kinds of disturbances and waves were observed in the boundary layer. As is shown by the investigations described below, it is possible first to classify two different kinds of disturbance:

a)   waves, which are brought about by disturbances in the stagnation area and

b)   waves, which are observed where the flow in the stagnation area is undisturbed, with a larger angle at circumference.

To a): Waves caused by disturbances in the stagnation area are characterized by lines of the same phase, which are at a 70° to 90° angle to the cylinder axis. Fig. 4.4 shows these waves and their change with the Reynolds number for ϕ_0 = 70°. The Tollmien-Schlichting waves are already observed in the vicinity of the stanation area (γ = 30°) and spread into a wedge-shaped area around the streamline direction. With increasing Reynolds number, a greater diffusion along the cylinder axis is possible until, at Re = 4 • 10^5 (R = 508), the disturbance becomes irregular and is so strongly excited that a laminar-turbulent turbulence takes place on the entire flank.   Similar processes are also observed for the sweep angle ϕ_0 = 65°. By using photographs, it could be proved that these waves propagate spatially.

Poll conducted intensive studies of the boundary layer in the stagnation area and came to the conclusion (see Section 2.3) that for critical Reynolds numbers of the boundary layer in the stagnation area,

R > 250

artificially introduced disturbances in the stagnation area are excited.

In these experiments, the characteristic Reynolds number for the stagnation area R falls between 250 and 440. The angle of roll of the bubble wire to the stagnation line is γ = 30°. Thus the mounting of the bubble wire, which lies upstream, is close to the stagnation area on the cylinder and could be a possible source of disturbances. Furthermore, the front mounting pin is attached at the transition of the head of the hemisphere to the cylinder, where the boundary layer has to overcome a rise in pressure within the stagnation area, making it unstable (cf. Poll [29]).

The experiments were repeated under somewhat modified conditions. The upstream mounting pin was moved forward into the area of pressure drop on the head of the hemisphere and the angle of roll of the bubble wire to the stagnation line was enlarged. It was then found that under these conditions, with sweep

44

angles ϕ_0 in the stagnation area between 65° and 55°, no waves could be observed with phase lines from 70° to 90° to the cylinder axis. These waves can, however, be brought back by causing additional artificial roughness near the stagnation line, as Fig. 4.5 shows for ϕ_0 = 55°, with the mounting pin moved forward and artificial disturbance.

To b): In order to investigate the characteristic instability of the three-dimensional boundary layer, care was taken that the stagnation area is free of potential sources of disturbance. As is already known from the plate experiment and from the experiments of Arnal [3], the cross flow instability causes a strong spanwise variation of the velocity component in the direction of the main flow. The time line method is well suited to making such structures visible and was therefore used in most of the experiments.

Fig. 4.6 shows two typical time line pictures. After a certain run length, the time lines, which are straight at first, show a regular distortion of increasing strength, which /64 corresponds to a spanwise variation of the velocity. Lines of the same phase (union of the "wave mounds" in the time lines) lie at the edge of the boundary layer in roughly the direction of the local streamlines. These structures are therefore attributed to the cross flow instability. When the distance of the wire is varied with all other conditions being equal, a clear and reproducible distortion of the time line could be observed only very deep within the boundary layer ($\delta^* \sim 0.5$). From this it can be concluded that the intensity of the disturbance due to cross flow instability decreases greatly toward the boundary layer edge.

The boundary layer flow was made visible for various parameters ϕ_0 and Q_∞ and evaluated with respect to three aspects:

- The first question was, for what smallest Reynolds number with a fixed sweep angle cross flow instabilites already became visible and at which Reynolds number the boundary layer becomes turbulent.

- Secondly, in images with regular excited cross flow instability, the wavelength was measured and compared with the results of other authors.

- Third, an attempt was made to make the occurrences in the boundary layer shortly before the actual turbulence visible.

Fig. 4.7 summarizes the results of initial excitation of cross flow instabilities and transition of the boundary layer. For every parameter combination ϕ_0 and Re for which experiments were conducted, it is recorded whether cross flow instabilities are observed (x) and whether turbulence was attained (T). In addition to the experiments, two curves for constant characteristic Reynolds number of the stagnation line boundary layer R = 250 and R = 570 are shown, and for purposes of comparison with Poll's results, so is the curve from painting images for the first

occurence of cross flow instability in the petroleum painting image (χ = 200) and the one for the appearance of turbulence at γ = 90°. For ϕ_0 = 65° and 60°, the Reynolds numbers at which transition takes place agree quite well with those from Poll's experiments. At ϕ_0 = 70°, transition begins very early. With this sweep angle, the flow is already very much influenced by the flow around the head of the hemisphere. A disturbance due to the mounting pin which has been moved forward might possibly still influence the flow field.

Surprisingly enough, the Reynolds number for the first possible observation of cross flow instabilities also comes quite close to Poll's observations for ϕ_0 = 65° and 60°. It would be reasonable to expect the instabilities to become visible in the boundary layer earlier than on the wall, since the disturbance velocities decrease toward the wall. Furthermore, the hydrogen bubble method is much more sensitive than the petroleum painting method used by Poll. A possible explanation lies in the different initial disturbances in the experiments. With the colored pigment-oil emulsion, Poll introduces an initial disturbance to his cylinder, even though a very small one, whereas in the water tunnel experiment both the surface of the model and the incoming flow are very low in disturbances. For ϕ_0 = 55°, cross flow instabilities were not observed until much larger Reynolds numbers. The reasons for this have not yet been discovered.

The appearance of regular structures in the time lines were observed for varying sweep angles ϕ_0, velocities Q_∞, and angles of roll of the bubble wire γ to the stagnation line. In one picture, the evolution of the time lines over angles at circumference of about 10° to 20° can be traced and observed. One finds that the number of waves and, thus, the wavelength does not change. Comparisons of the measured results at 40° and 80° angles of roll also reveal no deviations in the wavelengths beyond the accuracy of measurement. Thus, as in the experiments by Poll and Bippes using petroleum painting images, the wavelength of the cross flow instabilities does not change with the run length. The wavelength was measured perpendicular to lines with the same phase in the pictures and was transformed using a scale factor; the accuracy of the measurements is approximately 10%.

In Fig. 4.8, λ/d is plotted against the Reynolds number. The results of Poll and Bippes are also entered, as well as the experiments described here. Just as was the case for the experiments on the plate, a slight decrease wavelength with the Reynolds number becomes evident.

In Fig. 4.9, the wavelength was made non-dimensional with the value

$$\eta = \sqrt{d\nu/U_\infty} =$$

$$= \sqrt{d^2/(Re \cdot \cos\phi_o)}$$

46

characteristic of the boundary layer. Within the limits of the
accuracy of measurement, a constant value over the Reynolds number
of

$$\lambda/n = 8.7$$

results. The 99% boundary layer thickness on the cylinder does
not change much for a wide range of the angle of roll γ (30° to
70°) and takes on the approximate value

$$\delta^* \sim 2$$

when it is likewise made non-dimensional with n. Thus, as in the
experiment on the plate, the ratio of wavelength to boundary layer
thickness is approximately four:

$$\lambda/\delta = 4.4 \quad .$$

MAKING THE BOUNDARY LAYER VISIBLE SHORTLY BEFORE THE LAMINAR-
TURBULENT TRANSITION

It is very difficult to make the boundary layer visible just
before the laminar-turbulent transition, since the boundary layer
becomes very thin. In addition to the distortions of the time
lines, familiar from cross flow instabilities, the pictures showed
the appearance of waves with increasing Reynolds number. The
lines of equal phase of these waves do not follow the local
streamlines; they are at an angle of 70° to 90° to the cylinder
axis. Fig. 4.10 gives some typical examples. In detail a) of <u>/67</u>
the figure, cross flow instabilities can be observed in the left
part of the picture. The development of these cross flow
instabilities can be traced over a large run length. To the
right, the first thing observed is the typical distortion of the
time lines due to cross flow instability; then they are disturbed
by waves at a different angle. Likewise in detail b), the waves
with phase lines from an angle of 70° to 90° can be seen. At a
greater Reynolds number, these waves propagate over a larger
section along the y axis (c).

For waves in this direction, it could be demonstrated that
they propagate spatially. Also, stationary vortices are possible
only in the direction of flow, since such vortices are the only
ones that are free of force. The observed structures are
therefore categorized as travelling waves.

Thus, just as in the experiment on the plate, standing and
travelling waves are observed for the swept circular cylinder.
According to these experiments, the first thing observed is a
continuous excitation of the stationary vortices. It is necessary
when evaluating this result to take into account that the
experiments in the water tunnel were carried out with a flow which
had very few disturbances, causing the initial disturbances of
travelling waves to be very small. With growing Reynolds number
before the transition to turbulence, travelling waves (i.e. waves

with lines of equal phase in an angle to the cylinder axis of 70°
to 90°) were always observed as well.

5. SUMMARY AND OVERVIEW

In accordance with knowledge gained from preliminary trials, a
model proposed by Hirschel and Dallmann [17] consisting of a swept
plate with a displacement body impressing pressure was designed
and constructed for the 1-meter wind tunnel. In the course of the
experiments, this model was improved by the addition of lateral
plates, so that a quite satisfactory quasi-two-dimensional flow
occurred on the plate. On the plate, the pressure gradient   /68
impressed by the displacement body creates a boundary layer, which
becomes unstable and reaches turbulence. This unstable boundary
layer was studied using methods of making the flow visible
(petroleum painting and naphthalene methods) and by hot wire and
hot film measurements. In detail, results of the measurements
were:

- Stationary cross flow instabilities with a wavelength $\lambda = 4\delta$
  were observed in the unstable area. At the same time, a broad
  frequency band of travelling waves is also excited. The
  maximal excited frequencies are
  $\omega = 2\pi f = 0.11 \, Q_e / \delta$.

- Both disturbances are excited in roughly the same area. For
  the travelling waves, a constant cross flow Reynolds number
  $\chi = 115$ describes the location of the first observable
  appearance quite well.

- The RMS value of the travelling waves is modulated by the
  standing waves. Thus, there is an interaction between both
  disturbances.

48

- The generalized Orr-Sommerfeld equation can be used to describe the wavelength and the direction of the stationary modes as well as the frequency of the travelling waves.

In a further experiment in the model water tunnel, the boundary layer on a swept circular cylinder with a semispherical head above the wall was made visible using the hydrogen bubble method. It was possible to prove the existence in the boundary layer of stationary cross flow instabilities, which had hitherto been made visible only in petroleum painting and sublimation images on the surface of swept wings. The pictures were evaluated for different Reynolds numbers, sweep angles, angles of roll of the bubble wire to the stagnation line, and heights of the wire in the boundary layer wall. The results were:

- Cross flow instabilities can only be observed very deep within the boundary layer ($\delta \sqrt{U_\infty/v d} \leq 0.5$).

- The wavelengths of the cross flow instability also amount /69 to approximately 4δ

$$\lambda = 4\delta .$$

- At first, cross flow instabilities are observed on the cylinder in the water tunnel (where the oncoming flow is low in disturbances!); later, however, travelling waves with phase lines of 70° to 90° to the cylinder axis are as well.

- Before the transition to turbulence, travelling, greatly excited waves also are always observable.

For further experiments in the 1-meter wind tunnel, it would be advisable to improve several elements of the model. Should preliminary trials indicate that a smaller sweep angle also is sufficient to create an unstable boundary layer, it would be advisable to choose it in order to make better use of the free jet's potential core. By this means, it might be possible to maintain a better quasi-two-dimensional flow at the back part of the plate, too. In the course of follow-up studies of stationary instabilities, how their continuous excitation is related to initial disturbances should be investigated. This would require considering the influence of the tunnel's smoothing filters and of small initial disturbances on the plate. When looking further into the travelling waves, it would be interesting to ask whether it is possible to measure the direction of the travelling waves and to compare it to theory.

Several questions regarding the interaction of travelling and stationary waves remain unanswered. First, measurements with a calibrated hot wire could make a better quantitative comparison of the two types of disturbance possible. These measurements should be conducted with different distances from the wall. The results might shed some light on why the stationary instabilities show up so plainly in petroleum painting images in spite of such strongly excited travelling waves.

Another interesting topic would be to investigate the
influence of the pressure progression and sweep angle on the two
disturbance waves and the location of transition.

Precisely because the occurrences in the unstable three-
dimensional boundary layer are so complex, valuable contributions
can be made by making the flow visible. When continuing with
these experiments, it is necessary to study thicker boundary
layers at lower relative wind velocities, making possible better
resolution of the occurrences and minimalization of disturbances
caused by tne wire. Also, the water tunnel is especially well-
suited to studying the influence of artificially introduced
disturbances.

REFERENCES

[1] Anscombe, A.   Wind Tunnel Observations of Boundary Layer   /71
    Illingworth,L.N. Transition on a Wing at Various Angles of
                      Sweep Back.

                      ARC Report and Memorandum 2968,   May 1952 .

[2] Arnal, D.   Théorie de l'Instabilité laminaire et
    Habiballah, M.   Critères de Transition en Ecoulement bi- et
    Coustols, E.   tridimensionnels.

                      La Recherche Aérospatiale 2, März/April 1984,
                      S.125 - 143.

[3] Arnal, D.   Etude experimentale et théoretique
    Coustols, E.   de la Transition sur une Aile en flèche
    Juillen, J.C.   infinie.
                      La Recherche Aérospatiale 4, Juli/Aug. 1984 ,
                      S. 275 - 290.

[4] van den Berg, B. Measurements in a Three-Dimensional
    Elsenaar, A.   Incompressible Turbulent Boundary Layer
                      in an Adverse Pressure Gradient under
                      Infinite Swept Wing Conditions.

                      NLR-Bericht NLR TR72092 U.
                      National Aerospace Laboratory,1972 .

[5] Bieler, H.   DFVLR-Forschungsbericht, in Vorbereitung,

                      (1985).

[6] Bippes, H.   Experimentelle Untersuchung des laminar-   /72
                      turbulenten Umschlags an einer parallel ange-
                      strömten, konkaven Wand.

                      Sitzungsberichte zur Heidelberger Akademie der
                      Wissenschaften math. nat. Klasse
                      Jahrgang 1972, 3. Abhandlung.

[7] Boltz, F.W.   Effects of Sweep Angle on the Boundary
    Kenyon, G.C.   Layer Stability Characteristics of an
    Allen, G.Q.   Untapered Wing at Low Speeds.

                      NASA TN D-338 (Juli 1960).

[8] Böttcher, J.   DFVLR-Forschungsbericht,in Vorbereitung,

                     (1985).

[9] Coustols, E.   Stabilité et Transition en Ecoulement
                     tridimensionnel: Cas des Ailes en flèche.

                     These de Docteur-Ingénieur soutenue à l'ENSAE,
                     1983 .

[10]Cumpsty, N.A.   The Calculation of 3-D-Turbulent Boundary
    Head, M.R.   Layers, Part II: Attachment Line Flow on an
                     Infinite Swept Wing.

                     The Aeron. Quarterly Vol. 18   (1967),
                     S. 150 - 164.

[11] Gaster, M.   On the Effect of Boundary Layer
                     Growth on Flow Stability.

                     J. Fluid Mech. 66 (1974), S. 465-480.

[12] Gray, W.E.   The Effect of Wing Sweep on
                     Laminar Flow.

                     R.A.E. Technical Memorandum 255 (1952).

[13] Gregory, N.   Brief Wind Tunnel Tests on the Effect
     Walker, W.S.   of Sweep on Laminar Flow.

                     ARC Paper 14, 928 (May 1952).

[14] Gregory, N.   On the Stability of Three-Dimensional
     Stuart, J.T.   Boundary Layers with Application to the Flow
     Walker, W.S.   due to a Rotating Disk.

                     Phil.Trans.Roy.Soc.of London Series A,
                     248 (1955), S. 155 - 199.

[15] Habiballah, M. Analyse de l'instabilité des couches
                     limités laminaires et prévision de la
                     transition du régime laminaire au régime
                     turbulent.

                     These de Docteur-Ingénieur
                     Soutenue à l'ENSAE, 1981.

/73

[16] Herbert, Th.   Secondary instability of plane channel
                       flow to subharmonic three-dimensional
                       disturbances.

                       Phys. Fluids 26 (1983), S. 871-874.

[17] Hirschel, E.H.   Vorschläge für die experimentelle Unter-
     Dallmann, U.   suchung des Übergangs laminar-turbulent in
                       dreidimensionalen Grenzschichten

                       Interner Bericht, DFVLR, Göttingen, 1974.

[18] Kachanov, Yu.S.   Resonant Interactions of Disturbances
     Levchenko,V.Ya.   in Transition to Turbulence in a Boundary
                       Layer (russisch) (1982),
                       siehe auch
                       J.Fluid.Mech. 138 (1984),S. 209 - 247.

[19] Klebanoff, P.S.   The Three-dimensional Nature of Boundary
     Tidstrom, K.D.   Layer Instability.
     Sargent, L.M.
                       J. Fluid Mech. 12 (1962),S. 1 - 34.

[20] Kovasznay,L.S.   Detailed Flow Field in Transition.
     Komóda,H.
     Vasudeva,B.R.   Proc. of the 1962 Heat Transfer and Fluid
                       Mech.Inst.Standford University Press, 1962 .

[21] Landhäußer, A.   Kalibrierung einer 5-Lochsonde und
                       Erprobung eines Auswerteverfahrens zur
                       Strömungsfeldmessung.

                       Diplomarbeit Universität Göttingen 1986 .

[22] Mack, L.M.   Boundary Layer Linear Stability Theorie.

                       AGARD Report Nr. 709 (1984).

[23] Malik, M.R.   Effect of Curvature on Three-Dimensional
     Poll, D.I.A.   Boundary Layer Stability.

                       AIAA Paper Nr. 84 - 1672 (1984).

[24] Nishioka, M.   An Experimental Investigation of the
     Iida, S.   Stability of Plane Poiseuille Flow.
     Ichihava, Y.
                       J. Fluid Mech. 72 (1975),S. 731 - 752.

/74

[25] Owen, P.R.   Boundary Layer Transition on a Swept
     Randall, D.G.   Back Wing.

                         RAE Technical Memorandum 256 (1952).

[26] Owen, P.R.   Boundary Layer Transiton on a Swept
     Randall, D.G.   Back Wing - a Further Investigation.

                         RAE Technical Memorandum 330 (1953)

[27] Pfenninger, W.   Laminar Flow Control - Laminarisation.
                         Special course on concepts for drag
                         reduction.

                         AGARD Report 654, March 1977.

[28] Poll, D.I.A.   Some Aspects of the Flow near a Swept
                         Attachment Line with Particular Reference to
                         Boundary Layer Transtion.

                         College of Aeronautics, Report 7805 (1978).

[29] Poll, D.I.A.   Some Comments and Suggestions Relating
                         to the Experiments Currently being Performed
                         to Investigate Transition via Cross-Flow
                         Instability.

                         Interner Bericht, DFVLR, Göttingen, 1983.

[30] Poll, D.I.A.   Some Observations of the Transition Process
                         on the Windward Face of a Long Yawed Cylinder.

                         J. Fluid Mech. 150 (1985), S. 329-356.

[31] Reed, H.   Disturbance - Wave Interactions in
                         Flows with Crossflow.

                         AIAA Paper Nr. 85 - 0494 (1985).   .

[32] Reed, H.   Wave Interactions in Swept Wing Flows.

                         AIAA Paper Nr. 84 - 1678 (1984).

[33] Reshotko E.   Boundary - Layer Stability and Transition.

                         Annual Review in Fluid Mech 8 (1976),
                         S. 311 - 349.

[34] Saric, W.S.   Forced and Unforced Subharmonic
     Kozlov, V.V.   Resonance in Boundary Layer Transition.
     Levchenko,V.Ya.
                         AIAA Paper Nr. 84-0007 (1984).

[35] Saric, W.S.   Nonparallel Stability of Boundary
     Nayfeh, A.H.   Layer Flows.

                         The Phys. of Fluids, Vol.18 (1975) No. 8.

[36] Saric, W.S.   Experiments on the Subharmonic
     Thomas, A.S.W.   Route to Transition.

                         Proc. IUTAM Symposium on Turbulence
                         and Chaotic Phenomena in Fluids,
                         Kyoto, Japan , 1983.

[37] Saric, W.S.   Experiments on the Stability of Cross
                         Flow Vortices in Swept Wing Flows.

                         AIAA Paper Nr. 85 - 0493 (1985).

[38] Schlichting, H. Grenzschicht-Theorie.

Karlsruhe: Verlag G. Braun, 1958,
S. 16 und S. 367.

[39] Schraub, F.A.   Use of Hydrogen Bubbles for
     Kline, S.J.   Quantitative Determination of Time-
     Henry, J.   Dependent Velocity Fields in Low Speed
     Runstadler,P.W. Water Flows.
     Litell, A.

                      Report MD-10, Thermoscience Div. Mech.
                      Engr. Dept., Stanford University 1964.

[40] Schubauer, G.B. Laminar Boundary Layer Oscillations and
     Skramstad, H.K. Stability of Laminar Flow.

                      Journal of the Aeronautical Sciences 14
                      (1947) Nr. 2.

[41] Squire, H.B.   On the Stability of Three-Dimensional
                      Distribution of Viscous Fluid Between Parallel
                      Walls.

                      Proc. Roy. Soc. A 142 (1933).

PROFILE DATA FOR DISPLACEMENT BODY AND SLATS

The data are indicated in a Cartesian coordinate system.

Displacement body

x points perpendicularly from the trailing edge toward the front tangentially to the flat portion of the underside.

x [mm]	Lower Side y [mm]	Upper Side y [mm]
0	0	0
20	0	20
40	0	34
60	0	47
80	0	57
100	0	65
120	0	73
140	0	79
160	0	85
180	0	91
200	0	95
220	0	99
240	0	102
260	0	103
270	1	104
280	2	104
300	4	105
320	9	105
340	14	105
360	21	103
380	29	101
400	40	98
410	46	96
420	53	94
430	59	91
440	68	85
447	77	77

57 - 60

The x axis points perpendicularly from the trailing edge toward the front and touches the wing there tangentially.

x [mm]	Lower Side y [mm]	Upper Side y [mm]
0	0	0
10	5	10
20	9	17
30	11	22
40	13	27
50	14	30
60	12	32
70	8	33
80	2	32
90	0	28
95	2	25
100	7	18
102	13	13

REMARKS CONCERNING DISTURBANCES OF THE FLOW DUE TO THE HYDROGEN BUBBLE WIRE

As was mentioned in Section 4.2.5, caution is particularly called for in wire Reynolds numbers above 15-20. One notes in many experiments that from this Reynolds number, at regular intervals no bubbles are freed from the wire. Just which procedures are responsible for this behavior is a matter which has not yet been clarified. During the experiments, attempts were made to keep the wire's Reynolds number below the 15 to 20 range by suitable selection of the parameters. For a few experiments, however, this condition could not be met. It must therefore be determined whether this effect has any influence on the flow in the boundary layer.

First, studies were carried out to determine how the   /80
structures developed as a result of the wire could be separated from those generated by the flow.

In experiments by Böttcher involving a wire anemometer outside a boundary layer and also in experiments involving a cylinder in which no cross flow instabilities could be found, the same behavior was always observed in the bubble layer: at regular intervals, no bubbles are freed at the wire, these "bands without bubbles" continue in a natural way along the streamline. The surrounding layer of bubbles and the time lines are not influenced

by this behavior. On the contrary, structures develop that are produced in the bubble layer with an increasing run length as a result of an already present velocity field, as Fig. 4.6 shows. In this way, both structures can be distinguished simply.

During the experiments within the range of the parameters in which structures could be observed both as a result of the bubble wire as well as due to the cross flow instabilities, special attention was paid to determine whether any influence could be noted as a result of the flow. Various experiments showed that as a result of the poor production of bubbles, structures are formed that are the result of cross flow instabilities. The wavelength of the cross flow instabilities did not agree with the characteristic distances of the interrupted bubble layer. From this it can be concluded that the cross flow instability is not influenced by the wire. For purposes of evaluation, pictures were used that show this quite plainly.

8. LIST OF ILLUSTRATIONS

Fig. 2.1: Three-Dimensional Velocity Profile with the Profiles
Projected Tangentially and Normally to the Streamline
at the Edge of the Boundary Layer
1: Main Flow Profile
2: Cross Flow Profile
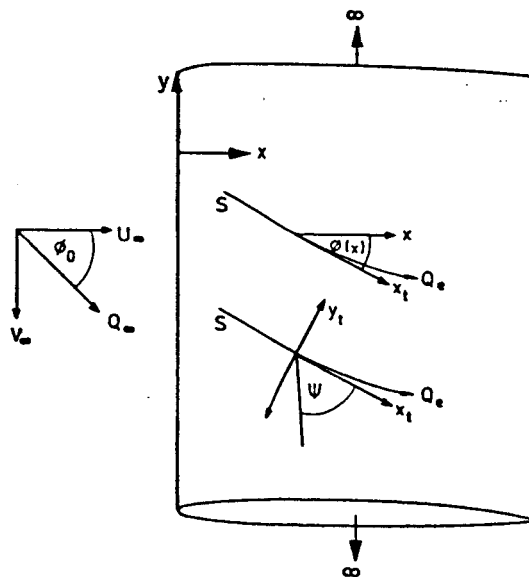
Fig. 2.2: Definition of the Coordinate System on an Infinitely
Long, Swept Model
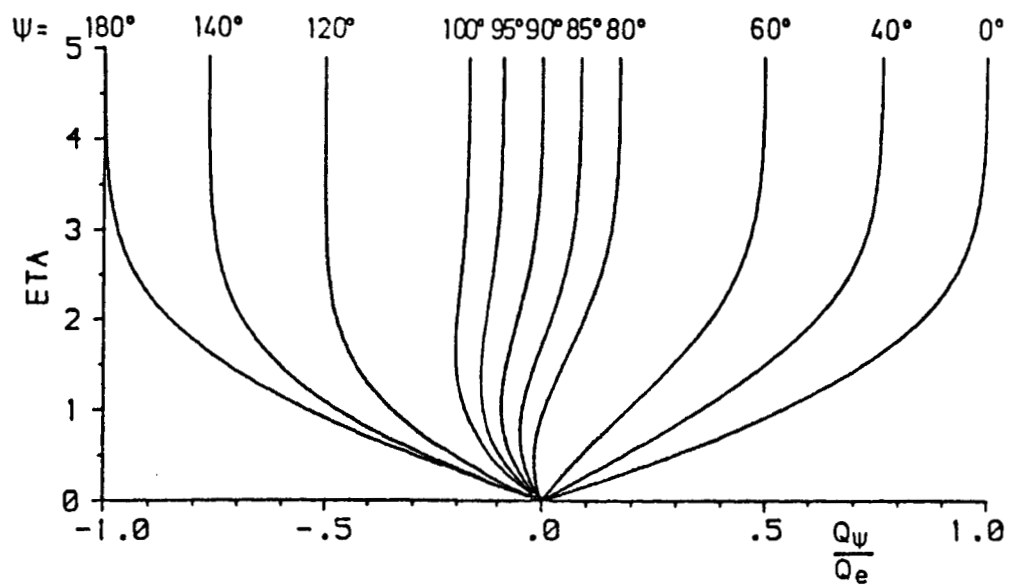
Fig. 2.3:   Projection Profiles of a Three-Dimensional Velocity
            Profile in Accelerated Flow Independent of Angle
            (Bieler 1985)
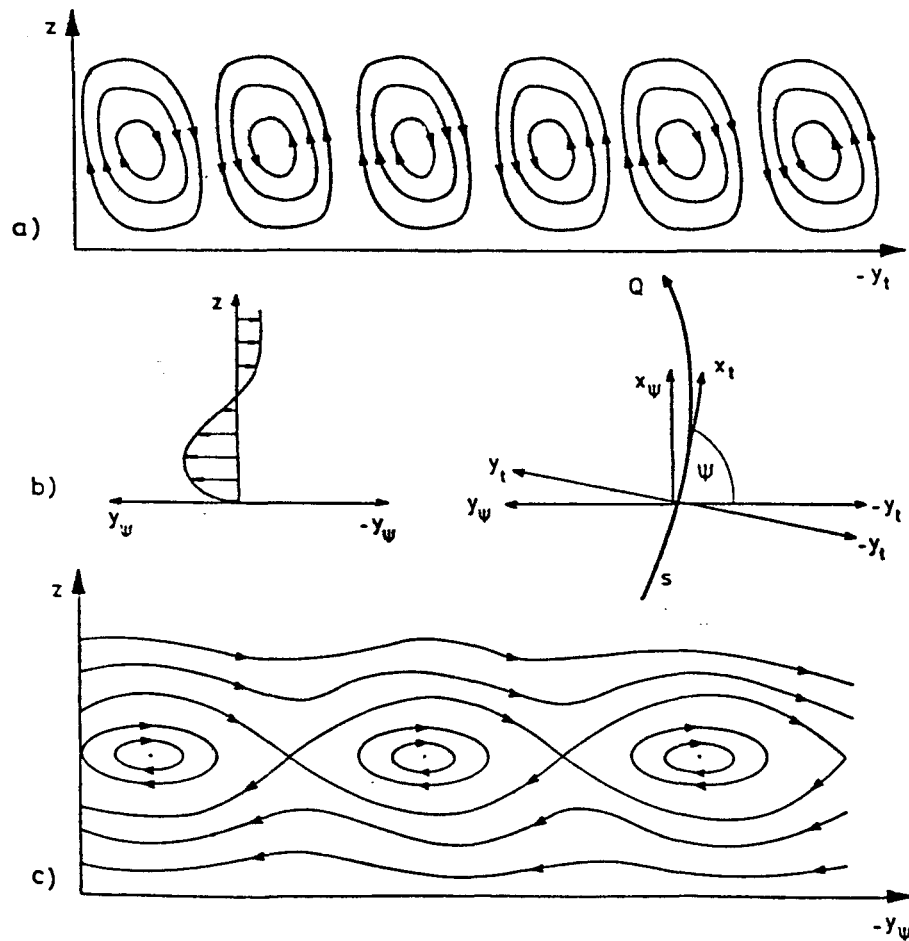
Fig. 2.4:   Streamline Image of the Stationary Cross Flow
            Instability
        a)   Streamline Image of the Disturbance
        b)   Projected Profile in Direction y_ψ
        c)   Streamline Image of the Overlapping of Disturbance
              and Main Flow
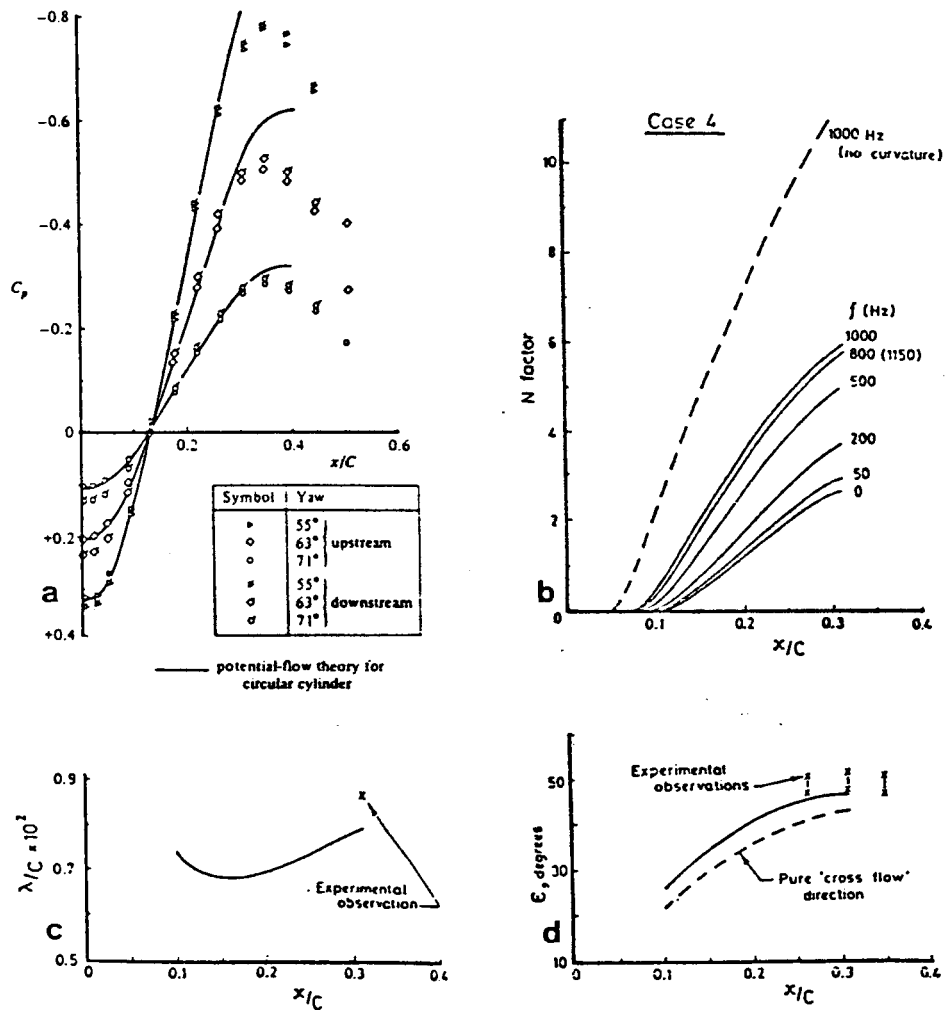
Fig. 2.5:   Poll and Malik's [23] Results on a Swept Cylinder
a) Pressure Progression
b) Excitation Factor n for Various Frequencies
c) Wavelength of the Stationary Cross Flow Instability
d) Direction of the Stationary Cross Flow Instability
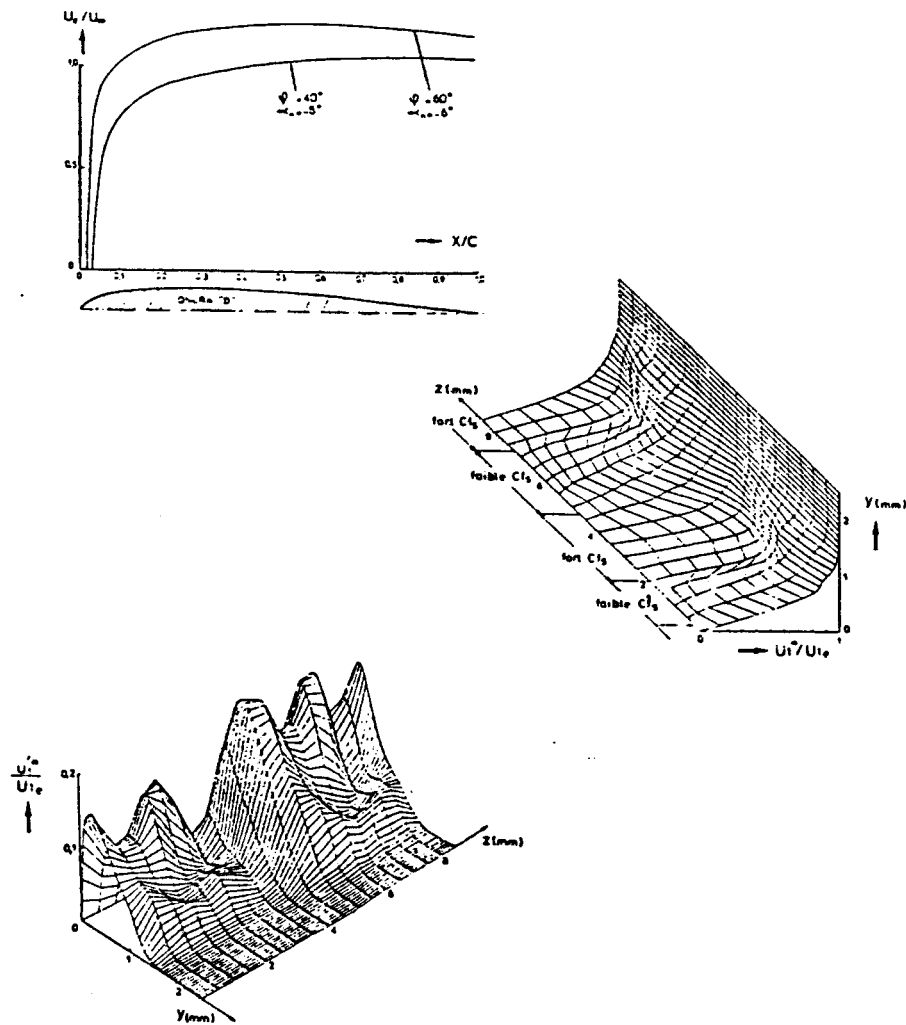
Fig. 2.6:   Results achieved by Arnal et al. [3] on the ONERA "D"
            Airfoil
            a)   Pressure Progression
            b)   Modulation of the Average Velocity Due to the
                  Cross Flow Instability
            c)   Modulation of the Effective Value of the
                  Variations in Velocity

Chordwise

a

b

Fig. 2.7:   Saric's [37] Results on a Swept Plate
        a)   Pressure Progression
        b)   Modulation of the Average Velocity Due to
              Stationary Cross Flow Instability

73

ORIGINAL PAGE IS
OF POOR QUALITY
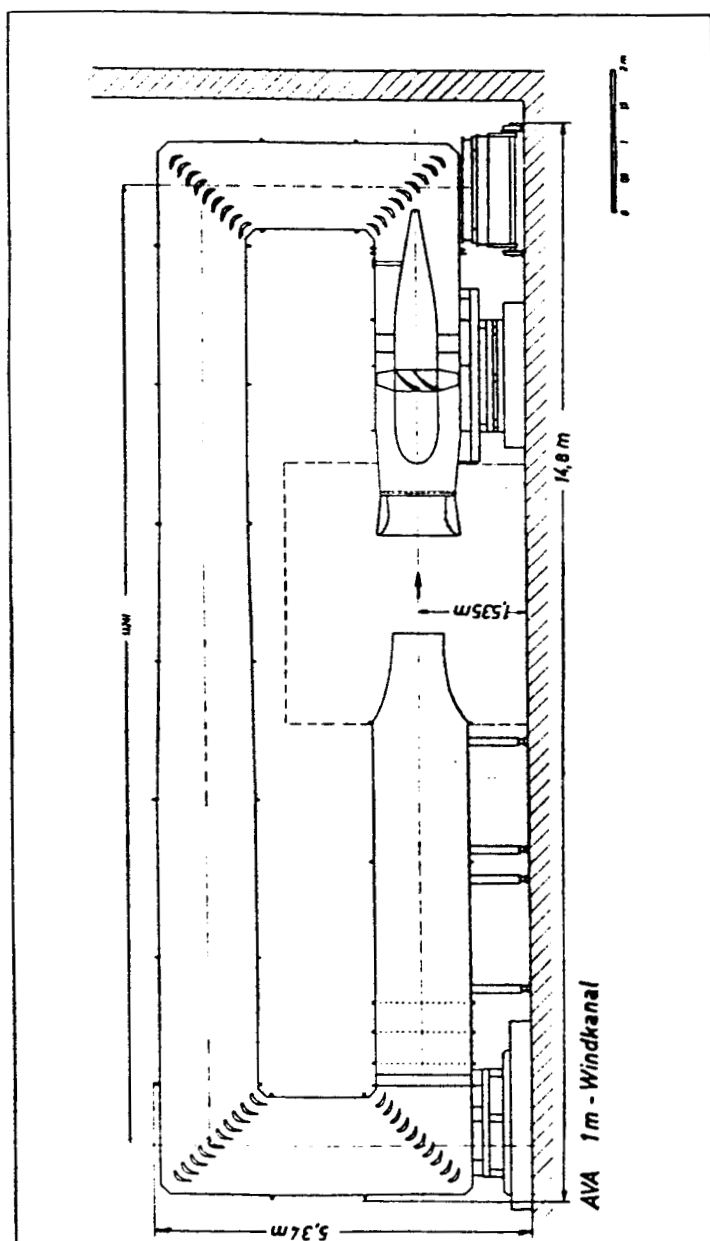
Fig. 3.1:   The 1-Meter Wind Tunnel
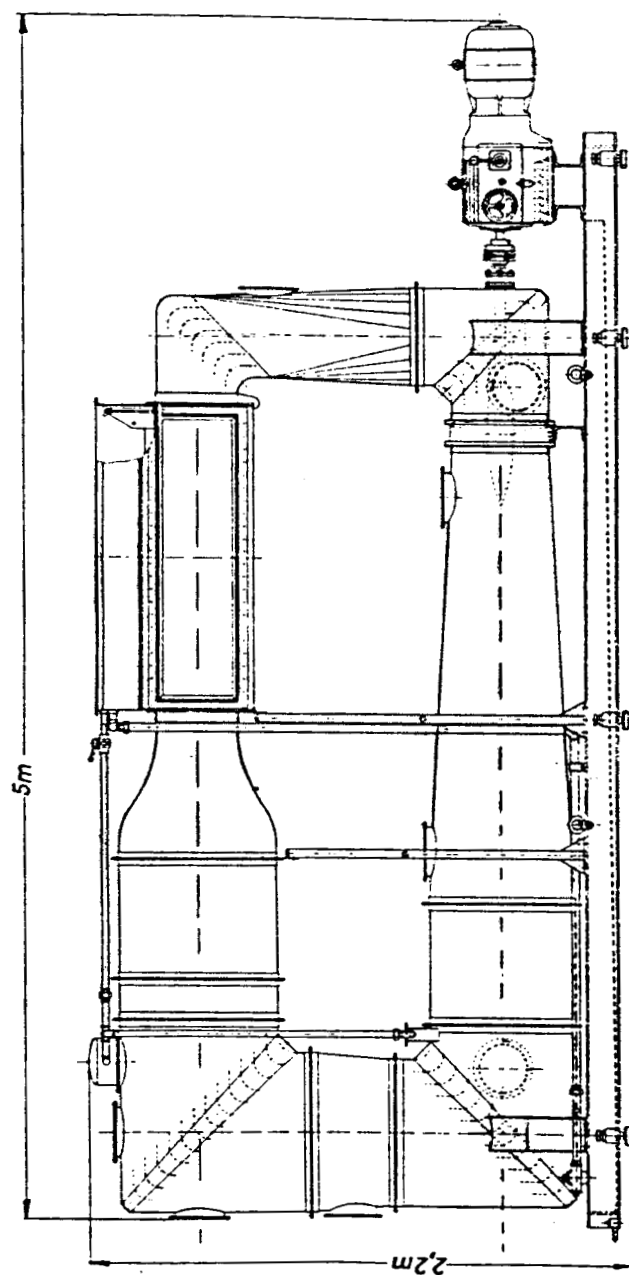
Fig. 3.2: The Circulating Water Tunnel
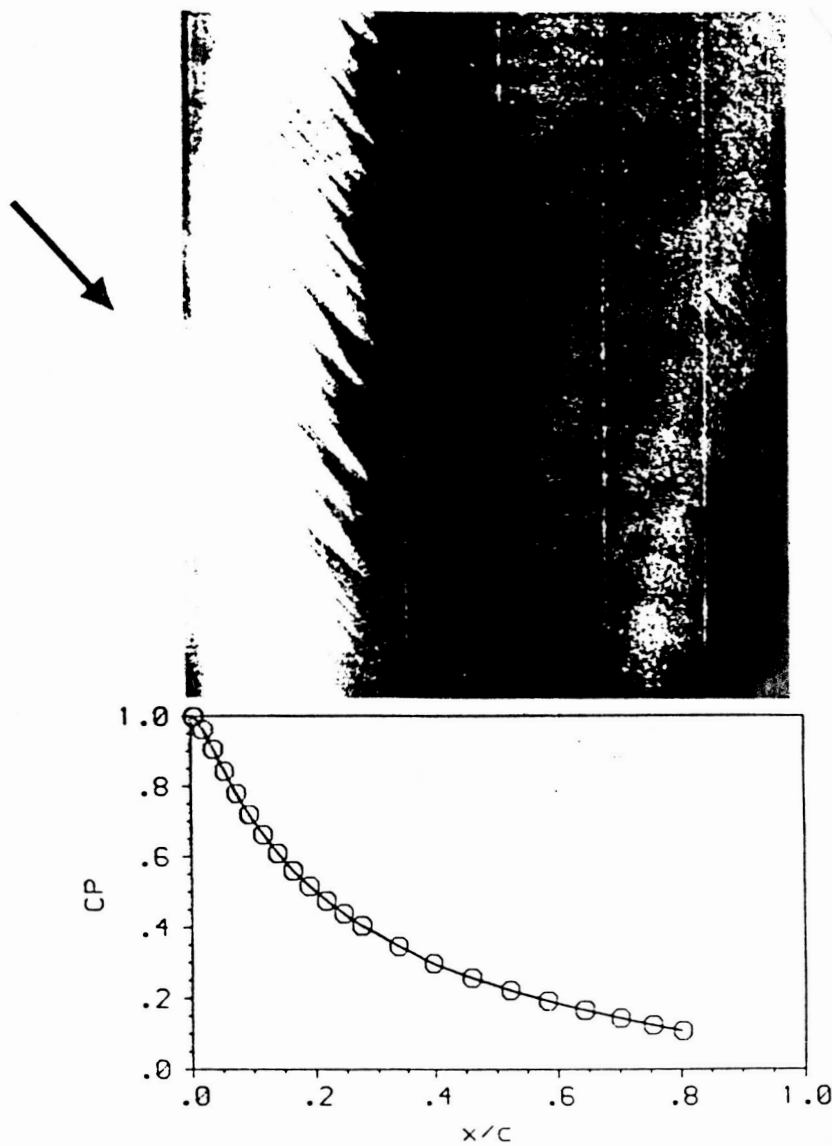
Fig. 3.3:   Rendering the Transition Site and the Cross Flow
            Instability Visible by Means of the Sublimation Method
            on the Pressure Side of the NACA-0010 Wing
            $Re = 1.5 \cdot 10^6$, $\alpha = 15°$, $\emptyset_o = 48°$
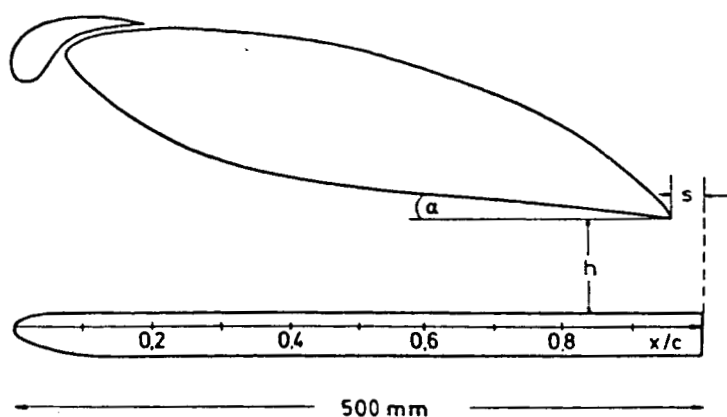
Fig. 3.4:   Cross-Section of the Plate and Displacement Body
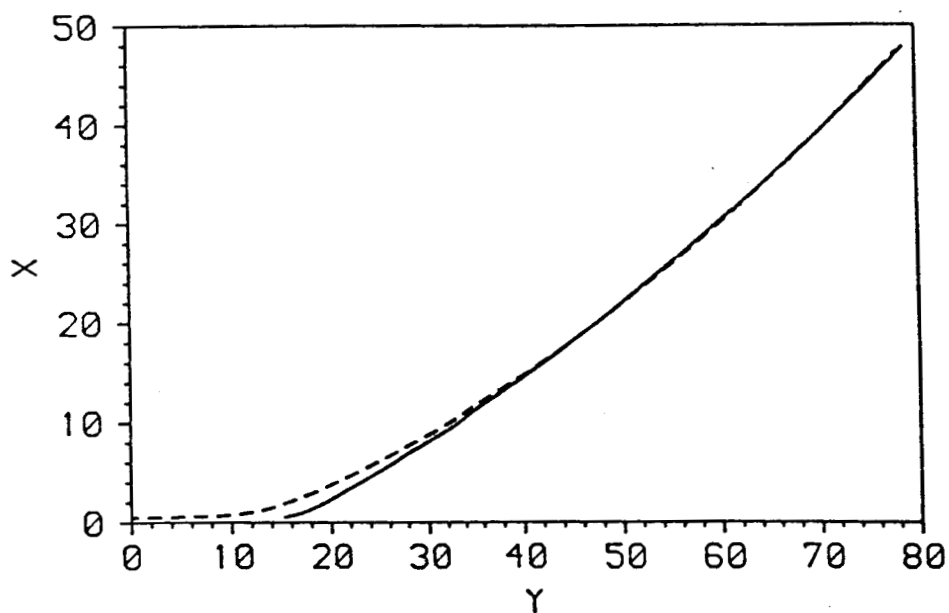
Fig. 3.5:   The Streamlines Calculated from Measured Pressure
            Progressions
            1:    From Measurements Prior to the Installation of the
                  Lateral Plates
            2:    From Measurements Following the Installagion of
                  the Lateral Plates

77
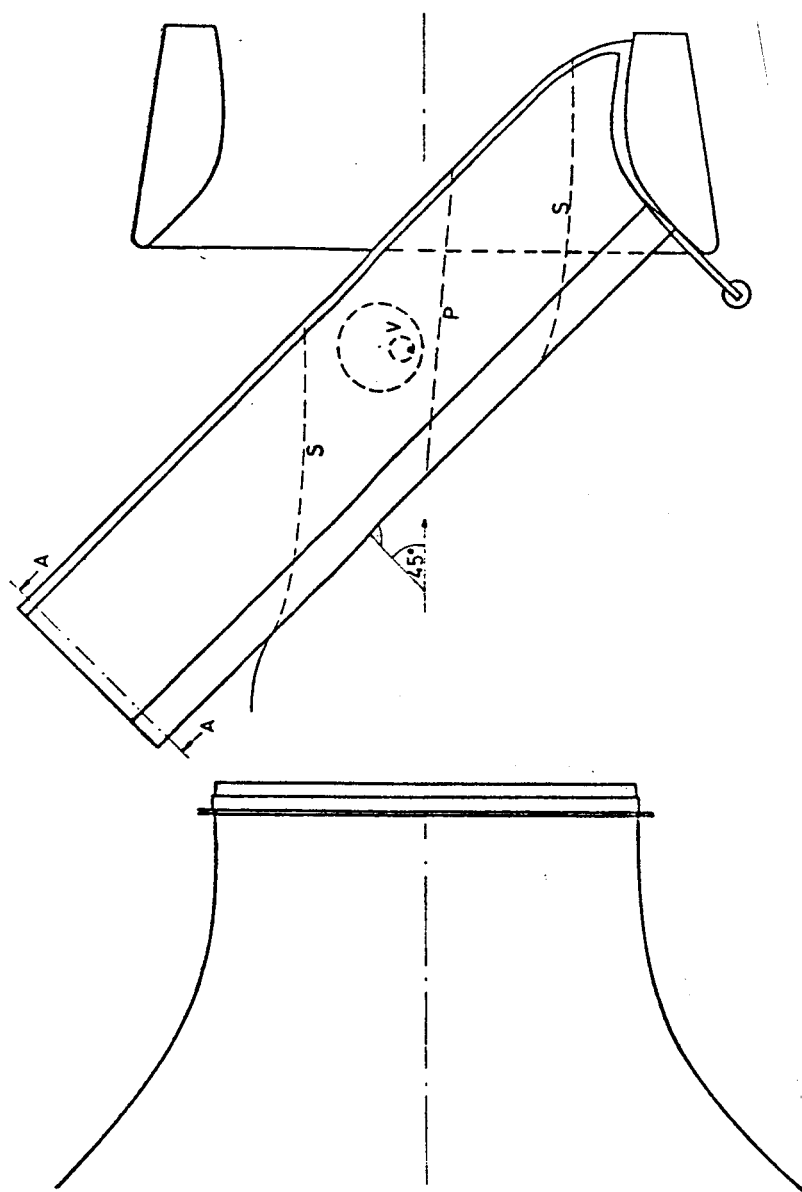
Fig. 3.6:   Structural Sketch of the Test in the 1-Meter Wind
            Tunnel
            S: Side Wall Shaped According to the Streamline
            P: Pressure Piercings
            V: Sweep Mechanism

Schnitt A-A
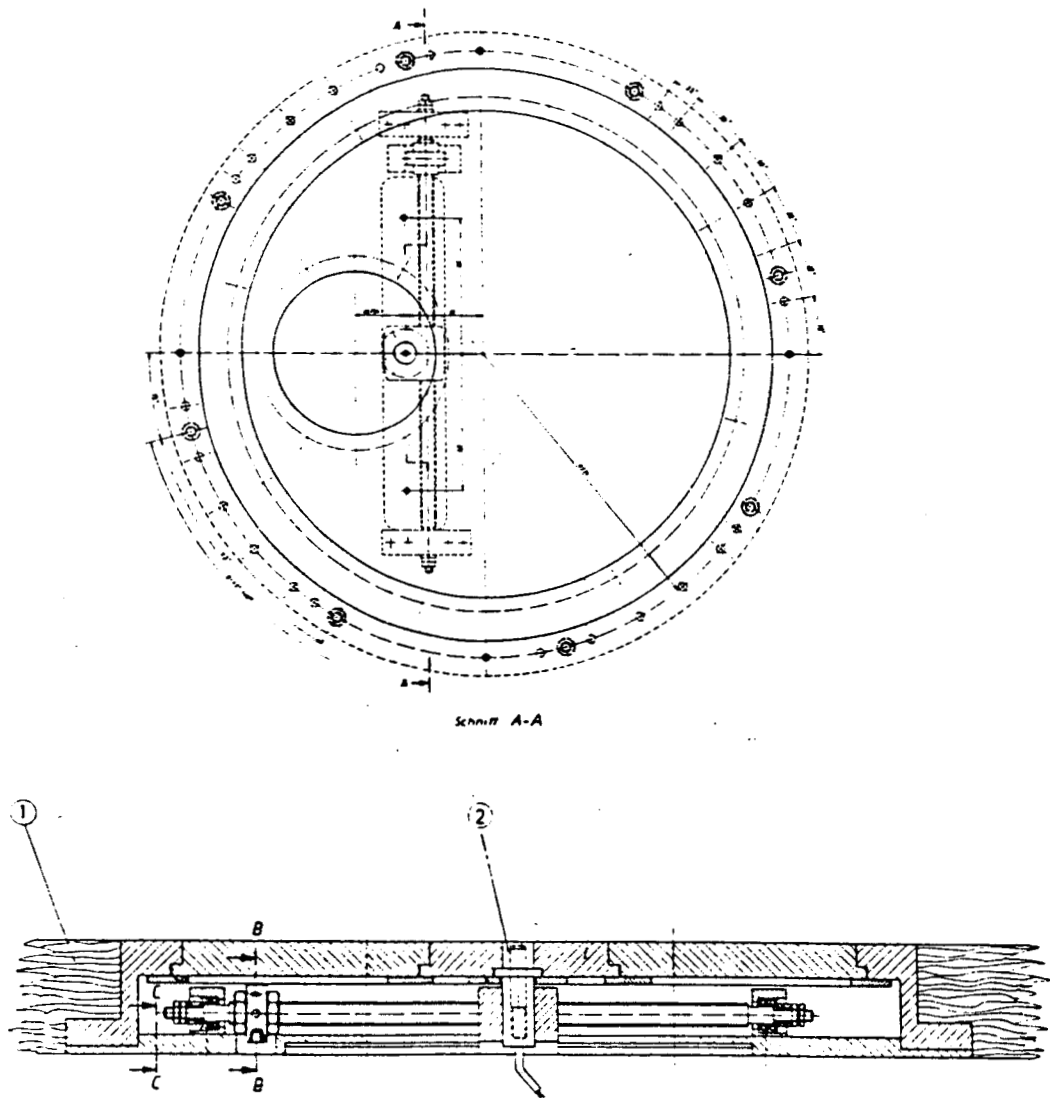
Fig. 3.7:   Sweep Mechanism for Hot Wire and Hot Film Anemometer
            1: Plate, 2: Mounting Cylinder for the Anemometers
            3: Section A-A
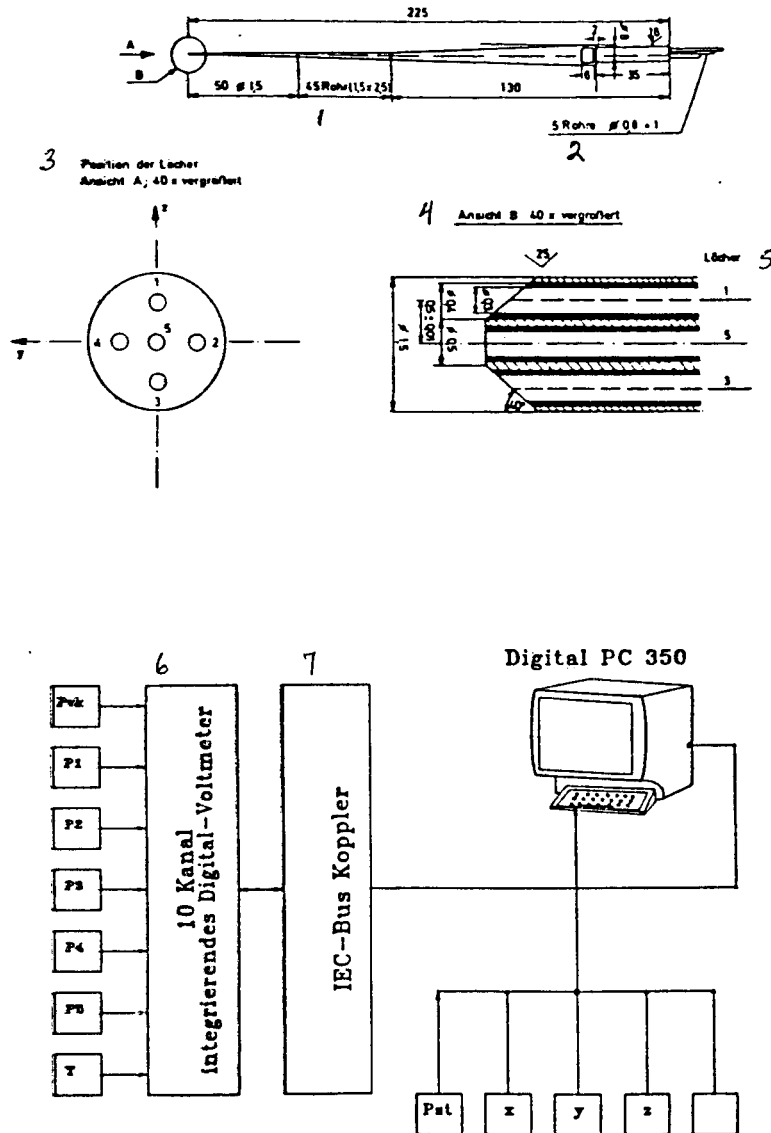
Fig. 3.8:   Sketch of the Five-Hole Anemometer with a Block
Diagram of the Data Acquisition System
1:45 Tube   2:5 Tubes   3:Position of the Holes, View
A, 40 Times Enlarged   4:View B, 40 Times Enlarged
5:Holes   6:10-Channel Integrating Digital Voltmeter
7:IEC-Bus Coupler
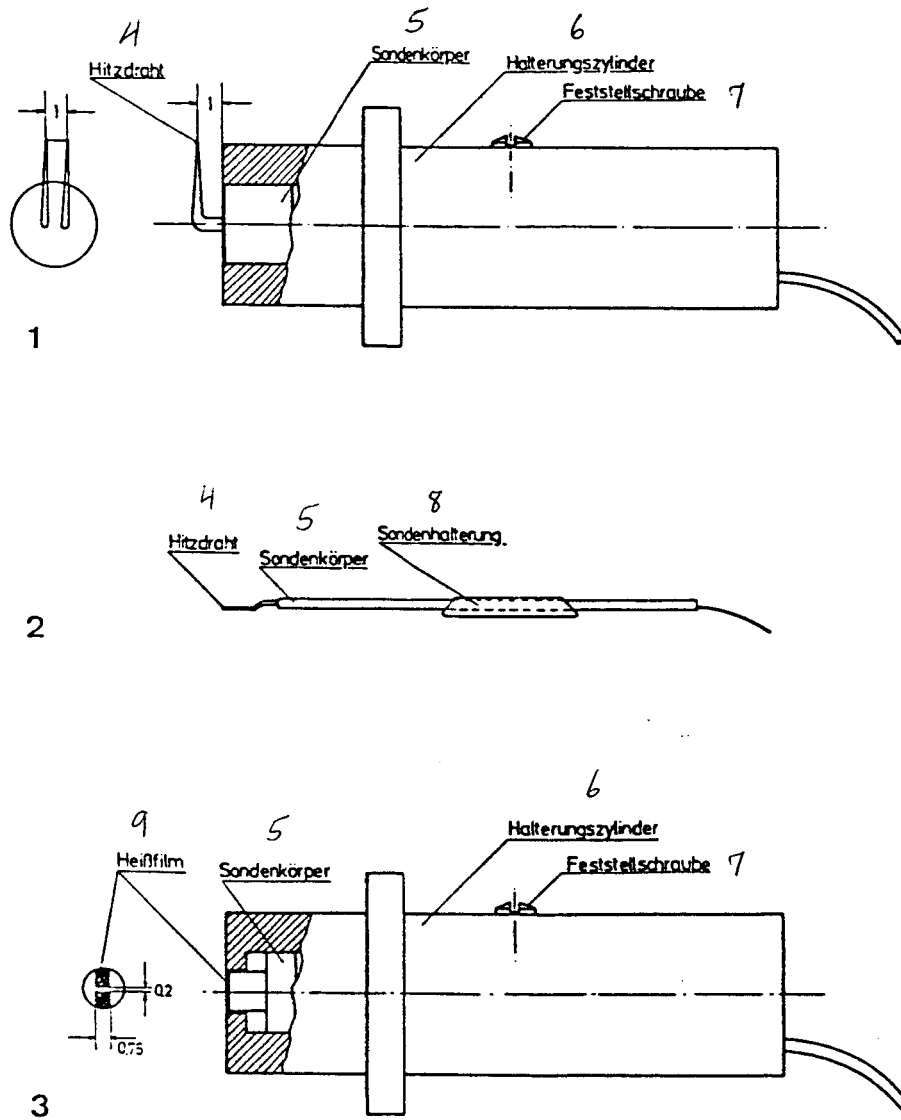
Fig. 3.9:   Sketch of the Hot Wire and Hot Film Anemometers
4:Hot Wire   5:Anemometer Body   6:Mounting Cylinder
7:Screw   8:Anemometer Mounting 9:Hot Film
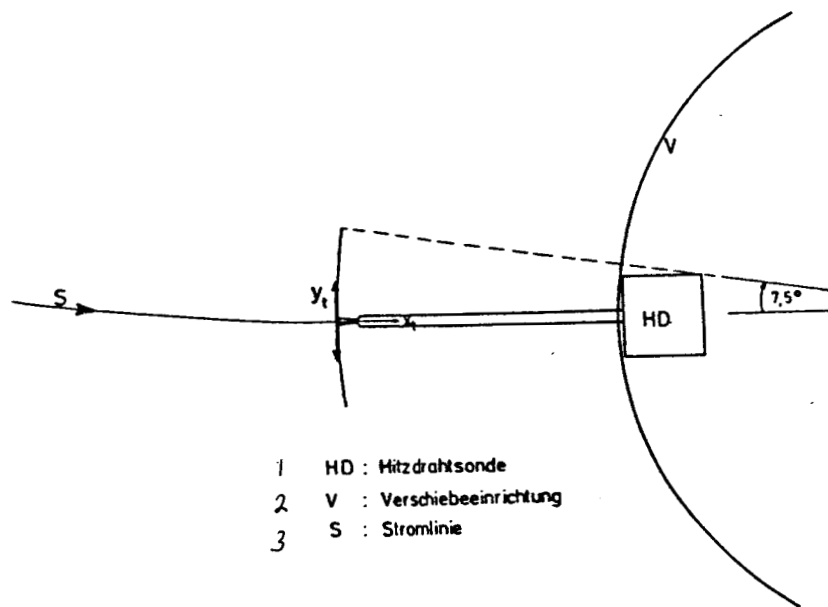
Fig. 3.10: Sketch of the Sweep of Hot Wire Anemometer 2 in the
Streamline-Oriented Coordinate System. 1:Hot Wire
Anemometer   2:Sweep Mechanism 3:Streamline
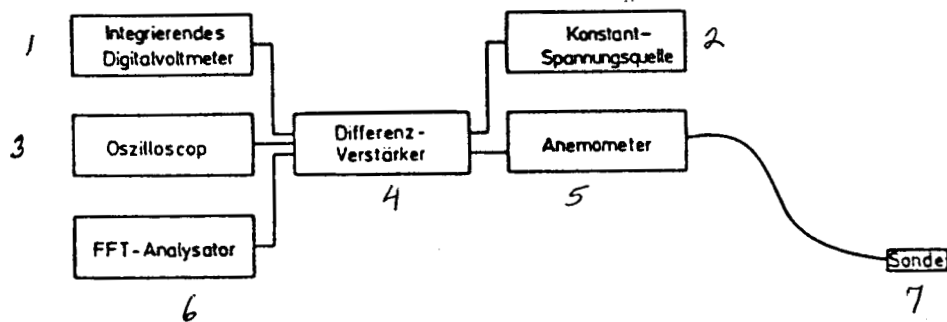
Fig. 3.11: Switching for Measurements Using the Hot Wire and Hot
Film Anemometers
1:Integrating Digital Voltmeter 2:Constant Voltage
Source   3:Oscilloscope   4:Difference Amplifier
5:Anemometer 6:FFT-Analyzer   7:Probe
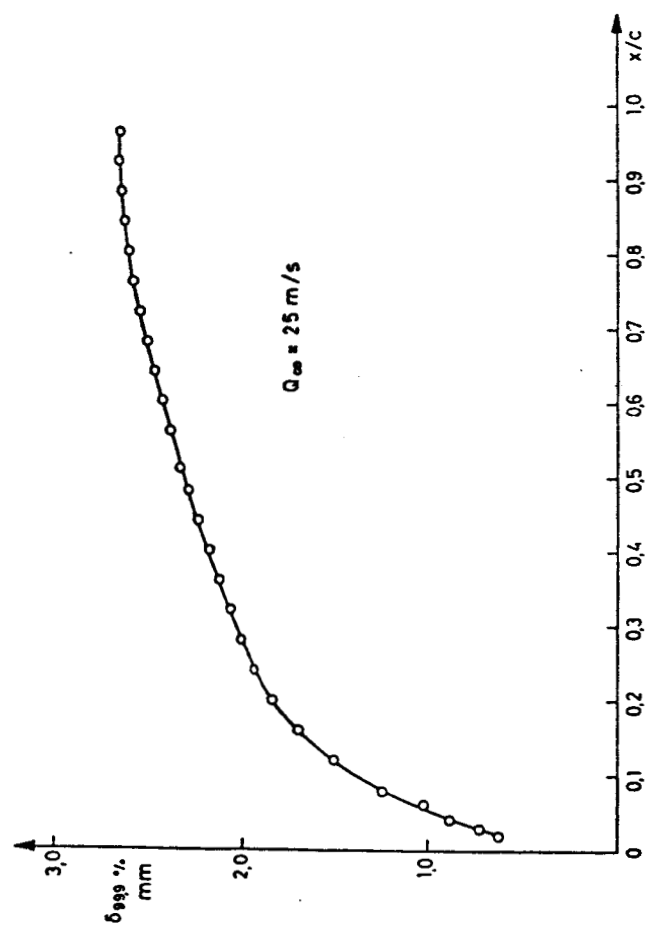
Fig. 3.12a: Course of the Calculated 99.9% Boundary Layer
              Thickness δ above x/c
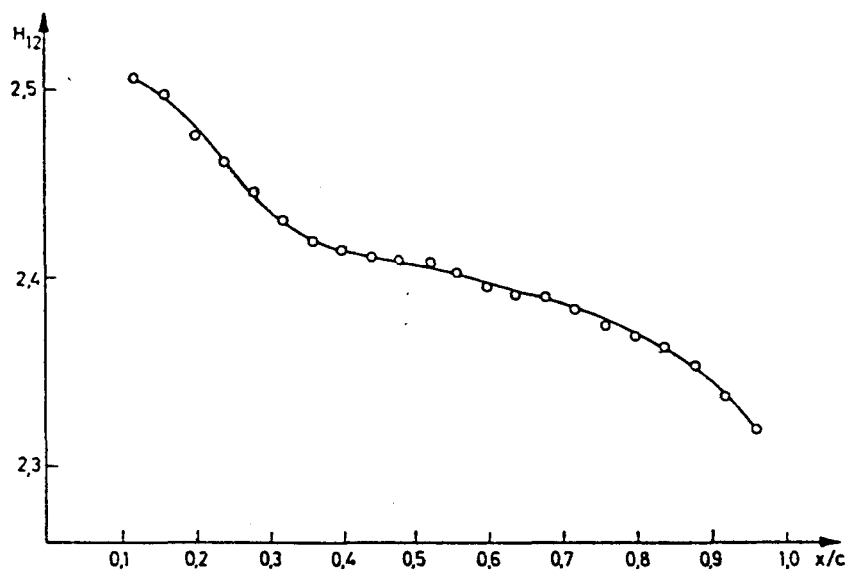
Fig. 3.12b: Course of the Shape Factor H_{12} of the Projected Velocity Profile above x/c in the Direction of the Main Flow (x_t)
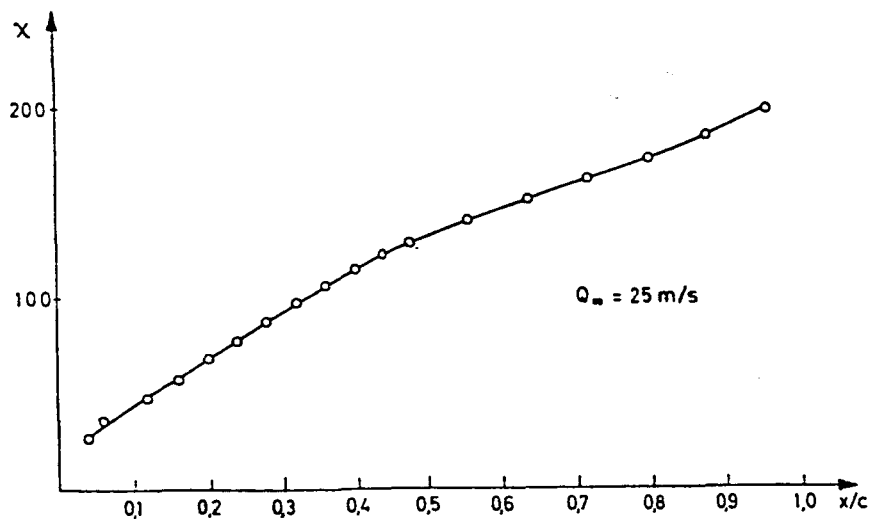
Fig. 3.12c: Course of the Cross Flow Reynolds Number χ above x/c
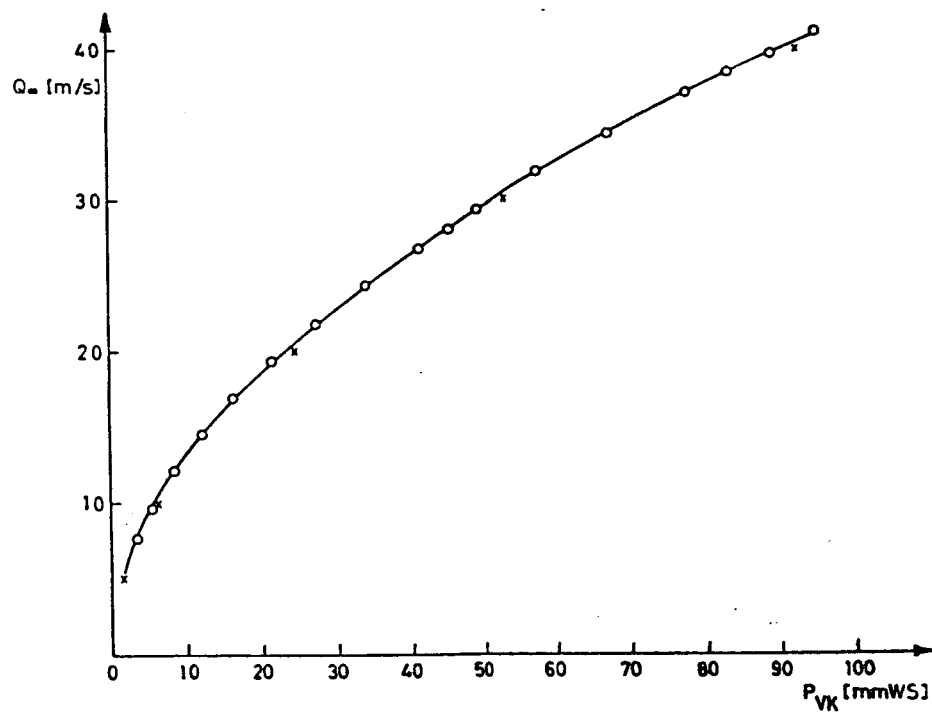
Fig. 3.13: Calibration Curve of the 1-Meter Wind Tunnel
            o: With Model
            x: Without Model
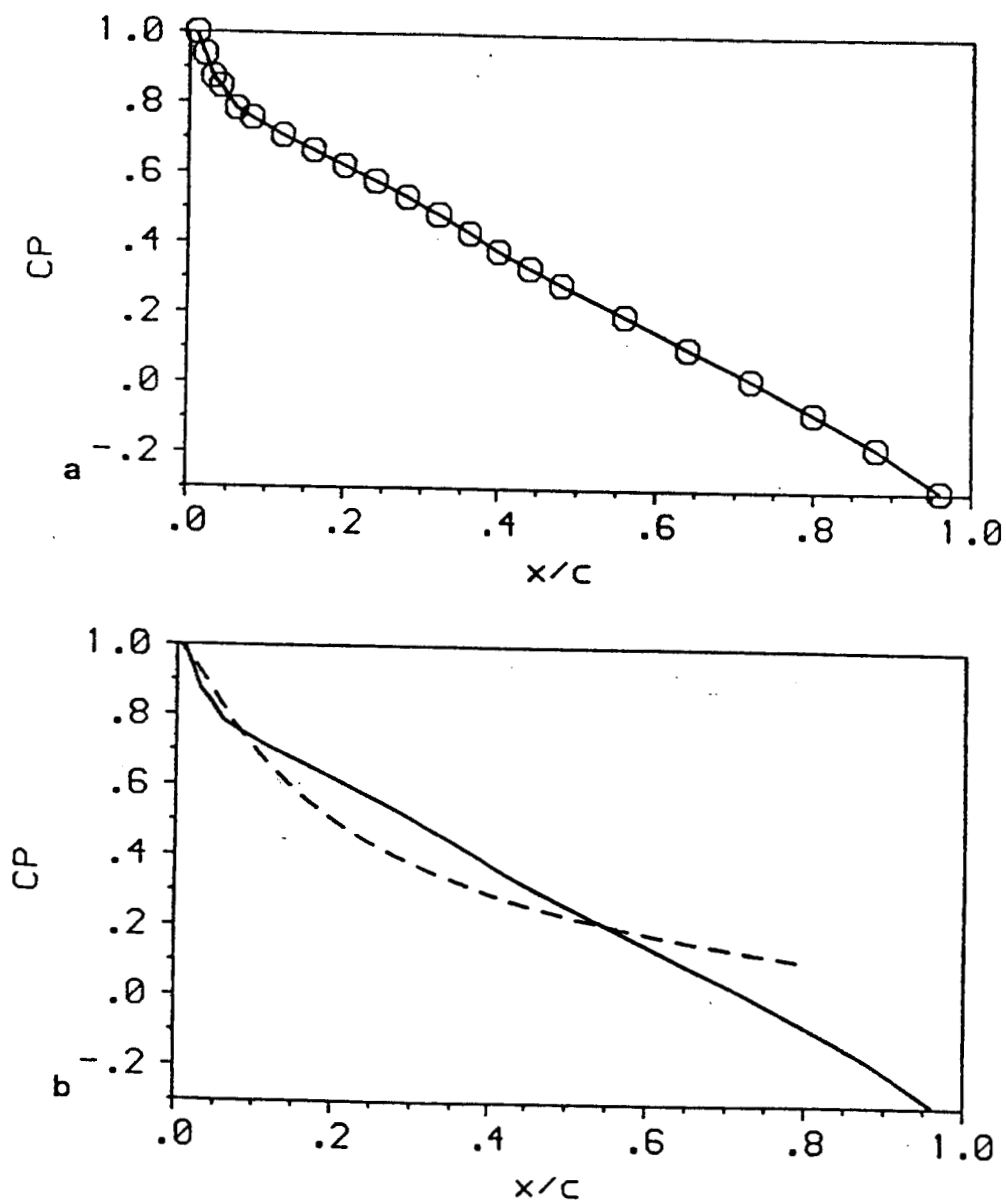
Fig. 3.14: Measured Pressure Progression on the Plate (a)
Compared with the Pressure Progression on NACA 0010 at
$\propto$ = 15°(b)
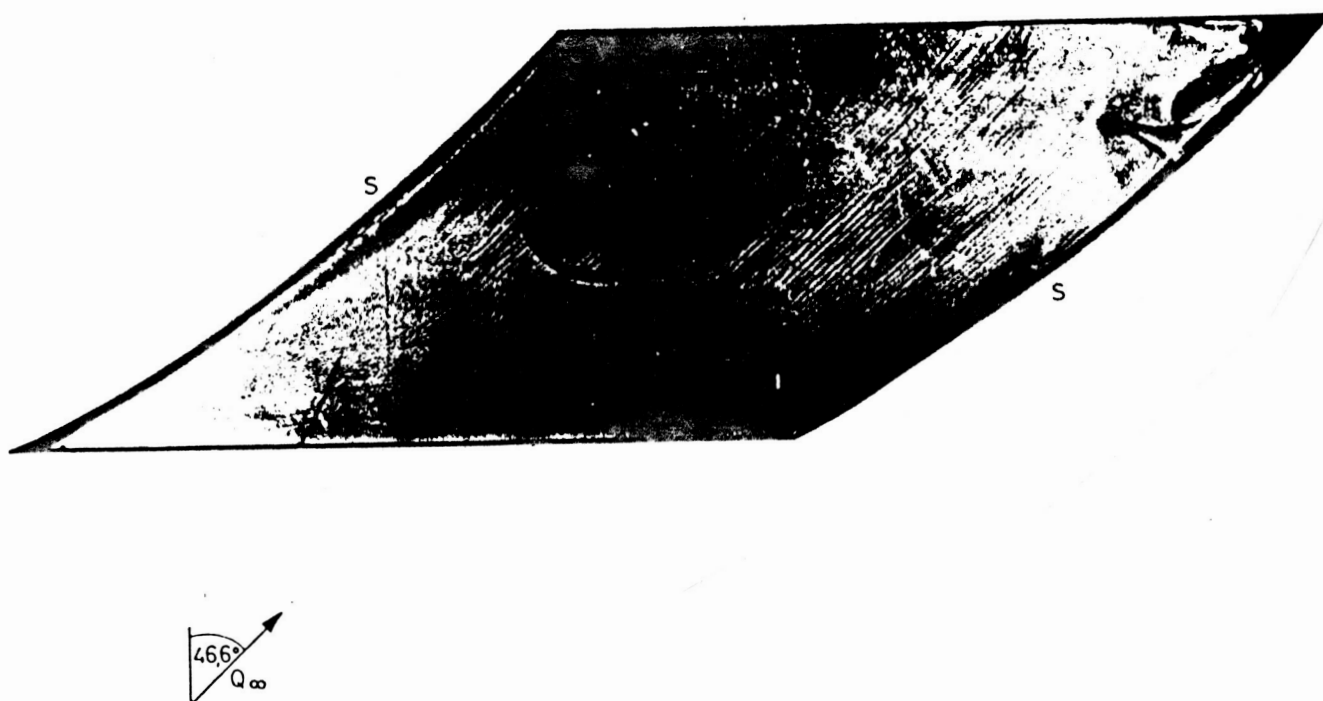
Fig. 3.15: Rendering the Wall Streamlines Visible on the Plate by Means of the Petroleum Painting Method, Re = 9.7 · 10^5 l:laminar   i:cross flow instability   t:turbulent

87

Fig. 3.16: Rendering the Site of Transition to Turbulence and the
Stationary Cross Flow Instabilities on the Plate
Visible by Means of the Sublimation Method,
$Re = 9.7 \cdot 10^5$
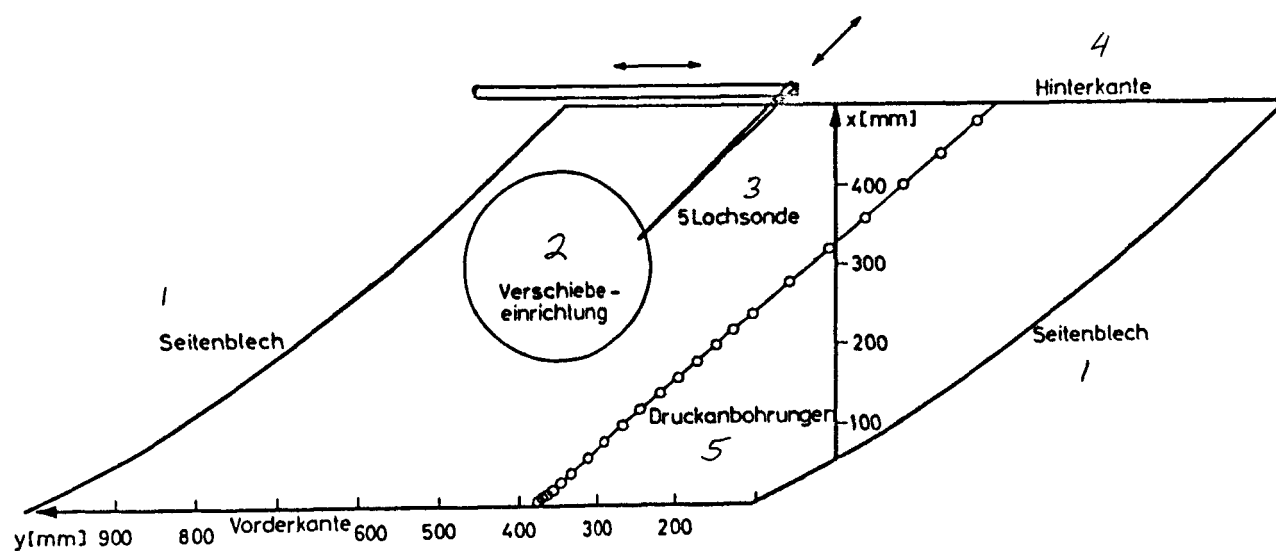
Fig. 3.17: Sketch of the Plate with the Arrangement of the Five-
Hole Anemometer in the Measurement of the Velocity
Vector at the Edge of the Boundary Layer
1:Lateral Plate   2:Sweep Mechanism   3:5-Hole Probe
4:Trailing Edge   5:Pressure Piercings
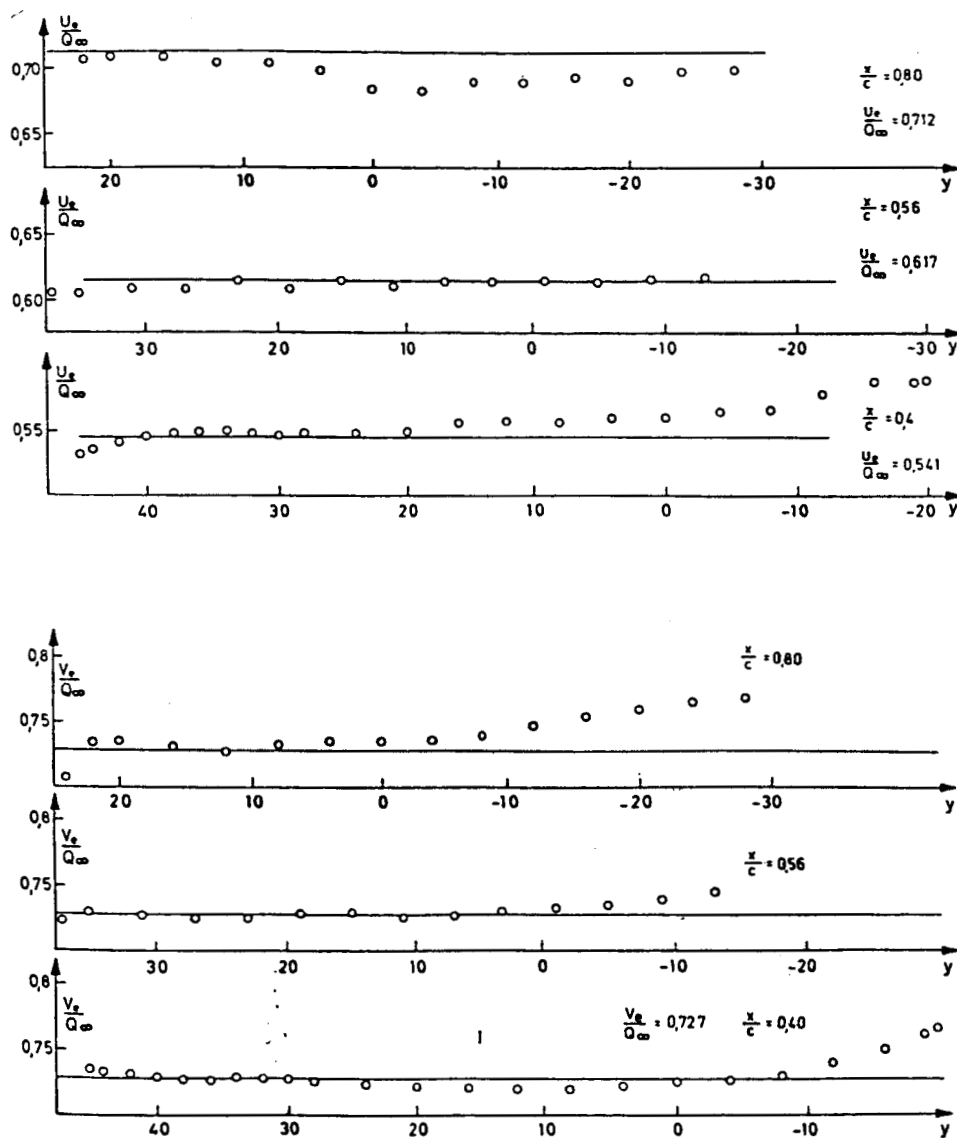
Fig. 3.18: Velocity Components Ue and Ve along Lines x/c = const.
When Compared with the Value Computed from the
Pressure Progression
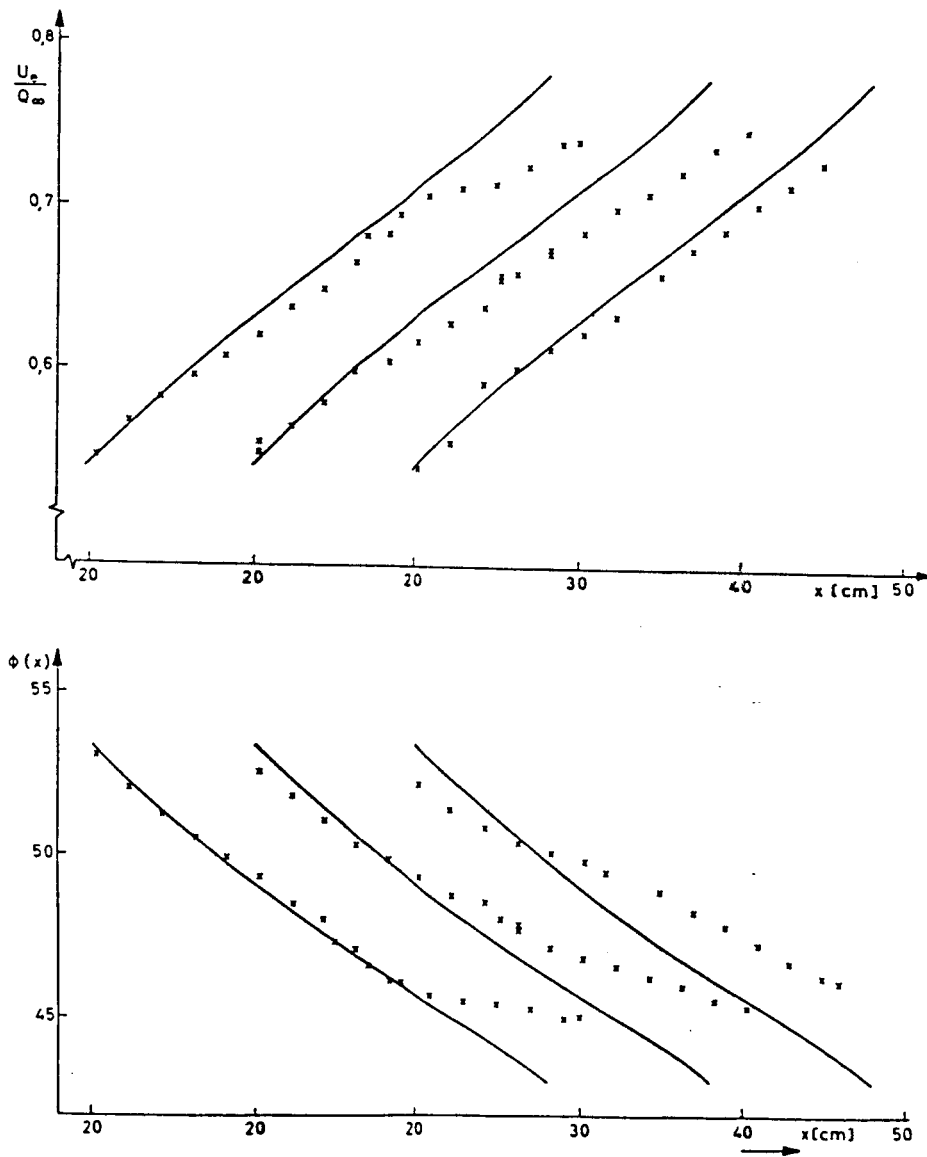
Fig. 3.19: Velocity Components U_e and Local Sweep Angle $\phi(x)$ of the Streamline on the Edge of the Boundary Layer along Three Straight Lines with a 45° Angle to the Leading Edge
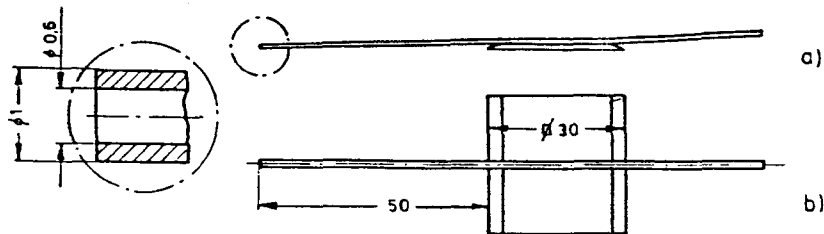
Fig. 3.20a: Diagram of the Preston Tube
a) Side View
b) Top View
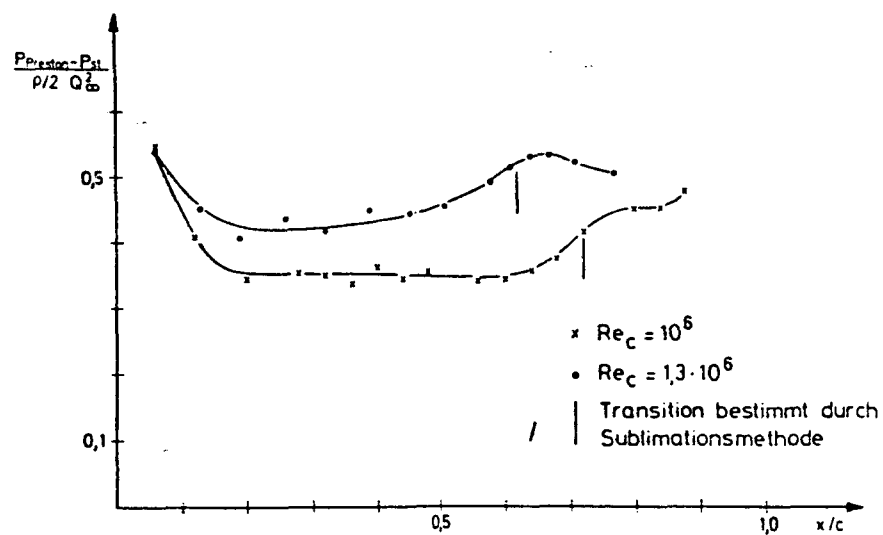
Fig. 3.20b: Measurement of the Preston Pressure along the Plate
Depth to Determine Transition
1:Transition determined by Sublimation Method
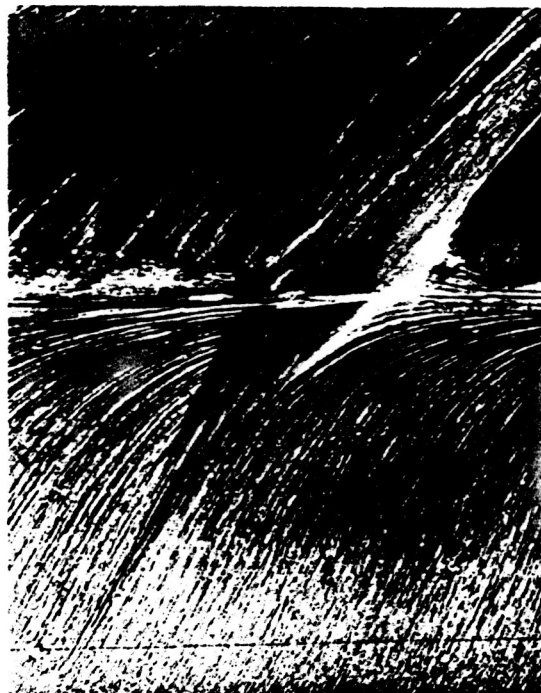
1: turbulent   1

2: laminare Ablösung   2

3: laminar mit einem
   turbulenten Keil   3
   durch eine Störung

Fig. 3.21: A Turbulent Wedge in a Laminar Boundary Layer Made
           Visible by the Petroleum Painting Method. The sepa-
           ration of the three-dimensional boundary layer is
           laminar; its touching down again is turbulent. The
           turbulent wedge causes a break through the separation
           bubble.
           1:Turbulent   2:Laminar Separation
           3: Laminar with a Turbulent Wedge Due to a Disturbance

93

1: turbulent

2: Umschlag

3: laminar

Fig. 3.22: The Laminar-Turbulent Transition Made Visible by the Petroleum Painting Method. Fewer pigment particles are left at the site of transition due to the rapid rise in wall shearing stress. The texture of the petroleum painting picture is finer in the turbulent area than in the laminar area.
1: Turbulent   2: Transition   3: Laminar
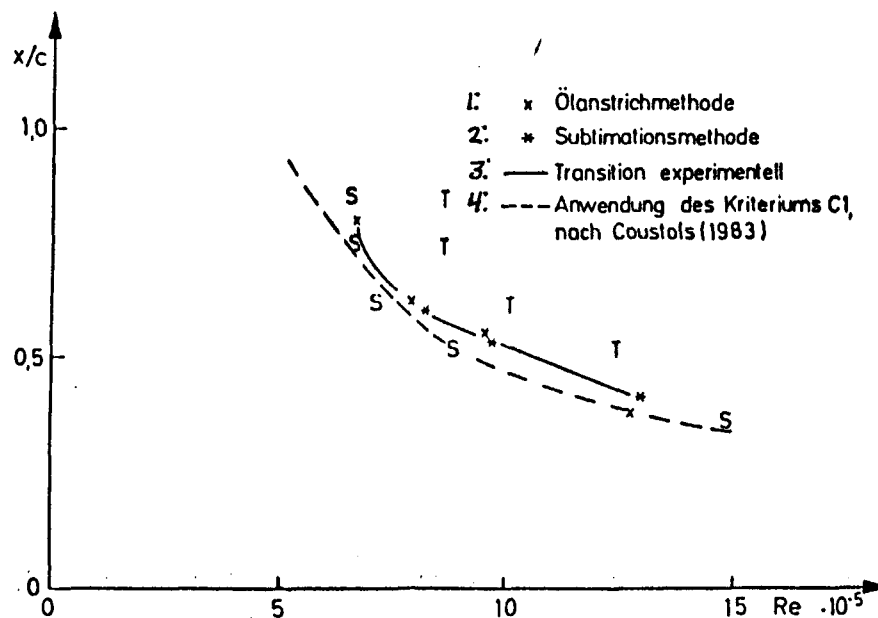
Fig. 3.23: Experimentally Determined Site of Transition to Turbu-
lence Depending on the Reynolds Number Compared to an
Empirical Criterion by Coustols (1983)
S: Turbulent Spots in the Hot-Wire Signal
T: Turbulent Hot-Wire Signal
1:Petroleum Painting Method   2:Sublimation Method
3:Experimentally Determined Transition
4:Application of the Cl Criterion by Coustols (1983)
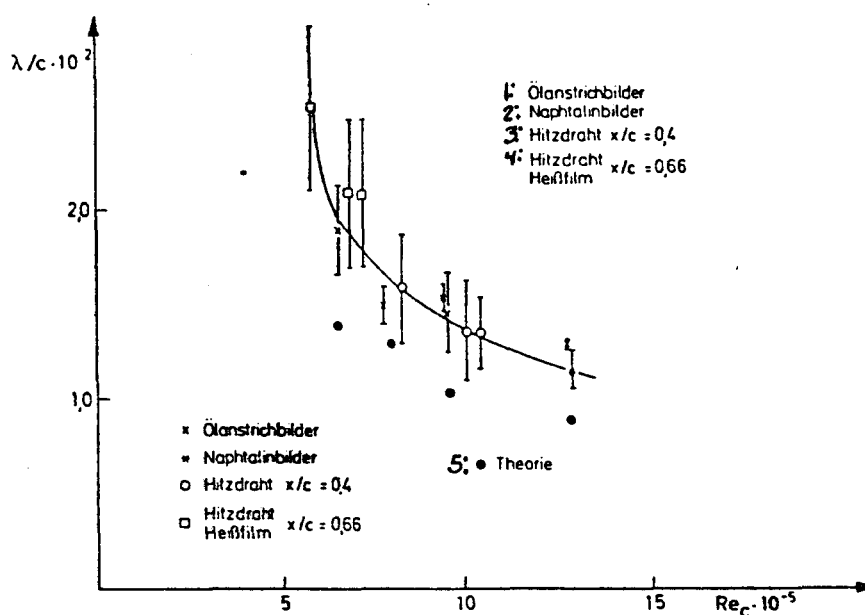
Fig. 3.24: Wavelengths of the Stationary Cross Flow Instability
Depending on the Reynolds Number
1:Petroleum Painting Pictures   2:Naphthalene Pictures
3:Hot Wire x/c = 0.4   4:Hot Wire Hot Film x/c = 0.66
5:Theory
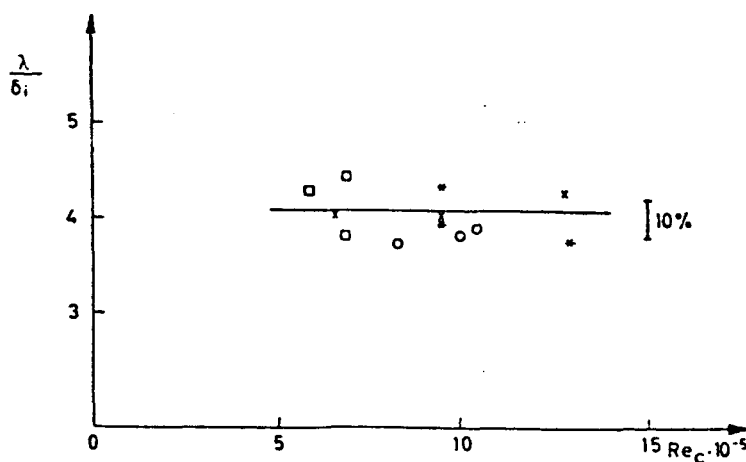
Fig. 3.25: Wavelength of the Stationary Cross Flow Instabilities
Normed by the Boundary Layer Thickness at the Site of
the Initial Observation
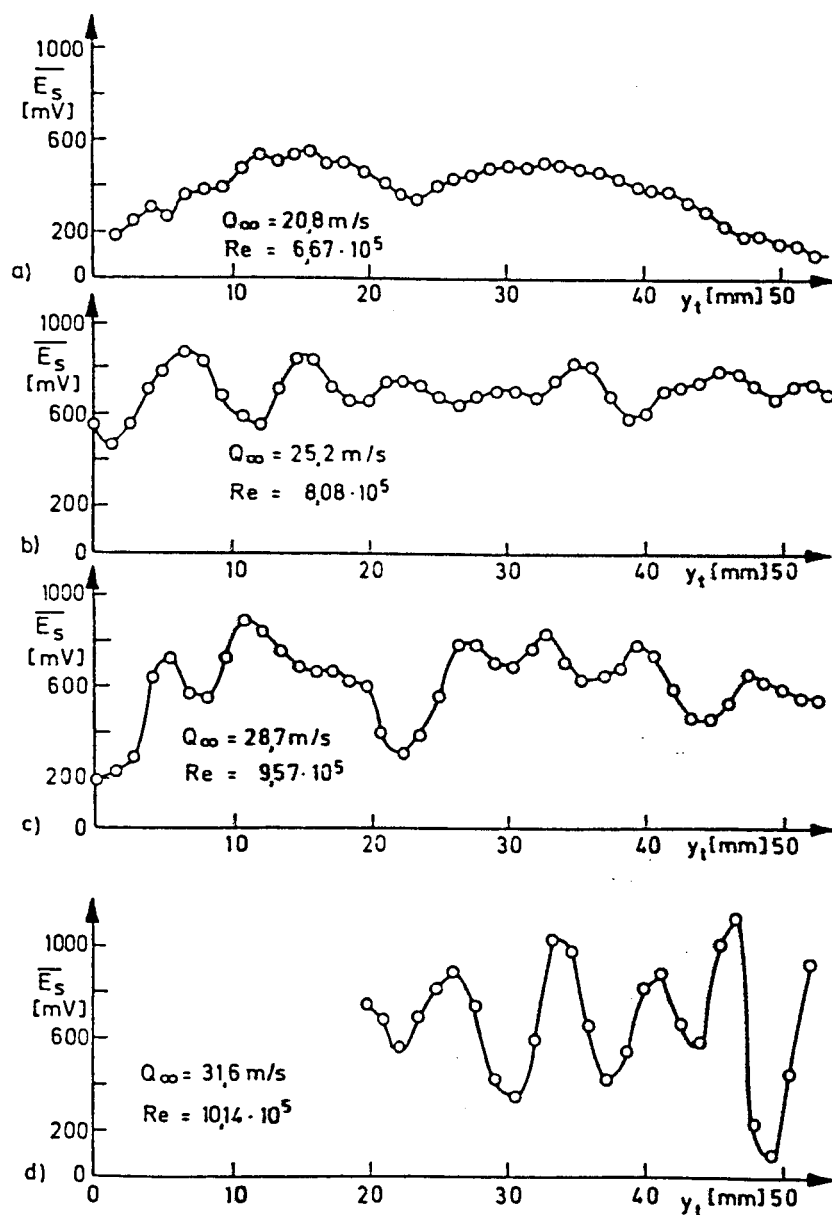
Fig. 3.26: Modulation of the Averaged Velocity and Wall Shearinga-
d Stress along y and y_t by the Cross Flow Instability,
Measured by Hot Wire Anemometer 2
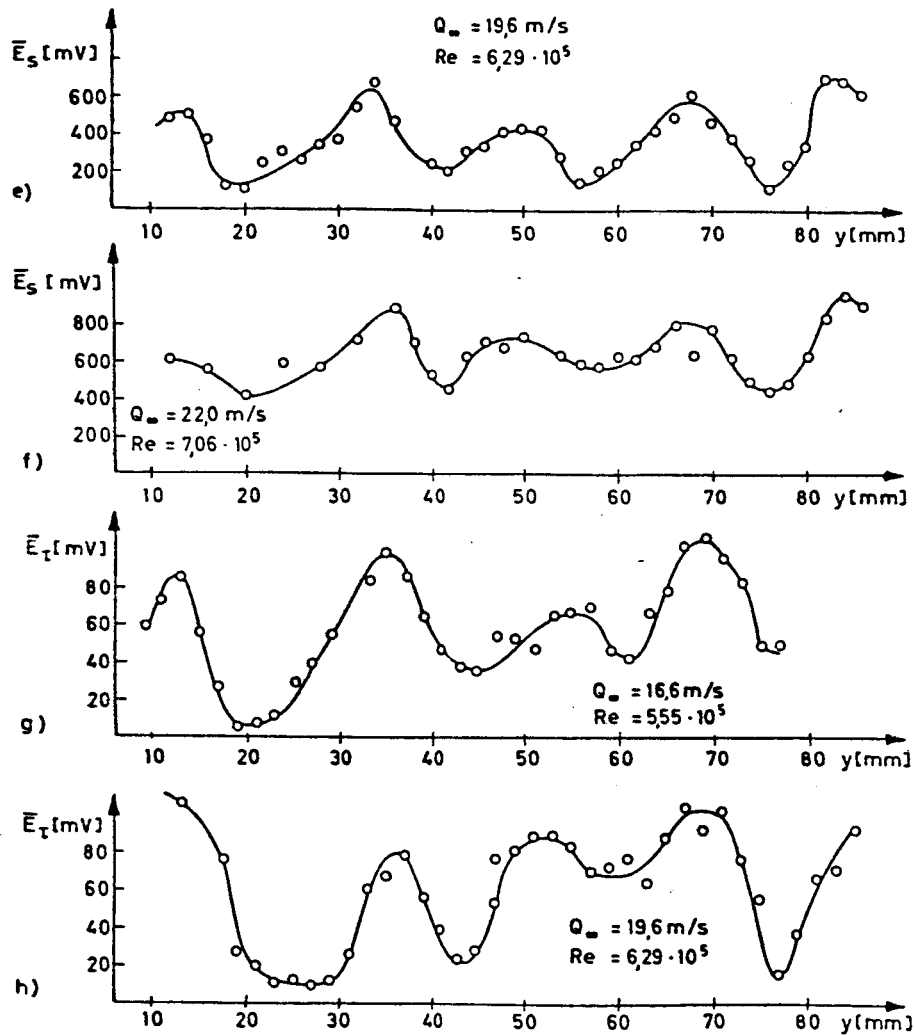
Fig. 3.26: Modulation of the Averaged Velocity (Es) and Wall
Shearing Stress (Eτ) along y and yt by the Cross Flow
Instability, Measured by Hot Wire Anemometer 1 and Hot
Film Anemometer 3

98
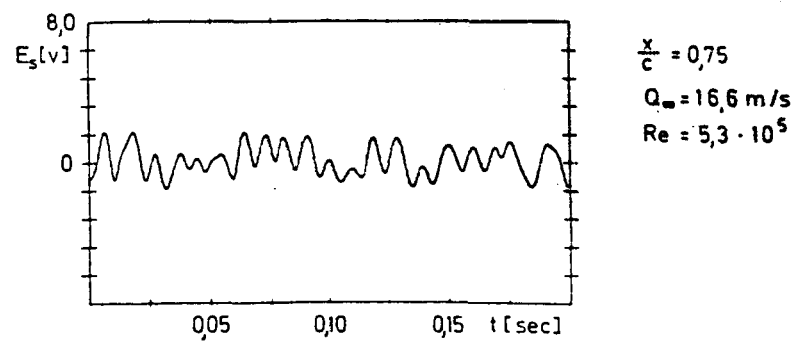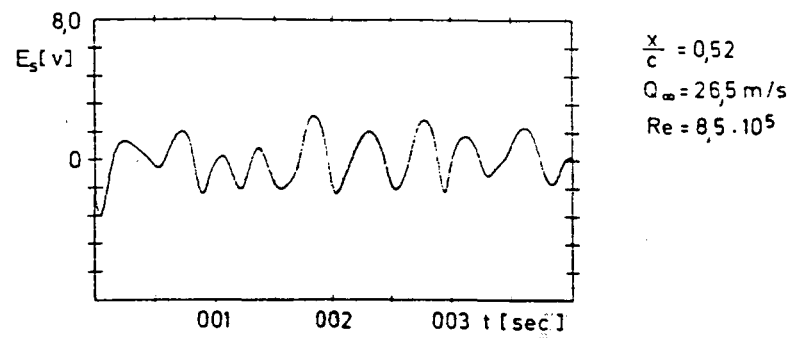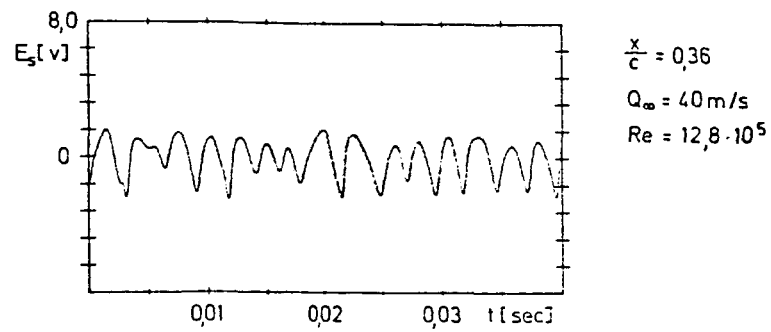
Fig. 3.27: Some Examples of the Hot-Wire Signals of Travelling Waves
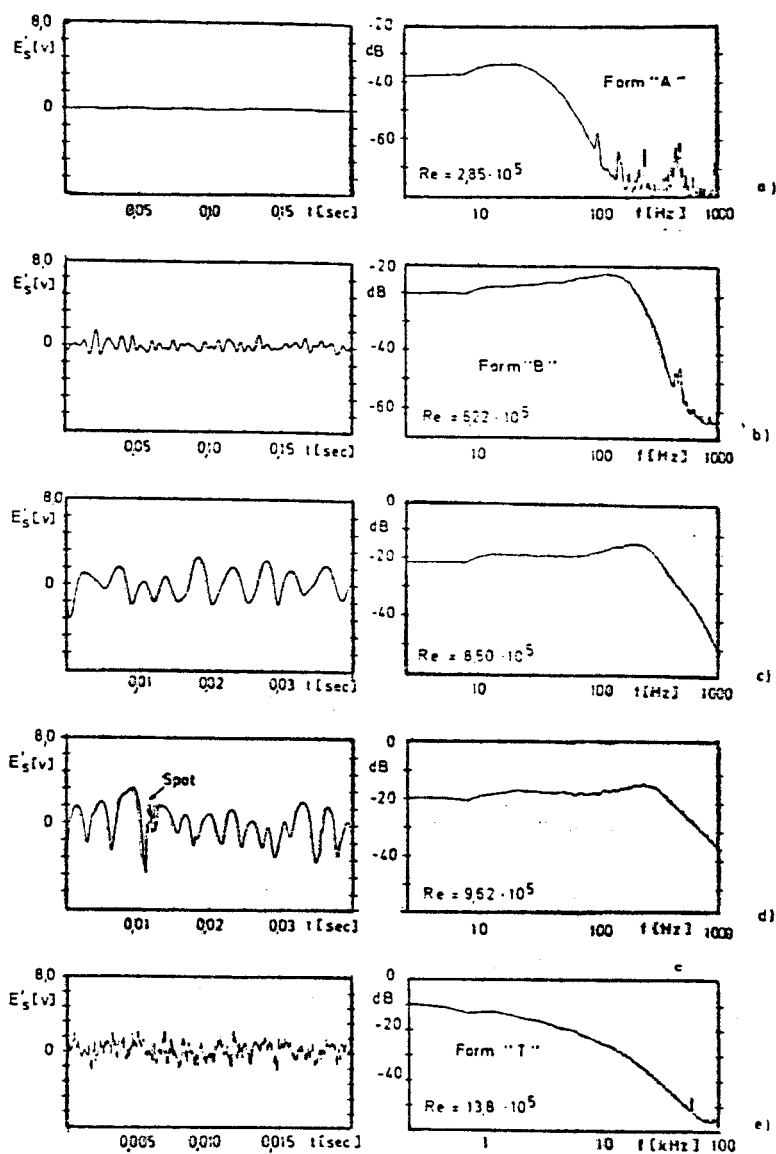
Fig. 3.28: Change in the Hot-Wire Signals of Travelling Waves and of Their Frequency Spectra as Velocity Increases – Ordinates of the Spectra: $20 \log(E_{RMS}/E_0)$
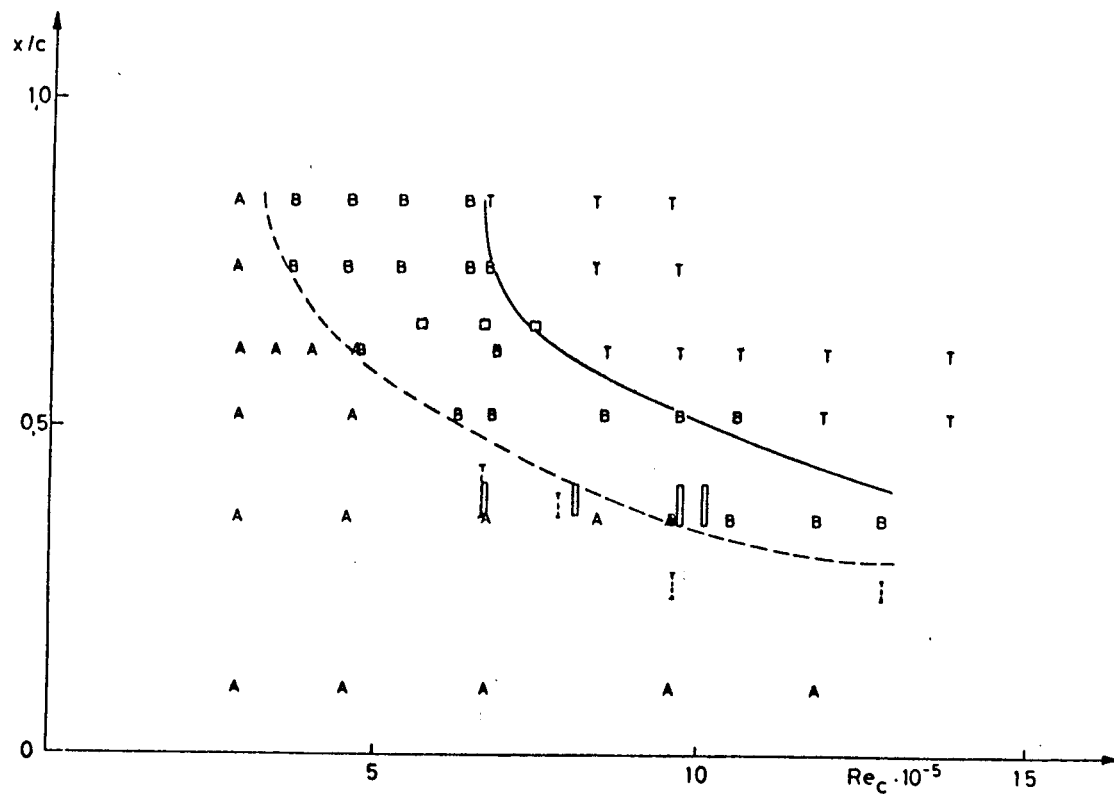
Fig. 3.29: Appearance of Travelling and Standing Waves Depending
on the Site x/c and the Reynolds Number Re, A: Undis-
turbed Flow, B: Travelling Waves, ----: χ = 115, !:
First Appearance of Stationary Cross Flow
Instabilities,   []: Hot-Wire Measurements
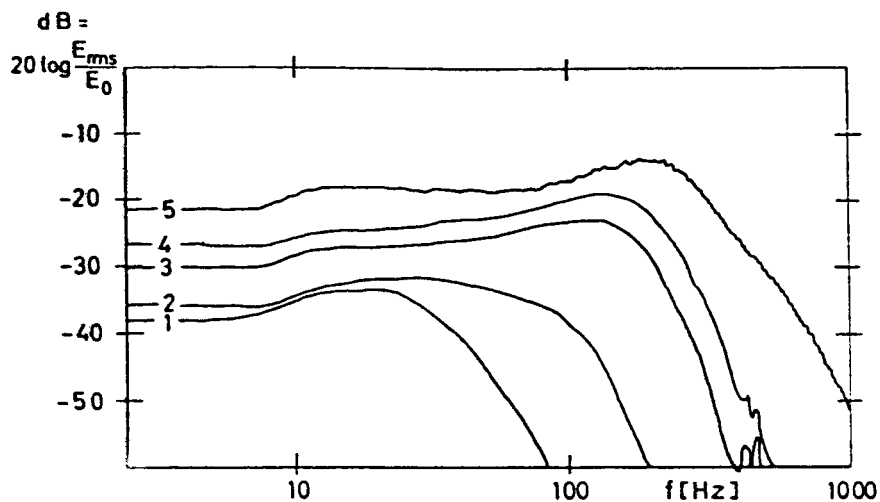
Fig. 3.30a: Change in the Frequency Spectra of the Hot Wire
              Signals with a Fixed Site x/c = 0.52, 1:
              Re = 2.85 • 10^5, 2: Re = 4.59 • 10^5, 3:
              Re = 6.22 • 10^5, 4: Re = 6.74 • 10^5, 5:
              Re = 8.50 • 10^5
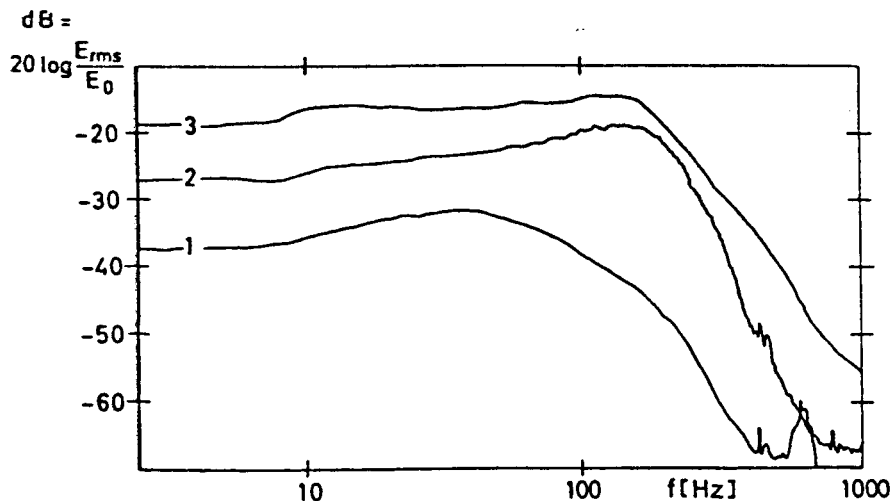
Fig. 3.30b: Change in the Frequency Spectra of the Hot Wire
              Signals with a Fixed Reynolds Number Re = 6.4 • 10^5,
              1: x/c = 0.36, 2: x/c = 0.52, 3: x/c = 0.62

C-2
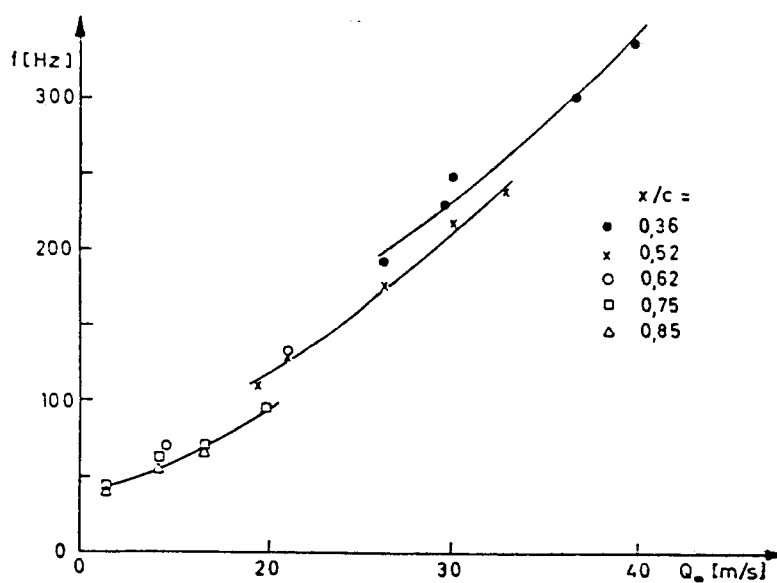
Fig. 3.31: Change in the Frequency of the Maximally Excited Waves
with the Site x/c and the Reynolds Number
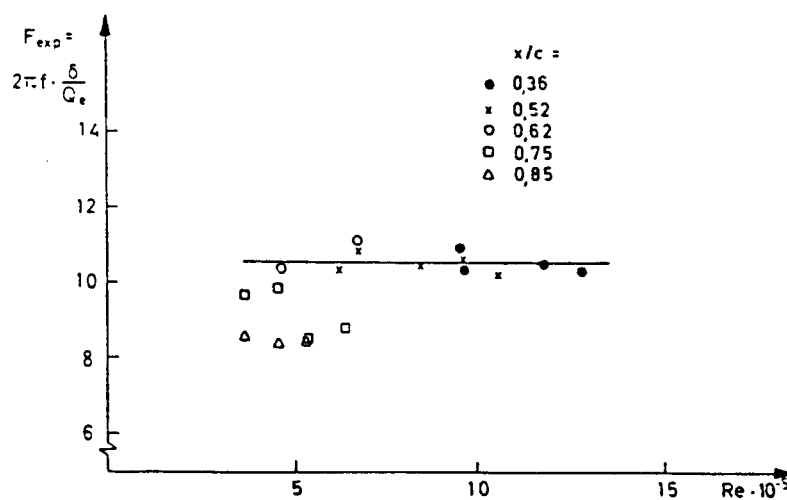
Fig. 3.32: Change in the Frequency of the Maximally Excited Waves
Normed by δ/Q_e
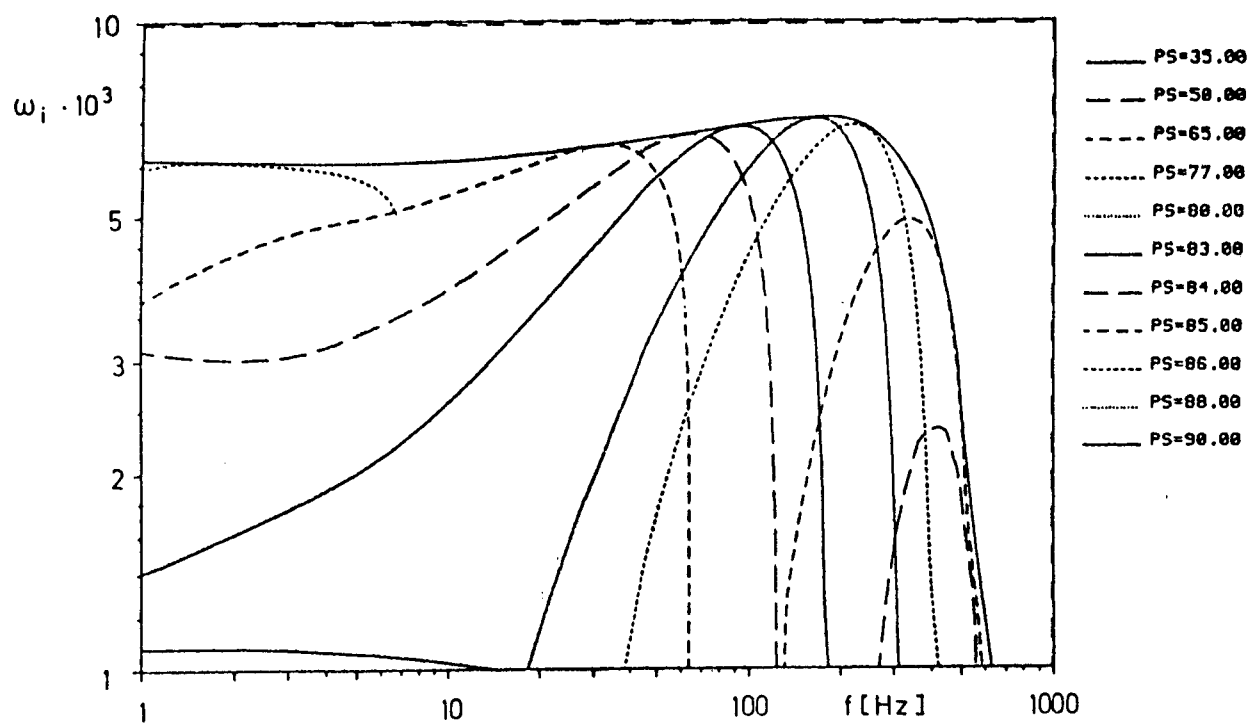
Fig. 3.33: Calculated Non-Dimensional Continuous Excitation of
        Travelling Waves for Various Propagation Directions
        ψ(PS) x/c = 0.52, Re = $8\cdot10^5$
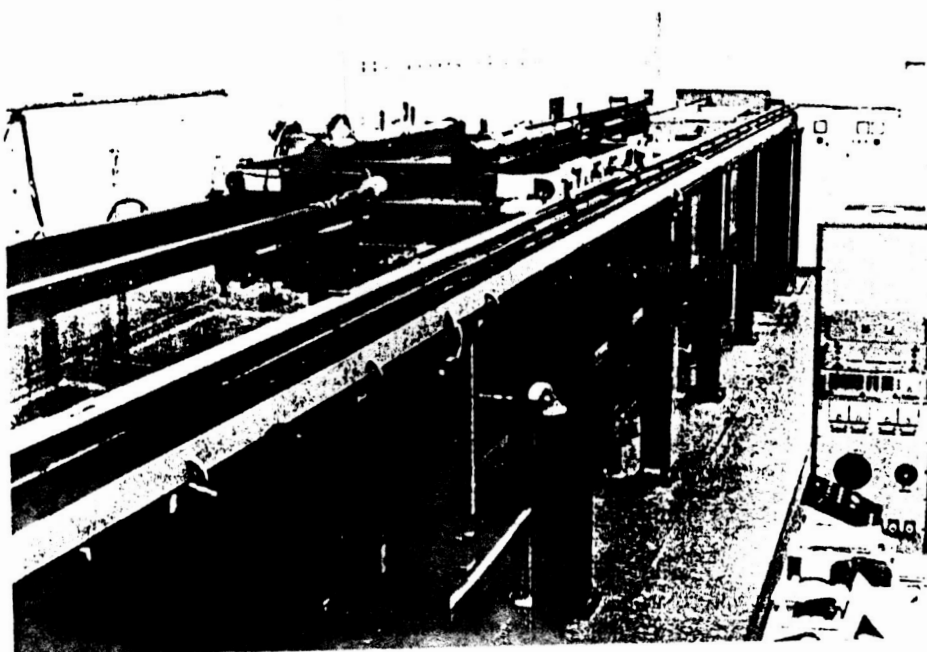
Fig. 4.1:   The Model Water Tunnel
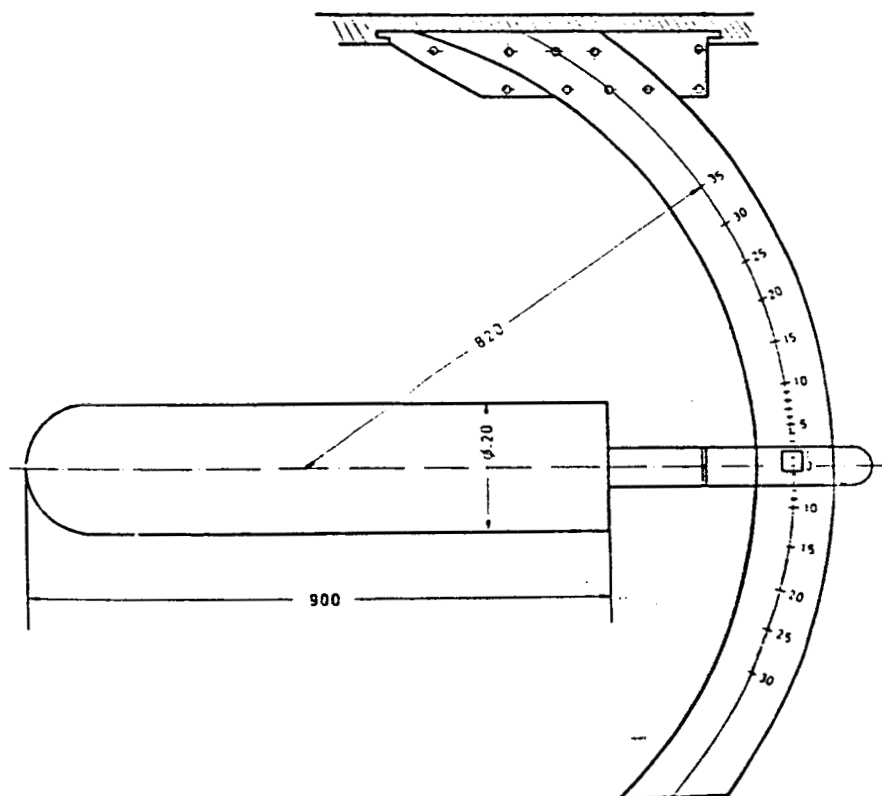
Fig. 4.2: Diagram of the Circular Cylinder with the Mounting
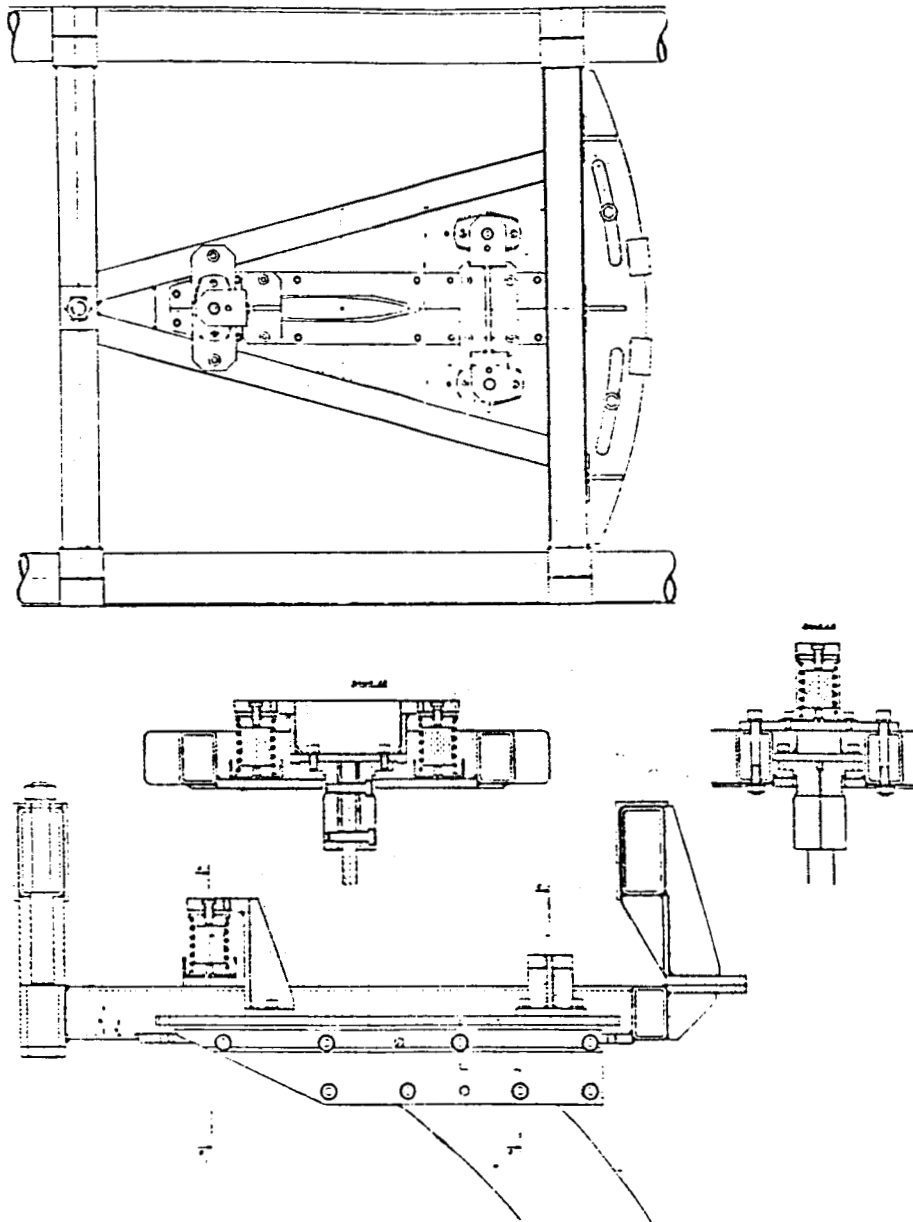
Fig. 4.3: Diagram of the Model's Vibration Insulation
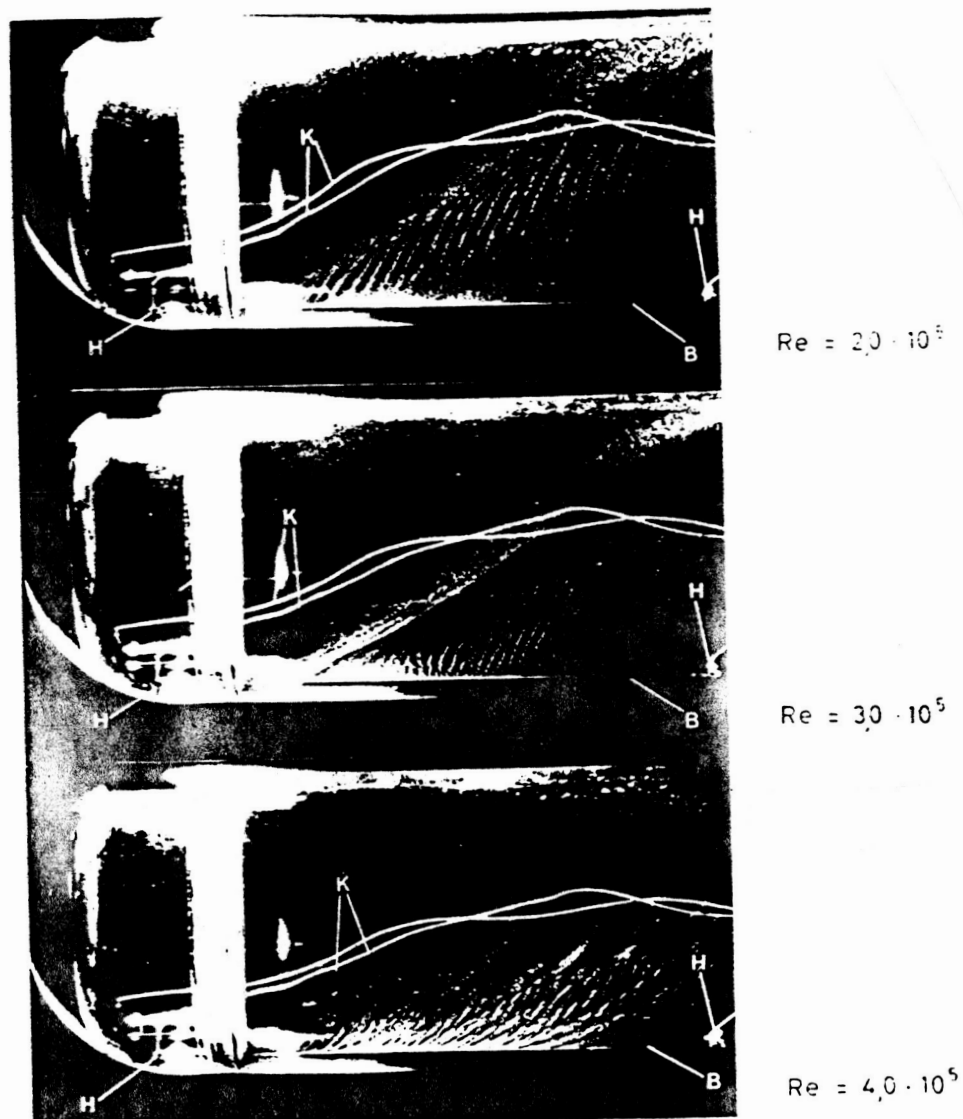
Fig. 4.4: Propagation of Travelling Waves Which Are Caused by a Disturbance of the Boundary Layer (Here: Mounting Pin) in the Stagnation Area, with Growing Reynolds Number and $\phi_0 = 70°$ B:Bubble Wire H:Bubble Wire's Mounting Pins K:Cable Inside Model

Fig. 4.5: Growth of a Turbulent Wedge and Travelling Waves Due
to Disturbance S of the Boundary Layer in the
Stagnation Area $Re = 3 \cdot 10^5$, $\phi_0 = 55°$

109
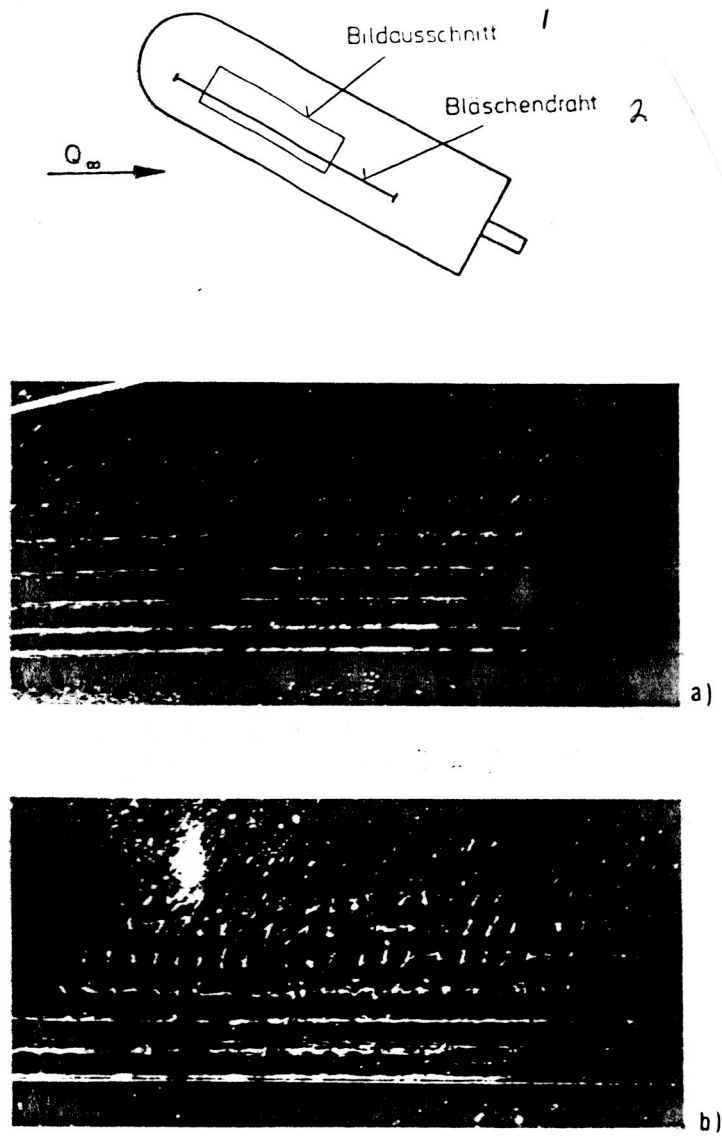
Fig. 4.6: Cross Flow Instability in the Boundary Layer Made
Visible by Time Lines
a)   Re = $3.0 y 10^5$, ϕ_0 = 60°,   Y = 40°
b)   Re = $3.5 y 10^5$, ϕ_0 = 65°,   Y = 60°
1:Detail   2:Bubble Wire
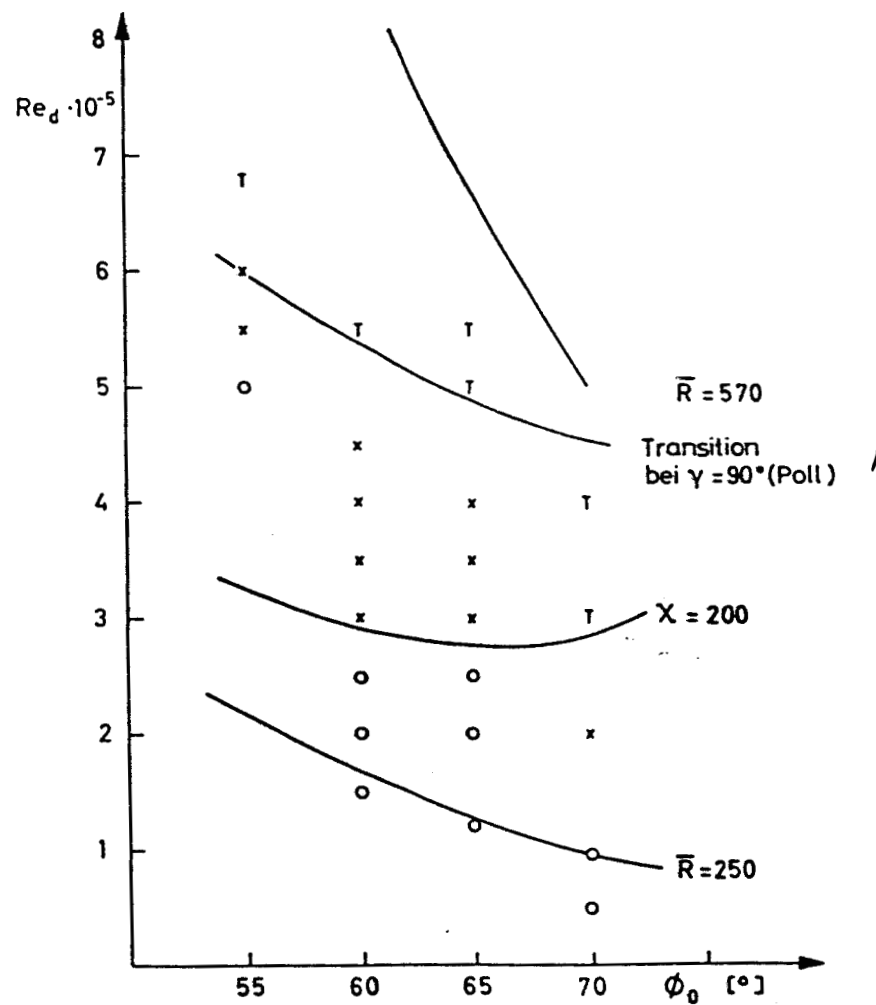
Fig. 4.7: Appearance of Cross Flow Instabilities and Transition
Depending on the Reynolds Number and the Sweep Angle
1:Transition with Y = 90° (Poll)
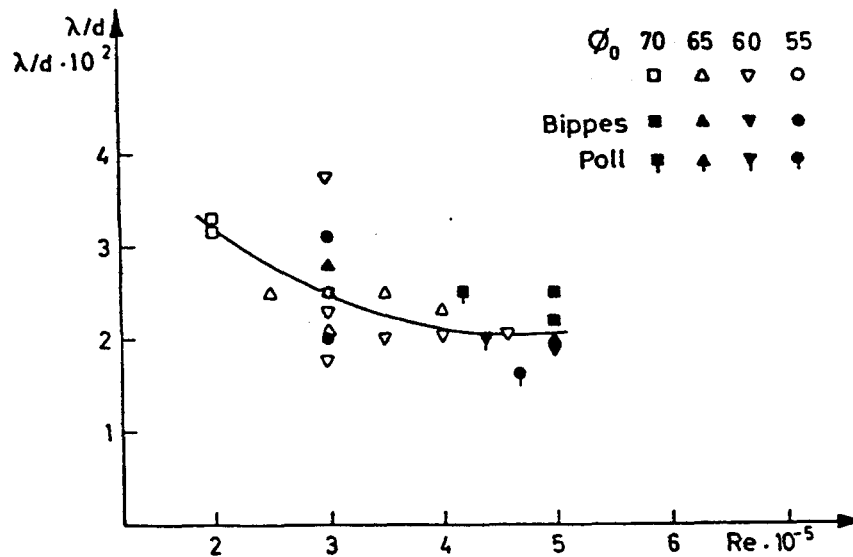
Fig. 4.8:   Wavelength of the Cross Flow Instability Depending on
            the Reynolds Number
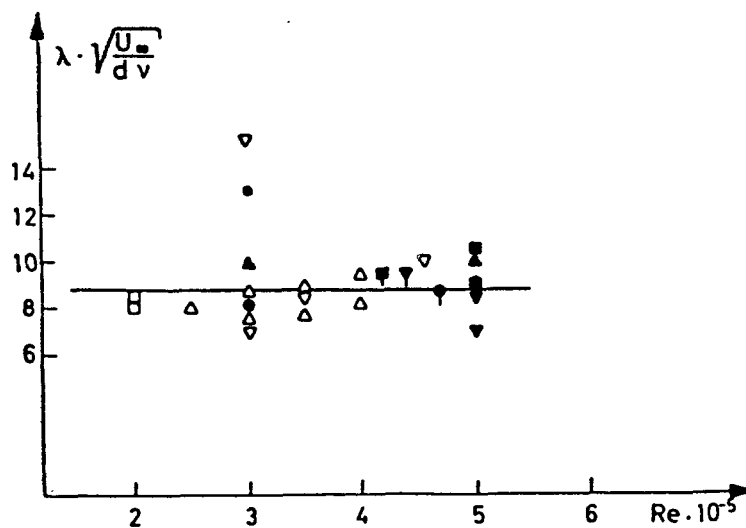
Fig. 4.9:   Wavelength of the Cross Flow Instabilities Normed by
            Depending on the Reynolds Number $\eta = \sqrt{d\,\nu/U_\infty}$
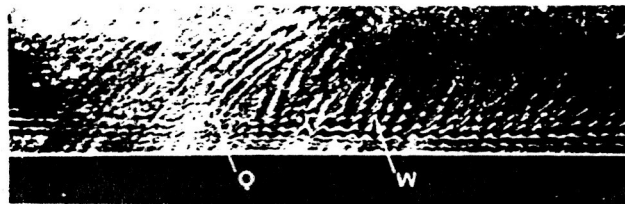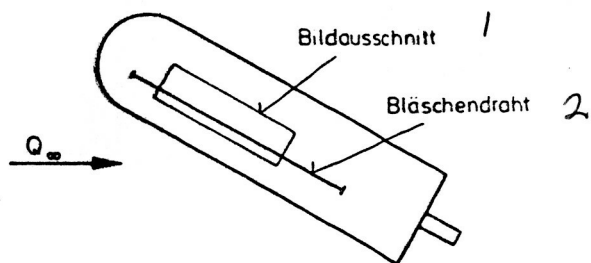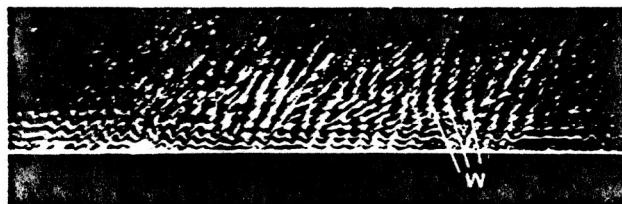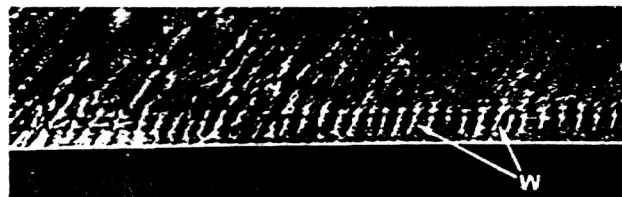
Fig. 4.10: Visualization of Cross Flow Instabilities Q and
Travelling Waves W in the Boundary Layer Shortly before
the Laminar-Turbulent Transition
1:Detail   2:Bubble Wire

113